The Dissertation Committee for Michael Shannon Waring certifies that this is the approved version of the following dissertation:

Indoor Secondary Organic Aerosol Formation: Influence of Particle Controls, Mixtures, and Surfaces

Committee:

_____
Jeffrey Siegel, Supervisor

_____
Richard Corsi, Co-Supervisor

_____
Atila Novoselac

_____
Glenn Morrison

_____
Benny Freeman

Indoor Secondary Organic Aerosol Formation: Influence of Particle Controls, Mixtures, and Surfaces

by

Michael Shannon Waring, M.S.E.; B.S.E.; B.A.

Dissertation

Presented to the Faculty of the Graduate School of
The University of Texas at Austin
In Partial Fulfillment
of the Requirements
for the Degree of

Doctor of Philosophy

The University of Texas at Austin
August 2009

Dedication

To my father and mother,
for always encouraging me to pursue my goals.

Acknowledgements

The majority of the research for this Ph.D. work was carried out in the Indoor Air Quality Research Group at the University of Texas at Austin, during 2005–2009, and a portion of it was conducted at the National Institute for Occupational Safety and Health (NIOSH) research facility in Morgantown, WV in 2008. The work was funded by many sources, including Harrington and THRUST Fellowships from The University of Texas at Austin, the American Society of Heating, Refrigerating and Air-Conditioning Engineers (ASHRAE), the International Society for Exposure Science (ISES), Consumers Union, and NIOSH. The research was also supported by the National Science Foundation Integrative Graduate Education and Research Traineeship (IGERT) grant DCE-0549428, Indoor Environmental Science and Engineering, at UT-Austin.

I have had many wonderful mentors. First, I would like to express my sincere gratitude to my graduate advisor, Dr. Jeffrey Siegel. I appreciate the educational instruction he has given, as well as the time and effort he has applied towards helping me establish my own place in the field of indoor air quality (IAQ). I would also like to thank Dr. Richard Corsi for his guidance and the tireless work he has put in over the years to make UT-Austin a world-class IAQ research institute. I would like to show appreciation to Drs. Atilia Novoselac and Glenn Morrison, from the Missouri University of Science and Technology, for many helpful discussions. My gratitude also extends to Dr. J. Ray Wells at NIOSH for providing me with a wonderful internship opportunity. Last but certainly not least, I am indebted to Dr. Neil Crain for his support and friendship during the last two years. His instruction in experimental methodology has improved my research greatly. Also, I would like to thank past and present fellow students, Donghyun Rim, Brent Stephens, Jim Lohaus, and Scot Waye, for support and friendship.

Finally, to the loved ones in my life—my family, Shannon, Carla, Melissa, Nate, Steve, Barb, Cindy, and Debbie, and my dear friends, Rachael, Wayne, Neil, Kathy, KB, Camron, Hunter, Jay, Sarah, Meagan, and Peter—thank you all for being in my life.

Indoor Secondary Organic Aerosol Formation: Influence of Particle Controls, Mixtures, and Surfaces

Publication No._____

Michael Shannon Waring, Ph.D.
The University of Texas at Austin, 2009

Supervisor: Jeffrey A. Siegel
Co-Supervisor: Richard L. Corsi

Ozone (O_3) and terpenoids react to produce secondary organic aerosol (SOA). This work explored novel ways that these reactions form SOA indoors, with five investigations, in two categories: investigations of (i) the impacts of particle controls on indoor SOA formation, and (ii) two fundamental aspects of indoor SOA formation.

For category (i), two investigations examined the particle control devices of ion generators, which are air purifiers that are ineffective at removing particles and emit ozone during operation. With a terpenoid source present (an air freshener), ion generators acted as steady-state SOA generators, both in a 15 m^3 chamber and 27 m^3 room. The final investigation in category (i) modeled how heating, ventilating, and air-conditioning (HVAC) systems influence SOA formation. Influential HVAC parameters were flow rates, particle filtration, and indoor temperature for residential and commercial models, as well as ozone removal by particle-laden filters for the commercial model.

For category (ii), the first investigation measured SOA formation from ozone reactions with single terpenoids and terpenoid mixtures in a 90 L Teflon-film chamber, at low and high ozone concentrations. For low ozone, experiments with only d-limonene yielded the largest SOA number formation, relative to other mixtures, some of which had three times the effective amount of reactive terpenoids. This trend was not observed for

high ozone experiments, and these results imply that ozone-limited reactions with d-limonene form byproducts with high nucleation potential.

The second investigation in category (ii) explored SOA formation from ozone reactions with surface-adsorbed terpenoids. A model framework was developed to describe SOA formation due to ozone/terpenoid surface reactions, and experiments in a 283 L chamber determined the SOA yield for ozone/d-limonene surface reactions. The observed molar yields were 0.14–0.16 over a range of relative humidities, and lower relative humidity led to higher SOA number formation from surface reactions. Building materials on which ozone/d-limonene surface reactions are predicted to lead to substantial SOA formation are those with initially low surface reactivity, such as glass, sealed materials, or metals. The results from category (ii) suggest significant, previously unexplored mechanisms of SOA number formation indoors.

Table of Contents

List of Tables in Research Summary

List of Figures in Research Summary

List of Symbols in Research Summary

A	nominal surface area (m^2)
CADR	clean air delivery rate (m^3/h)
C_{O3}	indoor ozone mass concentration ($\mu g/m^3$)
$C_{O3,m}$	indoor ozone molar concentration (ppb)
C_{seed}	indoor seed particle (i.e., not SOA) mass concentration ($\mu g/m^3$)
C_{SOA}	indoor SOA mass concentration ($\mu g/m^3$)
C_{terp}	indoor terpenoid mass concentration ($\mu g/m^3$)
$C_{terp,m}$	indoor terpenoid molar concentration (ppb)
d_p	particle diameter (μm or nm)
E_{O3}	emission rate of ozone (mg/h)
E_s	formation rate SOA from of ozone/terpenoid surface reactions (μg/h)
F_{RH}	model formation factor that adjusts for change in *RH* (-)
F_T	model formation factor that adjusts for change in *T* (-)
J	mass flux to a surface ($ug/m^2 \cdot h$)
k	bimolecular reaction rate constant between terpenoid and ozone ($ppb^{-1}\ h^{-1}$)
k_{ac}	decay of particles when the air cleaner was energized in CADR test (h^{-1})
k_{OH}	bimolecular reaction rate constant of a compound with the hydroxyl radical ($cm^3/molecule \cdot s$ or $ppb^{-1}\ h^{-1}$)
k_{ozone}	bimolecular reaction rate constant of a compound with ozone ($cm^3/molecule \cdot s$ or $ppb^{-1}\ h^{-1}$)
k_n	background decay of particles in CADR test (h^{-1})
k_{pseudo}	pseudo first-order reaction rate of ozone with a compound (h^{-1})
$k_{pseudo,i}$	initial pseudo first-order reaction rate of ozone with a compound (h^{-1})
MW_{O3}	molecular weight of ozone (g/mol)
MW_{SOA}	molecular weight of SOA (g/mol)
Q	volumetric flow rate through a chamber or indoor space (m^3/h)
r_{terp}	fractional coverage of a surface with adsorbed terpenoid (m^2 terpenoid/m^2 intrinsic surface area)
V	volume (m^3)
v_d	deposition velocity of ozone to a surface (m/h)
$v_{d,terp}$	ozone deposition velocity to adsorbed terpenoids (m/h)
$\langle v \rangle$	Boltzmann velocity (1.296×10^6 m/h for O_3 at 296 K)
$Y_{g,m}$	yield of SOA for homogenous reactions between the terpenoid and ozone (moles SOA formed/moles terpenoids reacted)
Y_g	yield of SOA for homogenous reactions between the terpenoid and ozone (mass SOA formed/mass terpenoids reacted)
$Y_{g,sr}$	size-resolved yield of SOA for homogenous reactions between the terpenoid and ozone (mass SOA formed/mass terpenoids reacted)
$Y_{s,m}$	yield to SOA of reactions of ozone with surface-adsorbed terpenoids (moles SOA formed/moles ozone reacted)

β_{O3}	deposition loss rate of ozone to surfaces (h^{-1})
β_p	size-resolved deposition loss rate of particles and SOA to surfaces (h^{-1})
Γ	conversion factor to change the units of SOA formation from ppb/h to $\mu g/m^3 \cdot h$
γ	reaction probability of ozone with a surface (-)
γ_o	reaction probability of ozone with a surface without terpenoid adsorption (-)
γ_{terp}	reaction probability of the adsorbed terpenoid (-)
η_{O3}	removal of ozone by an HVAC filter (-)
η_p	size-resolved removal of particles and SOA by an HVAC filter (-)
λ	air exchange rate (h^{-1})
λ_{cycle}	air exchange rate during the HVAC Cycle period (h^{-1})
λ_i	air exchange rate due to infiltration (h^{-1})
λ_{off}	air exchange rate during the HVAC Off period (h^{-1})
λ_r	air exchange rate due to recirculation (h^{-1})
λ_v	air exchange rate due to ventilation (h^{-1})
χ_g	ratio of the SOA number concentration formed and mass concentration formed for gas-phase reactions $(\#/cm^3)/(\mu g/m^3)$
χ_s	ratio of the SOA number concentration formed and mass concentration formed for surface-phase reactions $(\#/cm^3)/(\mu g/m^3)$

1. INTRODUCTION

Exposure to air pollution is an indoor as well as an outdoor issue. Many hazardous pollutants are present at equivalent or higher concentrations indoors than outdoors. Moreover, Americans spend the majority of their time indoors, and on average, the typical American spends 18 hours indoors for every hour spent outdoors (Klepeis et al., 2001). These potentially higher indoor concentrations coupled with the longer amount of time spent indoors means that, for many airborne pollutants, indoor exposure can dominate inhalation exposure.

Indoor pollutants are present in gas and particle phases. Common examples of gas-phase pollutants at notable concentrations indoors include ozone (O_3) due to outdoor-to-indoor transport (Weschler, 2000) or emission from ozone or ion generators or office appliances (e.g. Lee et al., 2001; Mullen et al., 2005; Britigan et al., 2006); hydroxyl radicals (OH) due to reactions of ozone with unsaturated organics (Atkinson et al., 1992; Weschler and Shields, 1996, 1997); and volatile organic compounds (VOCs) emitted indoors from building materials (e.g. Baumann et al., 1999a, 1999b; Hodgson et al., 2002; Salthammer et al., 2003) or consumer products such as cleaners, air fresheners, and perfumes (e.g. Nazaroff and Weschler, 2004; Corsi et al., 2007). Common examples of particle-phase indoor pollutants are particles of outdoor origin from automobiles or power plants (e.g. Seinfeld and Pandis, 1998); those from indoor combustion sources such as smoking (e.g. Klepeis et al., 2003; Nazaroff and Klepeis, 2004; Waring and Siegel, 2007) or cooking (e.g. Wallace et al., 2004; Wallace, 2006); and those that are resuspended from building surfaces (e.g. Thatcher and Layton, 1995; Ferro et al., 2004).

Consequences of exposure to gas-phase pollutants are diverse, from acute irritation to mortality. For example, exposure to different VOCs can lead to eye, nose, and throat irritation, headaches, loss of coordination, nausea, or damage to the liver, kidneys, or central nervous system (U.S. EPA). Formaldehyde (HCHO) is both an acute irritant and linked to naso-pharyngeal cancer (Cogliano et al., 2005). Ozone exposure has been associated with the development of asthma in adult males (McDonnell et al. 1999) and increases in human mortality (Bell et al., 2004; Ito et al. 2005; Levy et al. 2005).

Epidemiological studies have associated particle exposure with adverse health effects, such as premature mortality or aggravated asthma (Pope and Dockery, 2006). Particle sizes of interest for exposure range across approximately five orders of magnitude, from a few nanometers to approximately ten micrometers in diameter. The mass concentration of particles less than 2.5 μm in diameter, $PM_{2.5}$ ($\mu g/m^3$), is one indicator of particulate pollution used by the U.S. Environmental Protection Agency (EPA). However, research suggests that exposure to high particle number or surface-area concentrations may also be associated with observed health effects (Harrison and Yin, 2000). Ultrafine particles are those less than 0.1 μm in diameter, and they can negatively affect cardiopulmonary function independently of $PM_{2.5}$ (Pekkanen et al., 2002).

Gas-phase pollutants can undergo chemical reactions and yield products, which necessitates a distinction between primary versus secondary indoor pollutants. Most of the chemical reactions that occur indoors are oxidative in nature, and most known reaction mechanisms are driven initially by ozone. Ozone reacts with surface-phase compounds (e.g., Sabersky et al., 1973; Cano-Ruiz et al., 1993; Morrison and Nazaroff, 2000, 2002) or with airborne VOCs to yield secondary products such as formaldehyde, more complex carbonyls, and free radicals (e.g. Weschler, 2000; Fan et al., 2003).

Reactions between ozone and unsaturated organic compounds (i.e., those with at least one carbon-carbon double bond) can yield secondary pollutants in both the gas-phase and particle-phase, as is the case with one very common class of indoor chemical reactions, that between ozone and terpenoids. Terpenoids are formed of two or more isoprene units, which have a molecular formula of C_5H_8. Monoterpenes are the most common type of terpenoid indoors (Brown et al., 1994), are formed of two isoprene units, and have the molecular formula $C_{10}H_{16}$ and a molecular weight of 136.24 amu. Major sources of terpenoids indoors are emissions from consumer products (e.g. Nazaroff and Weschler, 2004) and building materials (Baumann et al., 1999a; Saarela, 1999).

Ozone/terpenoid reactions can occur indoors at fast enough rates to compete with loss due to air exchange (Weschler and Shields, 1996). Some products of these reactions have lower vapor pressure, increased polarity, and higher molecular weight with respect

to the parent compounds and may either self-nucleate and/or partition between the gas and condensed particle phases (Weschler and Shields, 1999, 2003; Wainman et al., 2000; Long et al., 2000; Rohr et al., 2003; Sarwar et al., 2003, 2004; Vartiainen et al., 2006; Sarwar and Corsi, 2007; Langer et al., 2008). The fraction of products that exist in the particle phase are known as secondary organic aerosol (SOA), which is the major focus of this dissertation.

The primary objective of this dissertation is to explore novel ways that products of ozone/terpenoid reactions yield SOA indoors. The research in this dissertation falls into two distinct categories:

(i) Exploration of the primary and secondary impacts of particle controls on indoor SOA formation (the research in Appendices A–C), and

(ii) Investigation of two fundamental aspects of indoor SOA formation (the research in Appendices D and E).

These research objectives are further explained in Chapter 3.

This dissertation is comprised of two major sections: (I) a Research Summary and (II) Appendices A–E, which include five journal articles. The purpose of the Research Summary is to report the major findings of the research that was conducted for this dissertation. The work summarized in the Research Summary is presented in full in Appendices A–E, which include five articles that are published or in preparation for publication in peer-reviewed journals. Specifically, the journal articles in Appendices A–E report the results of:

(A) An experimental characterization of residential-use ozone-emitting ion generators, including their size-resolved ultrafine and fine particle removal capability, ozone emission rates, and ability to form SOA in the presence of a terpenoid source;

(B) A field study in a residential room without/with a terpenoid source that investigated the influence of an ion generator on SOA and other pollutants;

(C) A modeling investigation of the influence of heating, ventilating, and air-conditioning (HVAC) systems on SOA formation and concentrations in residential and commercial buildings;

(D) An experimental examination of the variation in SOA formation with single terpenoids versus mixtures of pure terpenoids; and

(E) Experiments and modeling that explore how surface reactions between ozone and adsorbed terpenoids contribute to gas-phase SOA formation.

This work investigated previously-unstudied elements of indoor SOA formation, facilitating a more complete understanding of its sources and sinks in real indoor spaces.

2. LITERATURE REVIEW

This chapter provides a review of the literature relevant to this dissertation on indoor SOA formation. It is divided into four different sections: (2.1) Indoor ozone concentrations and influencing factors; (2.2) Indoor terpenoid concentrations and influencing factors; (2.3) Indoor secondary organic aerosol (SOA) formation; and (2.4) Particle removal and ozone emission by ion generators.

2.1. Indoor ozone concentrations and influencing factors

Ozone (O_3) is produced in the troposphere through photochemical processes, and it is a key component of smog (Seinfeld and Pandis, 1998). Ozone is one of six criteria pollutants for which the Clean Air Act requires the U.S. EPA to set National Ambient Air Quality Standards (NAAQS). There are adverse health effects associated with ozone exposure. One epidemiological study found that an increase of 10 ppb in the ambient ozone concentration of the previous week was associated with a 0.52% increase in mortality (Bell et al., 2004). Ozone is a strong oxidant, and some products of ozone-initiated indoor chemistry may be more harmful than ozone itself (Weschler, 2004).

Indoor ozone concentrations track those outdoors, with only a minimal lag in time (Sabersky et al., 1973). Indoor peak concentrations of 30–100 ppb are not uncommon in areas with high ambient concentrations, and measured indoor-to-outdoor (I/O) ratios range from 0.05 for tightly sealed buildings or those with activated carbon filtration to 0.85 for buildings with high air exchange rates (Weschler, 2000 and references therein). Naturally ventilated buildings typically have larger I/O ozone ratios than those with forced-air HVAC systems. Weschler (2006) summarized six studies on ozone exposure and estimated that indoor exposures are 43–76% of total daily ozone exposure, with an average of just below 60%. Sources of ozone in indoor air include ventilation air (Sabersky et al., 1973), devices such as photocopiers, laser printers, and ozone and ion generators (Lee et al., 2001; Mullen et al., 2005; Niu et al., 2005a; Tung et al., 2005; Britigan et al., 2006; Destaillats et al., 2008). Loss mechanisms of ozone from indoor air are air exchange, surface reactions (e.g. Sabersky et al., 1973; Morrison and Nazaroff,

2000, 2002; Reiss et al., 1995), and gas-phase reactions (e.g. Weschler and Shields, 1996; Weschler, 2000; Fan et al., 1993).

Sabersky et al. (1973) first reported that the primary loss mechanism of ozone in buildings involved heterogeneous surface reactions. The removal rate of ozone to a surface is often cast as $v_d \cdot A/V$ (h^{-1}), where v_d (m/h) is the deposition velocity of ozone to a surface, A (m^2) is the nominal surface area, and V (m^3) is the volume of air. The term $v_d \cdot A/V$ for all surfaces in an entire building is often referred to as β_{O3} (h^{-1}), and it has been measured for many buildings, ranging from 2.5–4.3 h^{-1} for offices and laboratories, 2.9–7.2 h^{-1} for residences (Weschler, 2000 and references therein), and 2.8 ± 1.3 h^{-1} for 43 homes in Southern California (Lee et al., 1999).

The deposition velocity of ozone to a surface, v_d (m/h), is a mass transfer coefficient and is defined as the ratio of the mass flux to a surface, J ($\mu g/m^2 \cdot h$), to the indoor ozone mass concentration, C_{O3} ($\mu g/m^3$). The deposition velocity depends on both the rate of transport through the concentration boundary layer and the rate of reaction with the surface (Cano-Ruiz et al., 1993; Reiss et al., 1994). Typical deposition velocities for ozone indoors approximately range from 0.0005 cm/s for plate glass or lacquered ash to 0.1 cm/s for carpet (Wang and Morrison, 2006) to 1.2 cm/s for bricks (Cano-Ruiz et al., 1993). The ozone surface reactivity of an indoor material can be parameterized by the reaction probability, γ (-), which is the ratio of the ozone removal rate to ozone collision rate (Cano-Ruiz et al., 1993). Measured reaction probabilities for ozone with different indoor surfaces range from 10^{-8}–10^{-7} for glass to 10^{-4} for bricks and carpet (e.g. Cano-Ruiz et al., 1993; Reiss et al., 1994; Morrison and Nazaroff, 2000).

The ozone reactions on interior building surfaces emit volatile organic compounds (VOCs) into the indoor air. These secondary emissions of VOCs are well-documented, and secondary emissions, particularly of carbonyls, result from ozone surface reactions with interior materials such as latex paints (Reiss et al., 1995), carpet (Weschler et al., 1992; Morrison and Nazaroff, 2002; Wang and Morrison, 2006), kitchen floors and countertops (Wang and Morrison, 2006), and HVAC components (Morrison et al., 1998). The carbonyl byproducts are due to ozone reactions with unsaturated organic compounds

that coat the surfaces, and in these studies, formaldehyde and nonanal are the most commonly identified products. Yields are high enough to affect pollutant concentrations in typical indoor environments (Reiss et al., 1995; Wang and Morrison, 2006).

Ozone reactions occur in heating, ventilating, and air conditioning (HVAC) systems, particularly on filters (Morrison et al., 1998; Bekö et al., 2006; Hyttinen et al., 2006; Zhao et al., 2007). Particles build up on the filter over its service life, and ozone is removed by the filter-cake. For example, Zhao et al. (2007) tested the steady-state ozone removal efficiency of filters and found that it ranged from 0–9% for 8 clean filters, had a mean of 10% for 8 particle-laden filters from residential environments, and had a mean of 41% for 6 particle-laden filters from commercial environments. Oxidation occurs with compounds on the filter surfaces, leading to adverse sensory impacts and likely emissions of irritating products (Bekö et al., 2006; Hyttinen et al., 2006). Moreover, Bekö et al. (2007) observed more ultrafine particles downstream of particle-laden filters relative to upstream with ozone present in an experimental system.

The air exchange rate, λ (h^{-1}) is the ratio of the flow through, Q (m^3/h), and the volume, V (m^3), of the space. The relative impacts of building surface removal and air exchange on the ozone removal rate may be directly compared. For example, the surface removal rate reported in Lee et al. (1999) of 2.8 h^{-1} implies that the surface reactions are removing ozone at a rate equal to an air exchange rate of 2.8 h^{-1}, with the important difference that air exchange does not lead to the formation of byproducts. Murray and Burmaster (1995) measured air exchange rates in 2,844 households and the mean was 0.76 h^{-1} and the median was 0.5 h^{-1}. Persily (1989) measured approximately 3,000 air exchange rates in 14 office buildings, and the mean was approximately 0.9 h^{-1}. In highly occupied spaces, such as conference rooms or lecture halls, air exchange rates should approach 4-6 h^{-1} (ASHRAE, 2005). Thus, in all but the most occupied buildings, surface removal should have a larger removal effect on ozone than air exchange.

Another removal mechanism of ozone indoors is gas-phase reactions (e.g. Weschler and Shields, 1996). The relative effect of this loss may be compared with that due to surface reactions and air exchange with the pseudo first-order reaction rate of

ozone with a compound, k_{pseudo} (h^{-1}), which is the product of the compound concentration and the bimolecular reaction rate constant of ozone with that compound. For a gas-phase reaction of ozone with compound to influence product concentrations indoors, k_{pseudo} must be at least on the order of the air exchange rate of the indoor space (Weschler and Shields, 1996, 2000). Common examples of reactive compounds in indoor air include camphene, isoprene, d-limonene, α-pinene, and styrene. These compounds are unsaturated organics, meaning they have one or more carbon-carbon double bonds present in the molecular structure. Terpenoids have at least one carbon-carbon double bond, and they are a class of compounds with fast enough rate constants for their reactions with ozone to influence indoor environments (Atkinson et al., 1992).

2.2. Indoor terpenoid concentrations and influencing factors

Terpenoids are a class of chemical compounds primarily emitted from biogenic sources in outdoor environments (Seinfeld and Pandis, 1998). The building block of terpenoids is isoprene, C_5H_8. Monoterpenes consist of two isoprene units and thus have the molecular formula, $C_{10}H_{16}$, and a molecular weight of 136.24 g/mol. Isoprene accounts for 44% of global biogenic volatile organic emissions, and monoterpenes account for 11% (Guenther et al., 1995).

The monoterpenes of d-limonene, α-pinene, and α-terpinene are the most common of indoor terpenoids (Brown et al., 1994). Although biogenic sources produce terpenoids in large quantities (Seinfeld and Pandis, 1998), most terpenoids indoors result from indoor sources, as illustrated by their large *I*/*O* ratios. Brown et al. (1994) summarized fifty studies conducted in over 1,200 buildings between 1978 and 1990 and reported *I*/*O* ratios of 23 for α-pinene and 80 for d-limonene. Background indoor concentrations for terpenoids are typically lower than 10 ppb (Brown et al., 1994), but concentrations can exceed 100 ppb from use of consumer products (Singer et al., 2006). The most common terpenoid-emitting consumer products include cleaners and air fresheners, as well as fragrances, perfumes, and colognes (e.g. Wallace et al., 1991; Weschler and Shields, 1996; Wolkoff et al., 1998; Nazaroff and Weschler, 2004; Singer et al., 2006; Corsi et al.,

2007). Odor thresholds of d-limonene and α-pinene are 440 ppb and 700 ppb, respectively (Devos et al., 1990; Mølhave et al., 2000). Odors of terpenoids are often detected as a result of the use of cleaning agents, air fresheners, and perfumes, so transient peak concentrations can exceed at least these limits.

Building materials that contain natural or engineered wood products also emit terpenoids and contribute to background concentrations. Saarela (1999) reported that plain oak emitted d-limonene and α-pinene at rates of 2 and 10 $\mu g/m^2 \cdot h$ (after 28-days), respectively, and plain pine emitted d-limonene and α-pinene at rates of 10 and 17 $\mu g/m^2 \cdot h$ (after 28-days), respectively. Baumann et al. (1999a) reported total terpenoid 48-hour average emission factors for different types of particle board and medium density fiberboard in the ranges of 15–284 $\mu g/m^2 \cdot h$ and 2.1–11.5 $\mu g/m^2 \cdot h$, respectively.

Since terpenoids are unsaturated and contain one or more carbon-carbon double bonds, ozone and terpenoids react readily, also yielding hydroxyl radicals (OH) that lead to secondary reaction products (Atkinson et al., 1992). Table 1 shows the structure, formula, and rate constants with ozone and the hydroxyl radical for select monoterpenes and terpene alcohols. The rate constants for gas-phase reactions between ozone and the two most common indoor monoterpenes are: d-limonene 2.0×10^{-16} $cm^3/molecules \cdot s$ ($0.018\ ppb^{-1}\ h^{-1}$) and α-pinene 8.4×10^{-17} $cm^3/molecules \cdot s$ ($0.0076\ ppb^{-1}\ h^{-1}$). These reactions can occur at fast enough rates to compete with air exchange loss indoors (Weschler and Shields, 1996). For instance, d-limonene indoors at a concentration of 28 ppb would yield $k_{pseudo} = (28\ ppb)(0.018\ ppb^{-1}\ h^{-1}) = 0.5\ h^{-1}$, which is the median air exchange rate for U.S. residences (Murray and Burmaster, 1995).

Table 1. Structure, formula, and rate constants with ozone (k_{ozone}) and the hydroxyl radical (k_{OH}) for select monoterpenes and terpene alcohols, in order of decreasing k_{ozone}. Rate constants from Atkinson and Arey (2003), except k_{ozone} and k_{OH} for α-terpineol (Wells, 2005) and k_{ozone} for linalool (Grosjean and Grosjean, 1998).

Compound	Structure	Formula	k_{ozone} (cm^3/molecule·s)	k_{OH} (cm^3/molecule·s)
α-terpinene	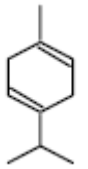	$C_{10}H_{16}$	2.1×10^{-14}	3.6×10^{-10}
terpinolene	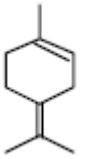	$C_{10}H_{16}$	1.9×10^{-15}	2.3×10^{-10}
linalool	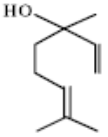	$C_{10}H_{18}O$	3.2×10^{-16}	1.6×10^{-10}
α-terpineol	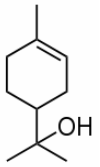	$C_{10}H_{18}O$	3.0×10^{-16}	1.9×10^{-10}
d-limonene	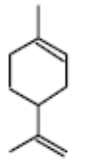	$C_{10}H_{16}$	2.0×10^{-16}	1.7×10^{-10}
α-pinene	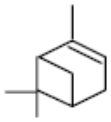	$C_{10}H_{16}$	8.4×10^{-17}	5.3×10^{-11}
Δ^3-carene	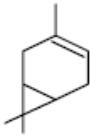	$C_{10}H_{16}$	3.7×10^{-17}	8.7×10^{-11}
β-pinene	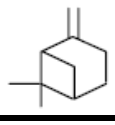	$C_{10}H_{16}$	1.5×10^{-17}	7.7×10^{-11}

Terpenoids also adsorb to interior surfaces from the gas-phase (Won et al., 2001; Singer et al., 2004), and they are also applied directly to surfaces in the form of cleaning products (Singer et al., 2006). Ozone can react heterogeneously with terpenoids adsorbed onto surfaces. Fick et al. (2005) studied ozonolysis of three monoterpenes in a test HVAC system. When the system surface area was doubled from 14.8 to 29.5 m^2, the reacted amount of Δ^3-carene increased by 2.8 (independent of ozone and reaction time), d-limonene by 2.3, and α-pinene by a statistically insignificant amount. Flemmer et al. (2007) continuously delivered 100 ppb of ozone-laden air for 72 hours to a vinyl tile surface onto which α-terpineol was applied before the experiment began, and the yield of one reaction product increased over 72 hours and the yield of another spiked after 36 hours and then decayed. Springs and Morrison (2008) observed that reaction probabilities for ozone and monoterpenes adsorbed to surfaces were 10 to 100 times more probable than gas-phase values. For model surfaces, reaction probabilities for Δ^3-carene ranged from 2.9×10^{-6} to 3.0×10^{-5} and d-limonene ranged from 2.8×10^{-5} to 3.0×10^{-4}.

2.3. Indoor SOA formation due to ozone/terpenoid reactions

Reactions between ozone and terpenoids produce some oxygenated organic compounds that have higher molecular weight, increased polarity, and reduced vapor pressure with respect to the reactant compounds (Kamens et al., 1999; Leungsakul et al., 2005). These products, which are primarily carbonyls and carboxylic acids, partition between the gas-, surface-, and particle-phases to yield secondary organic aerosol (SOA) in the ultrafine (< 0.1 μm diameter) and fine (0.1–2.5 μm diameter) particle ranges. SOA formation occurs through product nucleation or partitioning of products onto seed or already-nucleated SOA particles, and the relative influence of each depends largely on the initial particle concentrations (Sarwar et al., 2003).

Researchers have measured SOA formation from ozone reactions with both single terpenoids and consumer products, in both laboratory settings and indoor environments (Weschler and Shields, 1999, 2003; Wainman et al., 2000; Rohr et al., 2003; Sarwar et al., 2003, 2004; Hubbard et al., 2005; Sarwar and Corsi, 2007; Vartiainen et al., 2006;

Destaillats et al., 2006; Singer et al., 2006a; Alshawa et al., 2007; Zuraimi et al., 2007; Coleman et al., 2008; Langer et al., 2008).

Weschler and Shields (1999) first documented this effect indoors and separately introduced d-limonene, α-terpinene, and an α-pinene-based cleaner into two identical, unoccupied offices, with one office having ozone concentrations elevated to between 230 and 330 ppb with a dedicated ozone generator. SOA formation occurred for each combination, and the greatest was with d-limonene, which had 20 times the number of particles in the 0.1–0.2 μm diameter size range over the background. Also, elevated d-limonene concentrations in one office with ozone only due to outdoor-to-indoor transport yielded SOA formation, with number concentrations of 0.1–0.2 μm particles as much as 10 times greater than levels measured in the office without supplemental d-limonene.

Wainman et al. (2000) used a nested chamber system to observe SOA formation due to ozone and d-limonene (pure and consumer product) reactions. Measurable particle formation occurred almost solely in the 0.1–0.3 μm range, with the bulk of formation in the 0.1–0.2 μm range. Long et al. (2000) noted particle number concentrations 7–10 times relative to background in five of six sampling events when a pine oil-based cleaner was used to mop floors and clean toilets in Boston homes and concentrations of indoor ozone were solely due to outdoor-to-indoor transport. Rohr et al. (2003) noted significant steady-state particle growth in systems with ozone in combination with d-limonene and α-pinene, and non-reproducible steady-state growth for ozone and isoprene reactions. Sarwar et al. (2003) observed SOA formation in an 11 m^3 stainless-steel chamber due to reactions between ozone and α-pinene, as well as used the ICEM (Indoor Chemistry and Exposure Model) to predict SOA mass concentration based on detailed homogeneous chemistry and partitioning of semi-volatile products to particles. Sarwar and Corsi (2007) did the same for ozone and d-limonene reactions.

A group of researchers examined the resulting secondary pollutants from ozone reactions with a set of common consumer products, both in 50 m^3 chamber simulating transient use in a residential space (Singer et al., 2006a) and at steady-state conditions in a bench-scale 198 L Teflon-lined reaction chamber (Destaillats et al., 2006; Coleman et

al., 2008). With ozone initially present in the room at 60 ppb before consumer product use, Singer et al. (2006a) reported mean maximum $PM_{1.1}$ concentrations of 280 $\mu g/m^3$ with use of an orange oil degreaser, 134 $\mu g/m^3$ with a pine-oil cleaner, and 5.45 $\mu g/m^3$ with a liquid plug-in air freshener. For the bench-scale chamber with steady-state ozone concentrations of 0–25 ppb and total terpenoid concentrations of 439–658 ppb, Coleman et al. (2008) reported mean steady-state $PM_{1.1}$ concentrations of 189 $\mu g/m^3$ for the same orange oil degreaser, 120 $\mu g/m^3$ for the same pine-oil cleaner, and 52.7 $\mu g/m^3$ for the same liquid plug-in air freshener.

The effects of the following environmental parameters on indoor SOA formation have also been explored: air exchange rate, recirculation rate, ambient temperature, relative humidity (RH), and presence of nitrogen dioxide (NO_2). Particle concentrations were monitored after ozone and d-limonene were combined in an office with varying air exchange rates, and maximum SOA formation occurred at the low of 1.6 h^{-1} and no detectable formation at over 12 h^{-1} (Weschler and Shields, 2003). Higher recirculation rates lead to lower SOA formation, due to the increased deposition of ozone and particles (Zuraimi et al., 2007). The mass of SOA formed increases as temperature decreases (Leungsakul et al., 2005; Sarwar et al. 2003; Sarwar and Corsi, 2007), due to increased gas-to-particle partitioning. Decreasing RH for d-limonene/ozone reactions increases mass of SOA formed. As RH decreases, the water available for reactions becomes limited, and some products of the ozone and d-limonene reaction (stabilized Criegee intermediates) that can react with water instead react with other products of the ozone and d-limonene reactions (aldehydes) to form less volatile compounds, slightly increasing total SOA mass formed (Leungsakul et al., 2005). Finally, the presence of NO_2 reduces the magnitude of SOA due to reactions between ozone and terpenoids because it provides an additional loss mechanism for ozone (Nøjgaard et al., 2006).

2.4. Ion generator particle removal and ozone emission

Ionizers are air cleaning devices that charge particles with a corona so that they deposit on oppositely charged collector plates and/or building surfaces. One type of ionizer commonly used in residences is a portable ion generator, which has collector plates but no fan. Ion generators move small volumetric flows of air due to the opposite charges of the particles and collector plates. Another type of ionizer, an electrostatic precipitator (ESP), also has collector plates but moves air with a fan. Because of the fan, an ESP tends to have a much higher flow rate than an ion generator. Due to the corona, ionizers produce ozone as a byproduct of operation. The California Air Resources Board (2007) reports that 14% of California households own an air cleaner, and 10% own an air cleaner that produces ozone intentionally or as a byproduct. Figure 1 shows a schematic of the principle of ion generator operation.

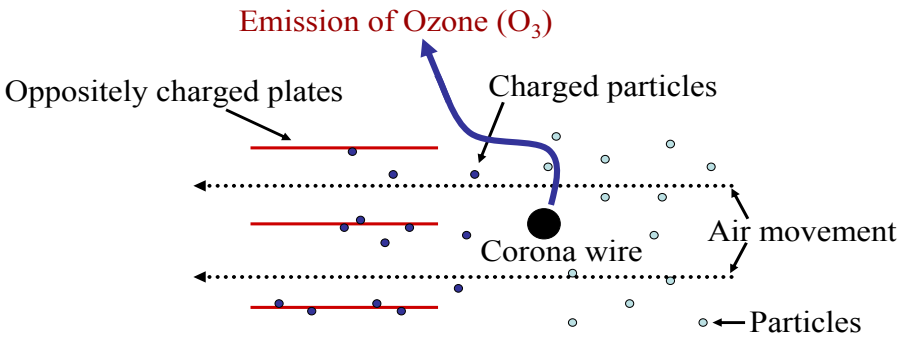

Figure 1. Schematic of the principle of operation of an ion generator.

The ability of an air cleaner to effectively remove particles is best quantified with the clean air delivery rate, or CADR (m^3/h). The CADR is the effective volumetric flow rate of clean (i.e., particle-free) air delivered by the air cleaner. The CADR is a function of particle diameter, and it is the best available metric to compare portable air cleaners because it takes into account (and is the product of) the flow rate through the air cleaner and the particle removal efficiency (Shaughnessy et al., 1994; Offermann et al., 1985; Shaughnessy and Sextro, 2006). Typical measured CADRs for particles associated with environmental tobacco smoke (ETS) range from 277–407 m^3/h for High Efficiency

Particulate Air (HEPA) air cleaners, 197–499 m^3/h for electrostatic precipitators, and 2–51 m^3/h for ion generators (Offermann et al., 1985; Shaughnessy et al., 1994). Most reported CADRs are not size-resolved and were determined with fine (0.1–2.5 μm diameter) or larger particles, rather than the ultrafine (< 0.1 μm) particle size range.

Measured ozone emission rates from portable ion generators range from 0.056–2.8 mg/h (Niu et al., 2005a), 0.23–2.1 mg/h (Tung et al., 2005), 0.74–4.0 mg/h (Mullen et al., 2005), and 0.16–2.2 mg/h (Britigan et al., 2006). In typical indoor environments with a significant terpenoid source (such as an air freshener or cleaning event), an ozone emission rate of this magnitude might lead to increases in ultrafine and fine particles due to SOA formation. It follows that if an ion generator had a low CADR for ultrafine and fine particles, it might operate as a net particle emission source, rather than a removal device, in certain size ranges. For instance, Alshawa et al. (2007) showed that injections of 15 and 45 mg of d-limonene into an office with an energized ion generator each led to a transient elevation in ultrafine SOA concentrations.

3. SPECIFIC RESEARCH OBJECTIVES

The literature review identified the major parameters affecting the formation of secondary organic aerosol (SOA) due to ozone/terpenoid reactions in indoor settings. In the literature, the major parameters that were varied and had their influence on indoor SOA formation studied can be broadly classified into these categories: the concentrations of ozone and single terpenoid or consumer products; the air exchange and recirculation rates; and the environmental parameters such as air temperature, relative humidity (RH), and NO_2 concentrations. Many opportunities for novel research still exist.

One opportunity relates to the secondary effects of particle controls on SOA concentrations, particularly on the potential negative effects of ion generators and the potential positive or negative effects of heating, ventilating, and air-conditioning (HVAC) systems. Alshawa et al. (2007) demonstrated that ion generators can lead to transient SOA formation, and others (e.g. Weschler and Shields, 1999; Hubbard et al., 2005) have shown that ozone generators operated in the presence of a terpenoid source can lead to steady-state SOA formation. Since research suggests that ion generators are poor at removing particles, and a byproduct of their use of a corona is a steady emission of ozone, ion generators could yield more SOA than they are able to remove in the presence of a terpenoid source (e.g. an air freshener), thus operating as a steady-state net producer of indoor particles. Additionally, HVAC systems are nearly ubiquitous in many regions of the U.S. These systems usually contain a filter(s) to control particles, and their components and operation can influence ozone and SOA concentrations.

Other opportunities exist for research of a more fundamental nature. For instance, there has been limited research into SOA formation from ozone reactions with mixtures of pure terpenoids, and instead research has focused on ozone reactions with single terpenoids or consumer products. Investigations with terpenoid mixtures are important because they help demonstrate the SOA formation differences that might occur from reactions with single terpenoids versus consumer products. Also, terpenoids are known to adsorb to indoor surfaces in buildings. However, the possibility that products of ozone

heterogeneous reactions with terpenoids adsorbed to buildings surfaces can contribute to indoor SOA formation has been given almost no attention.

Correspondingly, this dissertation investigates these research opportunities with objectives that fall into one of the two general categories outlined above, which are:

(i) Exploration of the primary and secondary impacts of particle controls on indoor SOA formation (the research in Appendices A–C), and

(ii) Investigation of two fundamental aspects of SOA formation indoors (the research in Appendices D and E).

For category (i), three different investigations were undertaken, with the objective of answering these three sets of questions:

(A) How effective are ion generators at removing particles in the size ranges typical of SOA? Can these devices operate as steady-state net particle producers in a laboratory chamber in the presence of a terpenoid source?

(B) Can ion generators operate as steady-state net particle producers in a real environment with a terpenoid source?

(C) What influence do HVAC systems have on SOA formation? What are the most effective HVAC strategies to reduce the total amount of SOA formation?

For category (ii), two different investigations were undertaken, with the objective of answering these two sets of questions:

(D) What are the differences in SOA number and mass formation from ozone reactions with single terpenoids versus mixtures of terpenoids? Are SOA mass yields from single terpenoids additive in a mixed-terpenoid environment?

(E) Do reactions between ozone and surface-adsorbed terpenoids contribute to gas-phase SOA formation? What factors determine if reactions on a surface will contribute to SOA formation?

The two categories and specific research objectives within are summarized in Figure 2. Objectives A and B together constitute a thorough study on the effects of operating an ion generator on SOA formation. As will be elaborated on in Chapter 4, the impetus for undertaking Objective E was an observation made during the study for Objective B.

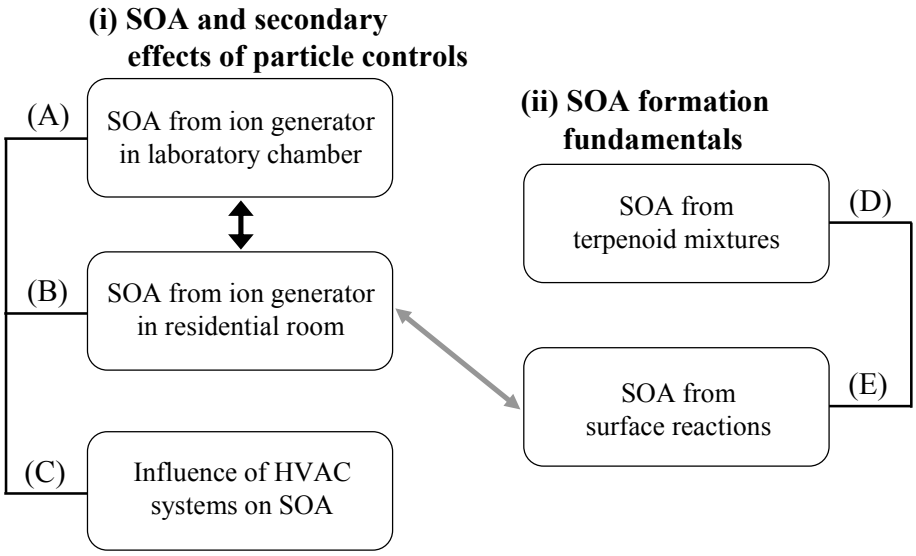

Figure 2. Summary of the two categories of research and the specific research objectives in this dissertation that focuses on indoor SOA formation.

The complete results of these five research objectives are presented in the five articles in Appendices A–E. Objective A is fulfilled by the article in Appendix A: "Ultrafine particle removal and generation by portable air cleaners" (published in *Atmospheric Environment* in 2008). Objective B is fulfilled by the article in Appendix B: "The effect of an ion generator on indoor air quality in a residential room" (submitted to *Environmental Science and Technology*). Objective C is fulfilled by the article in Appendix C: "The influence of HVAC systems on indoor secondary organic aerosol formation" (accepted to *ASHRAE Transactions*). Objective D is fulfilled by the article in Appendix D: "Secondary organic aerosol formation from ozone reactions with single terpenoids and mixtures of d-limonene, α-pinene, and α-terpineol" (in preparation for *Atmospheric Environment*). Finally, Objective E is fulfilled by the article in Appendix E: "The influence of surface reactions between ozone and d-limonene on secondary organic aerosol formation" (in preparation for *Environmental Science and Technology*).

4. DISCUSSION OF MAJOR RESEARCH FINDINGS

This chapter provides a summary of the studies exploring the formation of secondary organic aerosol (SOA) that fulfill objectives A–E, outlined in the previous chapter. This chapter is divided into five different sections, with one section per objective: (4.1) Quantification of size-resolved particle removal, ozone emission, and SOA generation by ion generators in a chamber; (4.2) The effect of an ion generator on SOA formation in a residential room; (4.3) The influence of HVAC systems on SOA formation; (4.4) SOA formation from ozone reactions with single terpenoids and mixtures of d-limonene, α-pinene, and α-terpineol; and (4.5) The influence on SOA formation of heterogeneous reactions on building surfaces between ozone and d-limonene. The study methodology is also briefly outlined in each section. The five journal articles in Appendices A–E have complete methodologies and results.

4.1. Quantification of size-resolved particle removal, ozone emission, and SOA generation by ion generators in a chamber

This section summarizes the experimental methods and results for the research presented in full in the article in Appendix A, which had the main purposes of: (1) to characterize the ozone emissions and size-resolved particle removal in the size range of SOA, and (2) to screen multiple ion generators and determine whether they act as steady-state net particle producers in the presence of a terpenoid source in a laboratory chamber.

For the first main purpose, five different portable air cleaners were characterized. This research investigated two ion generators (IG 1 and 2), one electrostatic precipitator (ESP), and two high-efficiency particulate air (HEPA) air cleaners (HEPA 1 and 2). The HEPA air cleaners were studied to provide a point of reference from which to evaluate the ion generators and the ESP. HEPA air cleaners operate by using a fan to push the air through a porous-media HEPA filter, which by definition filters 99.97% of particles 0.3 μm in diameter. These air cleaners are shown in Figure 3 in the test chamber. The full study determined the power draw, airflow rate, size-resolved (12.6–514 nm diameter)

clean air delivery rate (CADR) and single pass efficiency, and ozone emission rate for the air cleaners. For brevity, only the ozone emission and CADR results are presented here.

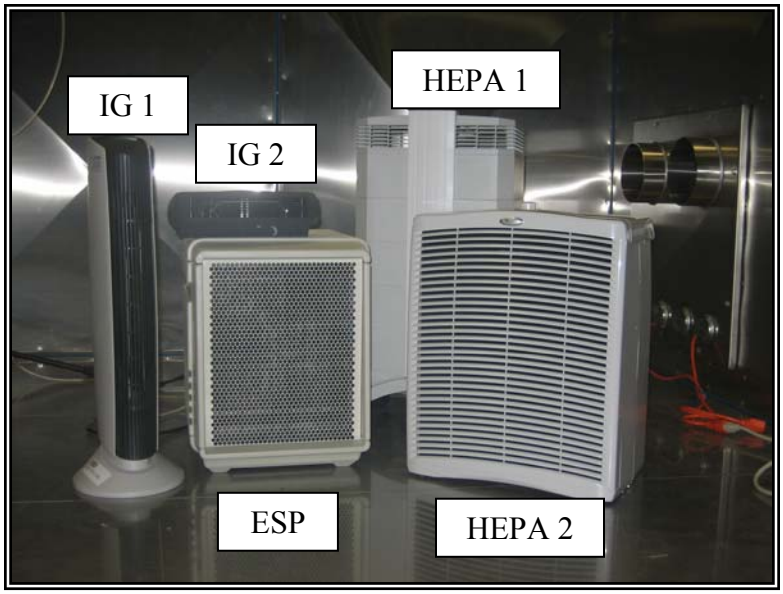

Figure 3. The five portable air cleaners tested for the first main purpose of objective A.

The ozone emission rates for the IG 1 and 2 and the ESP were determined by energizing the air cleaner in a stainless-steel 14.75 m^3 chamber, for which the inlet air was cleaned of incoming ozone with an activated carbon filter. Ozone concentrations were measured in one-minute averages, and once a steady-state was reached, the air cleaner was switched off, and the ozone decay with time was measured. Then a mass balance was used to determine the ozone emission rate, using the decay period to determine the deposition loss of ozone to the chamber surfaces, following the work of Niu et al. (2001a). Measured ozone emission rates for IG 1 were 3.3 ± 0.2 mg/h, IG 2 were 4.3 ± 0.2 mg/h, and the ESP were 3.8 ± 0.2 mg/h.

Ozone emission rates on this order can significantly affect indoor ozone concentrations. In a well-mixed 50 m^3 hypothetical space with an air exchange rate of 0.5 h^{-1} and a total ozone surface loss rate (β_{O3}) of 4.0 h^{-1}, an experimentally determined

value for offices and bedrooms (Weschler, 2000), predicted ozone concentration increases due to IG 1 are 7.5 ppb and due to IG 2 are 9.7 ppb.

The CADR (m^3/h) is the product of the airflow through the air cleaner (m^3/h) and the single-pass removal efficiency of the air cleaner (-). It was calculated by applying a mass balance to the 14.75 m^3 stainless-steel chamber and subtracting the background decay of particles, k_n (h^{-1}), from the decay when the air cleaner was energized, k_{ac} (h^{-1}): $CADR = V(k_{ac} - k_n)$ where V is the volume of the chamber (m^3) (Shaughnessy et al., 1994). The CADR is a function of particle diameter, and the size-resolved CADRs for the five tested portable air cleaners are displayed in Figure 4.

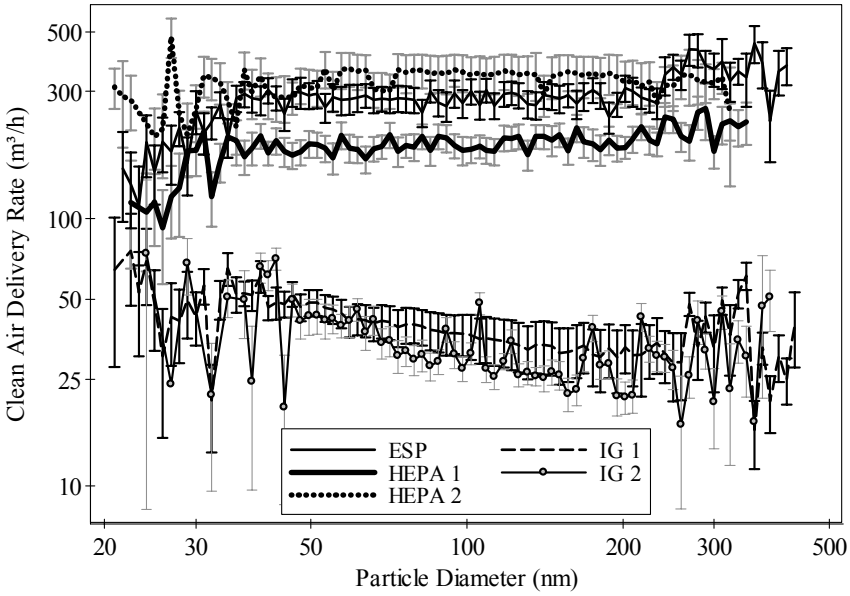

Figure 4. CADR as a function of particle diameter, with both axes plotted on log-scales. The whiskers represent the calculated uncertainty of the CADR for each size bin.

The two tested ion generators (IG 1 and 2 on the plot) both generally exhibited a CADR an order of magnitude lower than the other tested air cleaners. IG 1 had an average CADR (s.d.) of 41 (11) m^3/h, and IG 2 had 35 (13) m^3/h. HEPA 2 exhibited the largest average CADR of 324 (44) m^3/h. To effectively clean an indoor space, an air cleaner should have a CADR that is higher than the airflow through the space. Thus, for the hypothetical 50 m^3 space with an air exchange rate of 0.5 h^{-1}, the airflow through the

space is (50 m^3 × 0.5 h^{-1}) = 25 m^3/h, and the ion generators would be much less effective than the other tested types of air cleaners.

From a practical standpoint, this research illustrated necessary modifications to the procedure for determining the CADR of ion generators. Since, the CADR test is calculated with the difference in particle loss rates without and with the air cleaner operating, any source of particles in the chamber invalidates the calculation. Because of the ozone emitted by the ion generator, care must be taken to assure that no SOA formation inadvertently occurs during the CADR test. Thus, the test chamber for the ion generator CADR tests was modified to eliminate this potential bias. Ozone and unsaturated organic compounds were removed at the chamber inlet with activated carbon filtration, and ozone emitted by the ion generator was removed with 4 m^2 of activated carbon strips hung on the chamber walls, removing the majority of the ozone.

For the second main purpose of objective A, which was to screen multiple ion generators (IG 1, 3, 4, 5a, and 5b) and determine whether they act as steady-state net particle producers in the presence of a terpenoid source in a laboratory chamber, five different ion generators from two popular manufacturers were tested. Four of the five tested ion generators are shown in Figure 5.

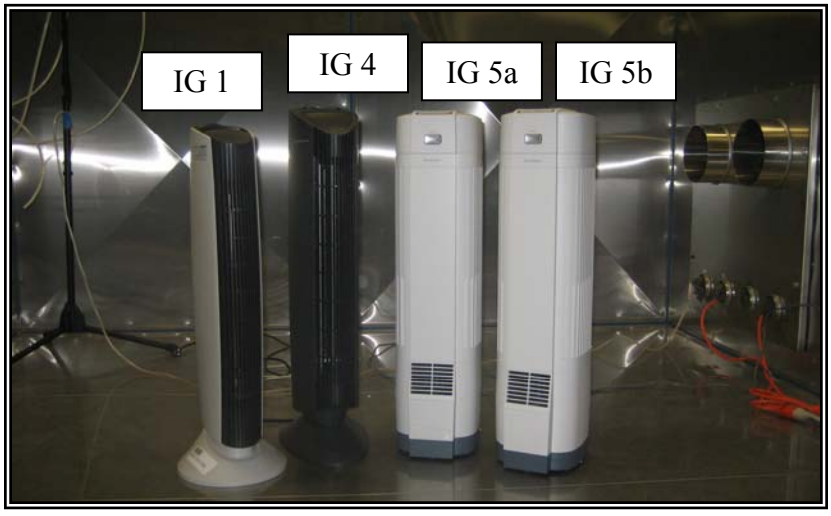

Figure 5. Four of five ion generators tested for the second main purpose of objective A.

The terpenoid source for each ion generator experiment was a different type of solid or plug-in air freshener. Ozone and size-resolved particles (4.61–157 nm diameter) were measured during 3 or 4 different test periods. The test for IG 1 had four distinct periods of testing:

- Background (BG) – no ion generator, no air freshener
- Air Cleaner (AC) only – ion generator, no air freshener
- Air Cleaner/Air Freshener (AC/AF) – ion generator, air freshener
- Air Freshener (AF) only – no ion generator, air freshener

The tests for IG 3, 4, 5A, and 5B did not include the AF period as no particle formation was seen during this phase for IG 1. Each period lasted until a steady-state condition was obtained. Size-resolved results for IG 1 are shown in Figure 6, and the total number results for all five ion generators are in Table 3 in Appendix A.

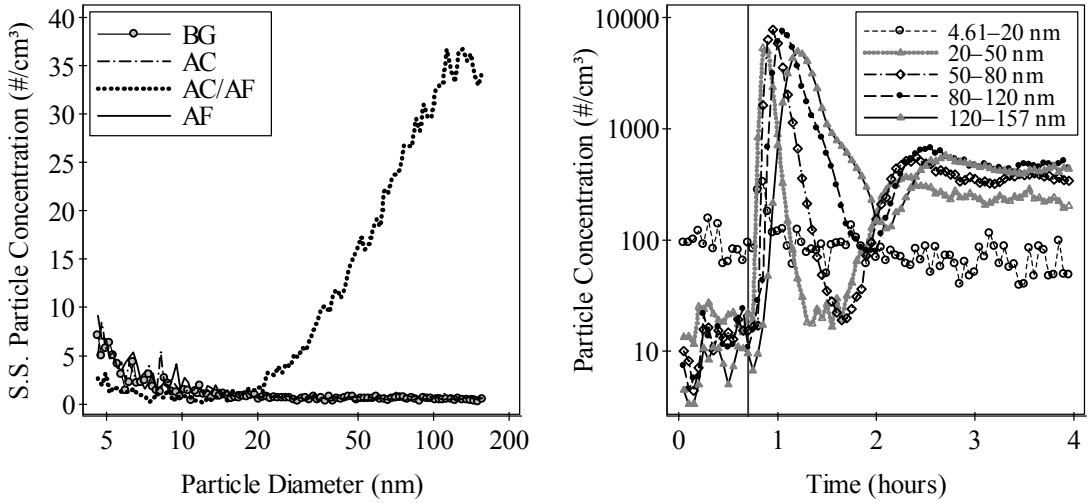

Figure 6. For IG 1, (a) steady-state particle concentrations as a function of particle diameter (x-axis on a log-scale), and (b) particle concentrations as a function of time (y-axis on a log-scale) after the plug-in liquid air freshener was energized (represented by the vertical line on the plot). BG = Background, AC = Air Cleaner only, AC/AF = Air Cleaner/Air Freshener, AF is Air Freshener only.

The steady-state results for each test period for IG 1 are in Figure 6(a), which shows that the size-resolved particle concentrations during the AC/AF period were elevated in all measured sizes over 20 nm. The time-resolved results for IG 1 are in Figure 6(b). After the air freshener was energized, particle number concentrations in the 20–50 nm size range increased on the order of 1,000 #/cm^3 and then declined before leveling off at a steady-state value. This trend was repeated in time sequentially by the remaining three size bins. The steady-state concentrations are controlled principally by the competition between the SOA formation due to ozone/terpenoid reactions and the loss of particles due to removal by the ion generator, deposition, and air exchange. Further research into the effects of ion generators on SOA concentrations is in the next section.

4.2. The effect of an ion generator on SOA formation in a residential room

This section summarizes the experimental methods and results for the research presented in full in the article in Appendix B, which had the purpose of experimentally assessing the impact of an ion generator on SOA formation and pollutant concentrations in a residential room. Determining the SOA formation due to ion generators in an actual indoor environment is necessary because of differences between real indoor settings and laboratory chambers. Real indoor environments have larger volumes and surface-to-volume ratios, as well as sources and sinks of particles, ozone, and other products of reactions between ozone and terpenoids.

Experiments were performed in a 27 m^3 unoccupied but furnished room. One HVAC duct supplied the room, and the HVAC system cycled on/off regularly from 9 a.m. to 11 p.m. (HVAC Cycle) and was switched off during each day of testing from 11 p.m. to 9 a.m. (HVAC Off). Four different room configurations were measured (RC 1–4), shown in the 2×2 matrix in Table 2. The original flooring of sealed/stained concrete was used for two configurations, and carpet with padding was installed for two others. There was no terpenoid source for two configurations, and a “Hawaiian” scented plug-in air freshener was used as a terpenoid source for two others (total emission rate = 1.5 g/day). The ion generator was IG 1 in the previous section and in Appendix A.

Table 2. Experimental matrix for the four room configurations (RC 1–4).

RC 1: Sealed/stained concrete floor, No terpenoid source	RC 2: Carpet with padding floor, No terpenoid source
RC 3: Sealed/stained concrete floor, Terpenoid source	RC 4: Carpet with padding floor, Terpenoid source

The room air for each configuration was sampled for at least one two-day period without an ion generator operating and at least one two-day period with an ion generator operating on its highest setting. Measurements included airborne sampling of size-resolved particulate matter (0.015–20 μm), terpenoids and C_1–C_4 and C_6–C_{10} aldehydes, ozone concentrations, and air exchange rates.

Twelve two-day-long tests were completed, with four of the twelve tests as experimental replicates. Two air exchange rates were measured, the rate during the HVAC Cycle period (λ_{cycle}) and the rate during the HVAC Off period (λ_{off}). At least one type of air exchange rate was measured for each two-day test. For all tests, the mean (s.d.) for λ_{cycle} was 1.3 (0.3) h^{-1} and for λ_{off} was 0.5 (0.1) h^{-1}. The air freshener effectively functioned as an experimental terpenoid source, and the predominate terpenoid emitted was d-limonene. Mean (s.d.) d-limonene concentrations without and with an ion generator, respectively, for RC 1 were 10 (9.1) ppb and 8.7 (8.1) ppb, for RC 2 were 2.6 (0.56) ppb and 6.7 (3.7) ppb, for RC 3 were 53 (10) ppb and 39 (4.4) ppb, and for RC 4 were 46 (5.4) ppb and 38 (3.3) ppb. Figure 7 displays a sample of the continuous particle and ozone concentrations measured for two different one-day tests.

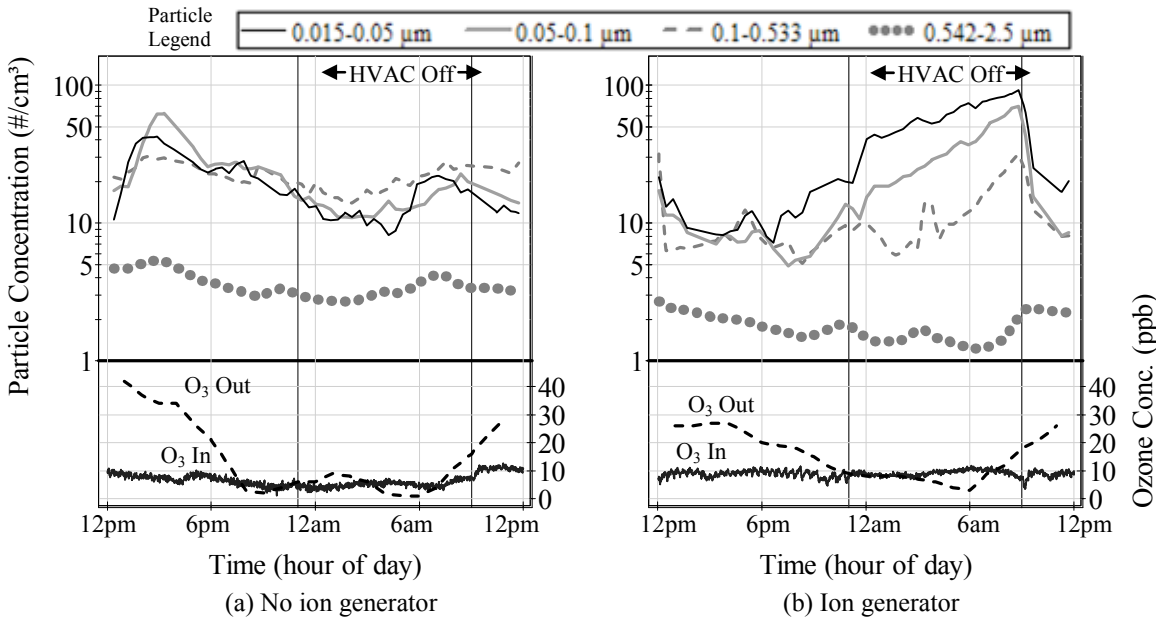

Figure 7. Typical indoor particle number and indoor and outdoor ozone concentrations versus time in a 27 m^3 test room, (a) without and (b) with an ozone-emitting ion generator operating (ozone emission rate = 3.3 ± 0.2 mg/h). The test room door was closed, and the room had a sealed/stained concrete floor and an air freshener present. The HVAC system cycled on/off from 9 a.m. to 11 p.m. and was off from 11 p.m. to 9 a.m. Mean air exchange rates for the HVAC Cycle period and HVAC Off period were approximately 1.3 and 0.4 h^{-1}, respectively.

These results represent typical days of testing in RC 3, which had sealed/stained concrete flooring and an air freshener. In Figure 7(a), the highest particle concentrations are during the HVAC Cycle period, around 3 p.m. These higher particle concentrations occur concurrently with elevated outdoor and indoor ozone concentrations, and their source is likely both SOA formation and infiltration of outdoor particles. The lowest particle concentrations are at night during the HVAC Off period. However, Figure 7(b) shows that with the ozone-emitting ion generator present, the trend is reversed. At about 6 p.m., concentrations for particles of less than 0.1 µm began to rise. After 11 p.m. near the start of the HVAC Off period, concentrations rose more sharply and continued to climb until the end of the HVAC Off period.

The measured concentrations of d-limonene for the test in Figure 7(a) was 49 ppb and in Figure 7(b) was 36 ppb, implying that some d-limonene likely reacted with ozone emitted by the ion generator. Detectable SOA formation occurred during the HVAC Off period because the air exchange rate decreased from λ_{cycle} to λ_{off}, increasing the residence time of ozone, terpenoids, and their reaction products. After the air exchange rate decreased, the SOA formation rate was high enough relative to the total particle loss rate to yield detectable SOA formation.

Figure 8 displays a summary of the effects of operating an ozone-emitting ion generator in RC 1–4. The solid lines separate the mean results into the four different room configurations, and within those, the dashed lines separate the results into no operation (N) and operation (IG) of an ion generator. Bars in Figure 8 are mean values for particle, ozone, formaldehyde, and nonanal room concentrations, for results during the HVAC Off period. The results during the HVAC Off period are the most appropriate to compare the effect of the ion generator across the different tests and configurations, since they occurred during the time of lowest outdoor ozone concentrations, lowest air exchange rates, and least activity in the home. Also, listed on Figure 8 are the % differences of the pollutants that are associated with operating the ion generator in RC 1–4, calculated with the mean concentrations as (no ion generator – ion generator)/(no ion generator). A positive % difference indicates that the ion generator increased that particular concentration in that room configuration.

Generally, Figure 8 shows that particle number concentrations decreased with the operation of the ion generator in RC 1 and 2 but increased with the operation of the ion generator in RC 3 and 4. The majority of the particle number increase was in the ultrafine range, and the particle % increases on Figure 8 are for ultrafine particles only. The particle generation due to the ion generator operation in RC 3 and 4, with the d-limonene source, was larger in magnitude than its removal in RC 1 and 2. Particles larger than the ultrafine range either decreased or were unaffected by the ion generator.

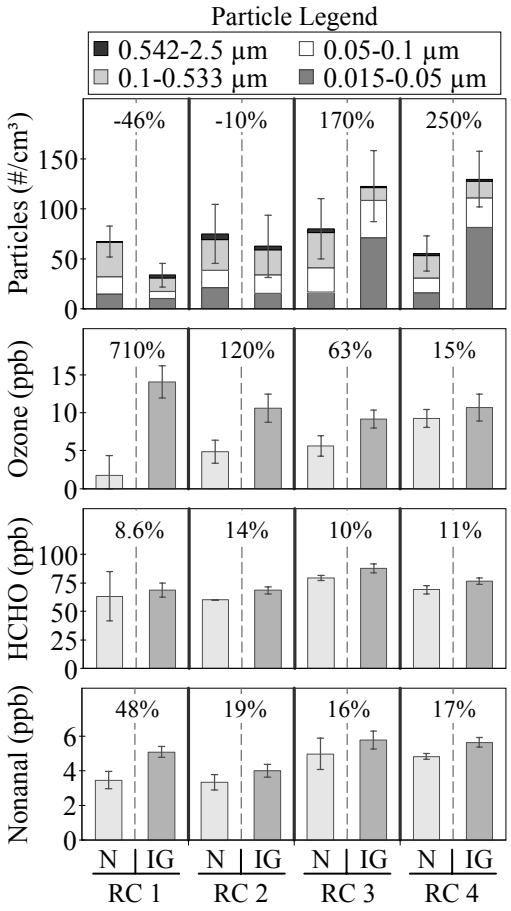

Figure 8. Summary particle, ozone, formaldehyde (HCHO), and nonanal concentrations in the four Room Configurations (RC 1–4), for tests without (N) and with (IG) an operating ion generator. Error bars represent one standard deviation from the mean. Percentages are % differences for each room configuration, and positive % differences indicate the ion generator increased concentrations.

Since the ion generator emitted ozone at a rate of 3.3 mg/h, it increased ozone concentrations in all room configurations. Ozone concentration increases were largest in RC 1, the second largest in RC 2, the third largest in RC 3, and were the smallest in RC 4. The successive decreases in the ozone concentration increases likely reflect the increasing reactivity of each room configuration with ozone. Concentrations of two aldehydes, formaldehyde and nonanal, also increased due to the operation of the ion generator in every room configuration. It was expected that aldehydes would increase in RC 1–4 since the ozone increased in RC 1–4. In RC 1 and 2, most of the increases in

aldehyde concentrations are likely due to ozone interactions with surfaces in the room since there was not a source of gas-phase unsaturated organics in the room. In RC 3 and 4, however, ozone also reacted with unsaturated organics emitted from the air freshener, likely leading to formaldehyde production as well (Singer et al., 2006a). Nonanal production is associated with ozone reactions with interior residential surfaces (Morrison and Nazaroff, 2002; Wang and Morrison, 2006).

The research presented in summary in Sections 4.1 and 4.2, as well as in full in Appendices A and B, constitute a thorough study into the effects of ion generators on indoor SOA concentrations. The work found that ion generators are capable of creating more SOA than they can remove if in the presence of an air freshener, and that they can increase concentrations of ozone, formaldehyde, and nonanal regardless of air freshener presence. Thus, their use in occupied spaces should likely be avoided.

4.3. The influence of HVAC systems on SOA formation

This section summarizes the modeling methods and results for the research presented in full in the article in Appendix C, which had the of purpose exploring the influence of HVAC systems on SOA formation. The HVAC system of a building can affect the mass of SOA formed by influencing the reactant concentrations, as well as the indoor air temperature and relative humidity (RH).

This investigation explored the influence of HVAC system design and operation on size-resolved SOA mass formation with models of typical residential (V = 392 m^3) and commercial (V = 1,000 m^3) buildings with HVAC systems. The following HVAC parameters were varied: (i) flow of ventilation and recirculation rates, (ii) filtration efficiency for particles, (iii) ozone removal due to particle loading on filters, and indoor (iv) temperature and (v) RH. Then a parametric analysis explored these HVAC system factors on SOA formation. This is the first investigation that I know of that has modeled SOA formation using size-resolved yields.

The simulations use the same building geometries and are similar to the size-resolved particle model in Waring and Siegel (2008), with the addition of gaseous

transport and emission and size-resolved SOA formation. The models assumed steady-state, well-mixed conditions, constant air density, and no indoor sources of particles other than SOA formation. These assumptions are not realistic over all indoor conditions, but this is an appropriate approach to compare the relative influence of HVAC system parameters on SOA formation. The indoor mass concentration of SOA, C_{SOA} (μg/m^3), was calculated in its steady-state form as Equation 1:

$$C_{SOA} = \left(F_T F_{RH}\right)\left(\Gamma C_{terp,m}\left(kC_{O3,m}\right)\right)\int_{d_p} \frac{Y_{g,sr}}{\beta_p + \lambda_i + \lambda_v + \lambda_r \eta_p} \mathrm{d}d_p \quad (1)$$

where F_T (-) and F_{RH} (-) are formation factors that adjust for changes in T and RH, respectively; k (ppb^{-1} h^{-1}) is the bimolecular reaction rate constant between the terpenoid and ozone; $C_{terp,m}$ (ppb) and $C_{O3,m}$ (ppb) are molar concentrations of indoor terpenoids and ozone, respectively; $Y_{g,sr}$ (μm^{-1}) is the size-resolved mass distribution yield of SOA formed by gas-phase reactions between ozone and the terpenoid, which is the ratio of the change in mass of SOA formed to the change in mass of terpenoid consumed; Γ (-) is a conversion factor to change units of ppb/h to μg/m^3·h; β_p is the size-resolved loss rate of particles, including SOA, to indoor surfaces; λ_i, λ_v, and λ_r (h^{-1}) are air exchange rates due to infiltration, ventilation, and recirculation, respectively; and η_p (-) is the size-resolved removal of particles, including SOA, by the HVAC filter. Equation 1 was integrated over a range of d_p = 0.01–10 μm. All terms in Equation 1 except k are influenced by the HVAC system and were varied in the parametric analysis. In reality, k is a function of indoor temperature and is also thus affected by the HVAC system, but the model incorporates this effect in the F_T term. All integration was performed numerically.

The varied HVAC parameters are listed in Table 3, with literature sources for the parameter values listed below. The residential flow cases considered duty (HVAC operation for one-sixth of the time) and continuous operation. The commercial flow cases considered continuous flow with 100% outdoor air (OA), 50% OA and 50% recirculated air (RA), and 10% OA and 90% RA. The PM Filtration cases used efficiency curves for new MERV <5, 6, 11, and 15 filters as well as an electrostatic

precipitator (ESP). The O_3 Filtration cases considered ozone removal, η_{O3} (-), by a new and a loaded (i.e. used) filter, assuming only the particle-laden filters removed any O_3. The ESP generates rather than removes ozone at a rate of E_{O3} = 21.6 mg/h when operating (Viner et al., 1992). Indoor temperatures were modeled as 18.3, 23.9, and 29.4 °C (65, 75, and 85 °F) and RH as 25, 50, and 75%, to account for a range conditions. Base cases were defined for each model and are in bold in Table 3.

Table 3. Varied HVAC system parameters. Base cases are listed in bold.

Parameter	Model	Case Title	Parameter Values
HVAC Flow[a]	Res.	**Duty;** Continuous	λ_i=**0.75**, λ_r=**0.67**; λ_i=0.75, λ_r=4 h^{-1}
	Comm.	100% OA; 50% OA/50% RA; **10% OA/90% RA**	λ_i=0.25, λ_r=0, λ_v=4; λ_i=0.25, λ_r=2, λ_v=2; λ_i=**0.25**, λ_r=**3.6**, λ_v=**0.4** h^{-1}
PM Filtration[b]	Res., Comm.	MERV <5; **6;** 11; 15; or ESP	η_p for MERV <5; **6**; 11; 15; ESP
O_3 Filtration[c]	Res., Comm.	New; **Loaded**	η_{O3} = 0; **10**% or η_{O3} = 0%; **41**%
Temperature[d]	Res., Comm.	18.3; **23.9**; 29.4 °C	F_T = 1.13, **0.98**, 0.83
RH[e]	Res., Comm.	25; **50**; 75%	F_{RH} = 1.02, **1.0**, 0.98

[a]Riley et al. (2002), Waring and Siegel (2008); [b]Waring and Siegel (2008), Wallace et al. (2004); [c]Zhao et al (2007); [d]Leungsakul et al. (2005), Sarwar and Corsi (2007); [e]Leungsakul et al. (2005).

The remaining parameters in Equation 1 are related directly to the reactants, and $C_{terp,m}$ and $C_{O3,m}$ were calculated for each modeled scenario in a manner similar to that of Equation 1. $C_{terp,m}$ was the result of a constant indoor emission of mopping with a pine-oil cleaner. For reactions with ozone, k = 0.05 ppb^{-1} h^{-1} and $Y_{g,sr}$ = 0.197 with unimodal lognormal distribution parameters of GM = 0.37 μm and GSD = 1.52 (Singer et al., 2006b; Coleman et al., 2008). $C_{O3,m}$ was modeled as due to outdoor-to-indoor transport and potential indoor emission from the ESP, in both an urban and rural setting with outdoor concentrations of 100 and 25 ppb, respectively. C_{seed} (μg/m^3), the indoor

concentration of seed particles (i.e., not SOA), is also calculated similarly to Equation 1, with urban and rural outdoor particle distributions as in Waring and Siegel (2008).

The complete methodology and parameter choices are shown in the Methodology in Appendix C. Also, the full article in Appendix C models scenarios in both a rural and an urban environment, but this Research Summary presents only the urban results. For the urban results presented in this chapter, the residential model had 162 unique scenarios and the commercial model had 243 unique scenarios.

SOA formation and other size-resolved parameters are log-normally distributed, so the median is used as a descriptive statistic. The median over 162 residential scenarios for C_{SOA} is 68.0 μg/m^3 (range of 14.7–108 μg/m^3) and over 243 commercial scenarios is 44.8 μg/m^3 (range of 11.6–105 μg/m^3). The base case C_{SOA} for the residential model is 90.9 μg/m^3 and the commercial model is 62.9 μg/m^3. These ranges are of the same order as reported in other studies (e.g. Weschler and Shields, 1999; Hubbard et al., 2005). Figure 9 shows the size-resolved distributions of SOA for these base cases, as well as the outdoor and indoor seed particle, SOA, and total particle distributions.

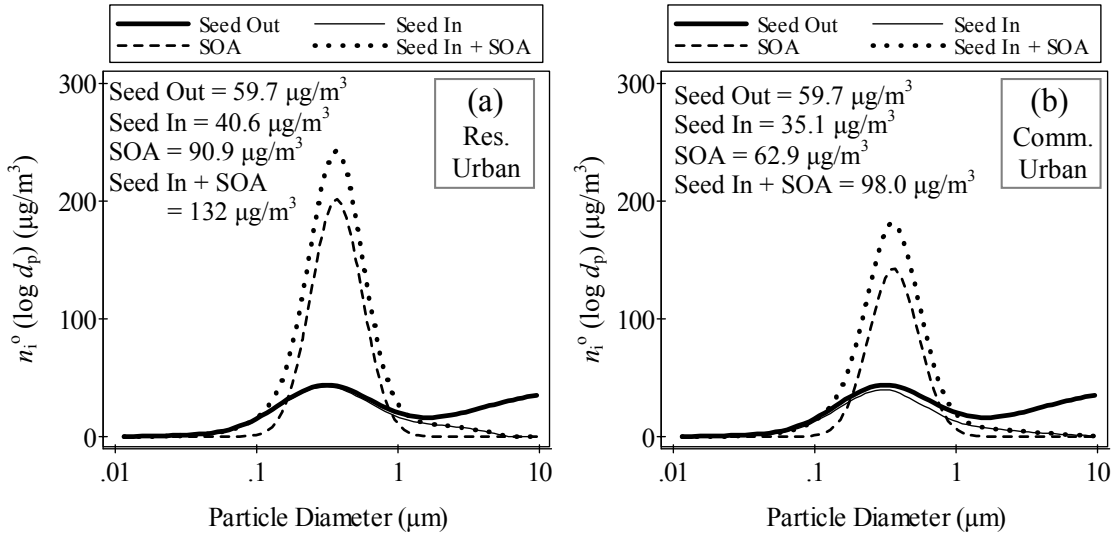

Figure 9. Outdoor and indoor seed (C_{seed}), SOA (C_{SOA}), and Seed + SOA particle distributions for urban (a) residential and (b) commercial base cases.

Parametric influence was determined with the SOA Change Ratio (SCR), listed in Table 4. The SCR = (adjusted SOA mass formed)/(base case SOA mass formed), and the adjusted SOA mass formed is the result of holding all parameters in the base case constant except for the varied parameter. Thus, the SCR is a measure of how sensitive SOA formation is to a change of a given parameter, relative to the base case. Non-influential parameters have SCRs at or near unity. Cases with less SOA formation have SCRs less than unity, and cases with more SOA formation have SCRs greater than unity.

Table 4. SOA Change Ratios for the Urban residential and commercial models.

				SOA Change Ratio (SCR)	
Parameter	Model	Base Case	Going To	Residential	Commercial
HVAC Flow	Res.	Duty	Continuous	0.86	
	Comm.	10% OA/90% RA	50% OA/50% RA		0.51
			100% OA		0.71
PM Filtration	Res., Comm.	MERV 6	MERV <5	1.01	1.04
			MERV 11	0.80	0.44
			MERV 15	0.62	0.22
			ESP	0.85	0.68
O_3 Filtration	Res., Comm.	Loaded	New	1.00	1.37
Temperature	Res., Comm.	23.9 °C	18.3 °C	1.15	1.15
			29.4 °C	0.84	0.84
RH	Res., Comm.	50%	25%	1.02	1.02
			75%	0.98	0.98

The most influential HVAC parameters are in the Flow, PM Filtration, and Temperature cases for the residential and commercial models, as well as O_3 Filtration for the commercial model. In the residential model, going from the Duty to the Continuous case decreases the SOA formed since continuous air flow causes the HVAC filter to remove more ozone, seed particles, and SOA. Changing to different HVAC Flow cases in the commercial model has an even larger relative effect, since airflow is always continuous with an air exchange rate through the HVAC system of 4 h^{-1}. Pollutant

concentrations of indoor origin, C_{SOA} and $C_{terp,m}$, decrease as the fraction of outdoor air increases, though $C_{O3,m}$ increases as more outdoor air is introduced.

SOA concentrations generally increase with lower efficiency filters and decrease with higher efficiency filters. An increase in filter efficiency has a larger relative effect within the commercial than the residential model due to the continuous flow and larger volumetric flow rates through the HVAC filter. In the residential model, the O_3 Filtration had little effect on the SCR since there was an η_{O3} of 10% and the HVAC system operated on a duty cycle. However, the commercial model exhibited a large SCR since it had an η_{O3} of 41% within a continuous flow case with 90% of its volumetric flow recirculated. The Temperature and RH cases affect the total mass of SOA formed with F_T and F_{RH} in Equation 1, and their SCRs equal the change caused by the factors.

More nuanced trends in the SOA formation can be determined by examining summary results from a size-resolved perspective, also within the context of parametric influence on C_{SOA}. These results are presented in the full article in Appendix C.

4.4. SOA formation from ozone reactions with single terpenoids and mixtures of d-limonene, α-pinene, and α-terpineol

This section summarizes the experimental methods and results for the research presented in full in the article in Appendix D, which explored the SOA formation due to reactions of ozone with single terpenoids and mixtures of pure terpenoids. Studies with terpenoid mixtures are important because they help bridge the gap between studies with single terpenoids and with consumer products. Concentrations of d-limonene, α-pinene, and α-terpineol were combined in different mixtures, at both low and high ozone initial concentrations, and the resulting SOA number and mass concentrations were analyzed.

Two phases of experiments were performed in a 90 L Teflon-film reaction chamber that was operated as a batch reactor with a flexible volume that decreased as samples were withdrawn. In Phase I, known amounts of a single terpenoid or a mixture of terpenoids were introduced with diluent air into the chamber. Once the chamber was filled, it was then connected to a size-resolved (10–500 nm) particle counter. After one

count (2 min), a known amount of ozone was introduced into the chamber and 24 more particle counts were taken (48 min), for a total time of 50 min. In Phase II, SOA mass yields (Y_g = mass SOA formed/mass terpenoids reacted) for ozone reactions with single terpenoids were determined. Then results from Phase II were applied to results from Phase I to explore whether SOA mass yields from single terpenoids can predict total SOA yields in a mixed terpenoid environment.

There were 13 experiments for Phase I, which measured the time- and size-resolved formation of SOA due to ozone reactions with single terpenoids and mixtures of pure terpenoids. Initial concentrations in Phase I were chosen to yield initial pseudo first-order reaction rates of terpenoids with ozone, $k_{pseudo,i}$, that were either equivalent or integer-factors of each other. Mixture experiments with equivalent $k_{pseudo,i}$ eliminates an initial bias of ozone reacting preferentially with one terpenoid over another. The experimental initial terpenoid reactant concentrations, [$terp_i$] (ppb), are referred to as [d-lim_i] for d-limonene, [α-pin_i] for α-pinene, and [α-$terp_i$] for α-terpineol. Experiments 1–9 were conducted with [$terp_i$] of between 50 and 118 ppb, depending on the terpenoid, and initial ozone concentrations, [$O_{3,i}$] (ppb), of 25 ppb to represent low ozone conditions. Experiments 10–13 were conducted with identical [$terp_i$] to Experiments 1, 2, 4, and 6, but with [$O_{3,i}$] = 100 ppb to represent high ozone conditions.

Table 5 lists the [$terp_i$], $k_{pseudo,i}$, the first peak of the total number concentrations, and the final total number and mass concentrations for Phase I experiments. The lognormal distribution parameters for both the first peak and final SOA number concentrations are listed in Table 2 in Appendix D. For Experiments 1–9 with low [$O_{3,i}$] = 25 ppb, Experiment 1 with [d-lim_i] = 50 ppb yielded the largest peak total number concentration, larger than any experiment with a single terpenoid or a mixture, even larger than those with three times the total $k_{pseudo,i}$. Also, the final number concentrations for Experiment 1 were the third largest observed, at 93 and 98% of the final number concentrations for Experiments 6 and 9, which each had three times the total $k_{pseudo,i}$.

Table 5. Phase I initial reactant concentrations, $k_{pseudo,i}$, and the first peak number and final number and mass SOA concentrations.

	Initial Reactant Concentrations					SOA Formation		
						Number		Mass
Exp.	$[O_{3,i}]$ (ppb)	$[\text{d-lim}_i]$ (ppb)	$[\alpha\text{-terp}_i]$ (ppb)	$[\alpha\text{-pin}_i]$ (ppb)	$k_{psuedo,i}$ (h^{-1})	Peak (#/cm^3)	Final (#/cm^3)	Final (μg/m^3)
1	25	50	0	0	0.9	13,628	7,430	4.2
2	25	0	33	0	0.9	547	486	0.33
3	25	0	67	0	1.8	7,257	5,626	7.2
4	25	50	33	0	1.8	8,567	5,991	4.6
5	25	50	67	0	2.7	11,284	9,064	8.9
6	25	50	33	118	2.7	12,854	7,578	7.7
7	25	0	0	118	0.9	4,044	1,985	2.1
8	25	0	33	118	1.8	9,232	4,406	6.6
9	25	0	67	118	2.7	12,693	7,982	11
10	100	50	0	0	0.9	16,326	17,699	3.7
11	100	0	33	0	0.9	20,857	21,014	34
12	100	50	33	0	1.8	39,022	30,383	31
13	100	50	33	118	2.7	50,152	40,787	84

The results of Experiments 1–9 reflect the elevated potential of ozone/d-limonene reaction products to nucleate at these low ozone, low RH conditions. For experiments with identical $[\text{d-lim}_i]$, the addition of another reactive terpenoid appears to lessen its nucleation potential greatly, which is illustrated by the results of Experiments 4, 5, and 6 exhibiting lower peak number formation. Experiment 2, with $[\alpha\text{-terp}_i]$ = 33 ppb and $[O_{3,i}]$ = 25 ppb, resulted in the lowest peak and final particle number concentrations, illustrating the low number formation potential of α-terpineol at these conditions.

Plotting the results of Phase I further illuminates trends in the SOA formation. Figure 10(a) and (b) display the first peak of the total number concentrations versus ($[O_{3,i}] \times k_{pseudo,i}$) for each experiment. Plotting the SOA formation results versus ($[O_{3,i}] \times k_{pseudo,i}$) normalizes the SOA formation by the initial amount of reactive material in the system. In Figure 10(b), the different shades of the bars represent the fractional contribution of each terpenoid to the total $k_{pseudo,i}$ of the mixture.

Figure 10(a) and (b) show that results of SOA peak number formation from ozone reactions with pure terpenoids at low $[O_{3,i}]$ (Experiments 1, 2, 7) are much less predictable than results for the remainder of the experiments. For $([O_{3,i}] \times k_{pseudo,i}) \geq 45$ ppb/h, the relationship between $([O_{3,i}] \times k_{pseudo,i})$ and peak number concentration is approximately linear. This approximate linearity holds true whether the reactive mixture is composed of a single terpenoid (Experiments 3, 10, and 11) or a mixture of terpenoids (Experiments 4–6, 8, 9, 12, and 13). For the terpenoids studied and combined as herein, the prediction of peak SOA number concentration appears possible with knowledge of $([O_{3,i}] \times k_{pseudo,i})$, if $([O_{3,i}] \times k_{pseudo,i}) \geq 45$ ppb/h.

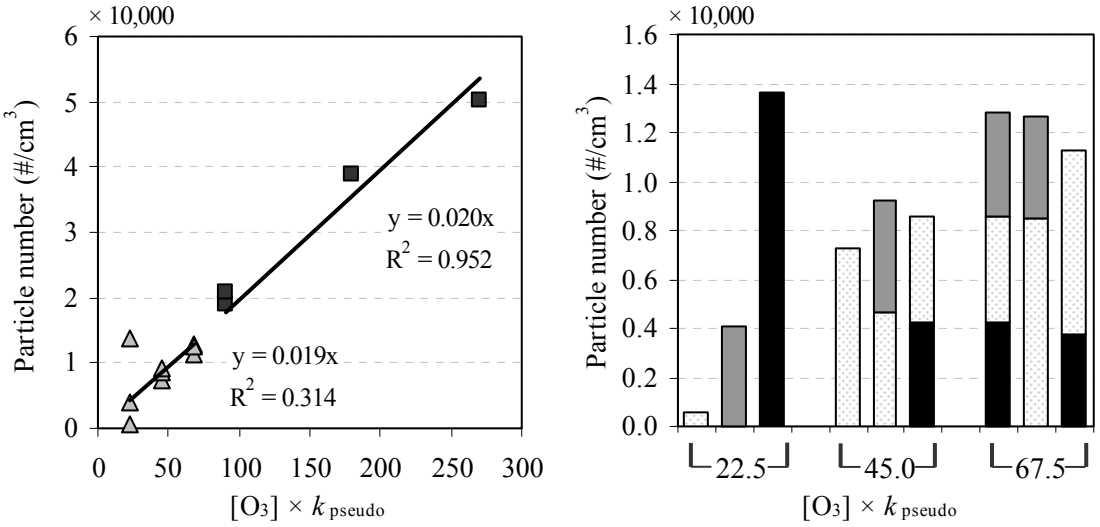

Figure 10. SOA number concentration versus the product of the initial ozone concentration ($[O_{3,i}]$) and the pseudo first-order loss rate of the terpenoids(s) with ozone ($k_{pseudo,i}$). Plot (a) shows peak number concentrations for Experiments 1–13 on a linear x-axis. Plot (b) is a bar graph with peak number concentrations for Experiments 1–9. For (b), the different shades represent the fraction of each terpenoid of the total $k_{pseudo,i}$. Black is d-limonene, gray is α-pinene, and dotted white is α-terpineol. Italicized numbers correspond to the experiment number.

The reason for the large nucleation potential of products of ozone/d-limonene reactions at low ozone conditions appears to be more complicated than simply that less ozone is available to react with d-limonene in a mixture, since the same trend was not observed with Experiment 10, which had equivalent $[\text{d-lim}_i]$ but at high $[O_{3,i}]$. Reactions

of ozone with d-limonene, which has two unsaturated carbon-carbon bonds, is a complex process that can lead to first or second generation products, depending on whether ozone is limited or in excess (Ng et al., 2006). For the experiments at low $[O_{3,i}]$, ozone was the limiting reagent, so first generation products were likely responsible for the nucleation. It is speculated that the ozone-limited reaction with d-limonene yields a set of byproducts with higher nucleation potential than those that occur with ozone reactions with mixtures of terpenoids or ozone-excess reactions with d-limonene. (Mass SOA formation results for Experiments 1–13 are discussed in Appendix D.)

Eleven experiments in Phase II were performed, which determined the gas-phase SOA yields, Y_g (mass SOA formed/mass terpenoid reacted), for ozone reactions with the single terpenoids of d-limonene, α-pinene, and α-terpineol. In a system with no other organic particle mass, Y_g is a function of the SOA mass concentration, C_{SOA} (μg/m^3), since partitioning of semi-volatile reaction products into the condensed organic phase in particles increases with organic phase mass (Pankow, 1994). Results for Y_g for experiments with different initial ozone and terpenoid concentrations are in Table 3 and Figure 3 in Appendix D, and yields increased with the concentration of SOA formed. Parameters were fit that describe the behavior of Y_g, according to the relationship in Odum et al. (1996).

The Y_g for single terpenoids determined in Phase II was used with Phase I results to estimate whether Y_g for single terpenoids are additive for mixtures. This analysis is useful because mass yields for many different terpenoids are available in the literature (e.g. Ng et al., 2006). The final terpenoid concentrations were not measured in Phase I experiments, so they were estimated for each concentration for 48 minutes after ozone injection by using a numerical approach. The full analysis is in Appendix D, but overall, the results show that Y_g for single terpenoids can be used to predict SOA mass yields in mixed terpenoid environments reasonably well. The percent differences between the measured and predicted values of the SOA mass formation range from −30 to 62%. The mean (s.d.) percent difference for all 13 experiments was 13 (29)%.

This research highlights the need for further experiments that investigate SOA number formation from ozone reactions with single terpenoids and mixtures, particularly for experiments at low ozone concentrations. Further attention should be focused on SOA number formation at low initial concentrations of ozone and terpenoids. Also, related topics that need investigation are the influence of preexisting particles, as well as the influence of transient versus steady-state conditions, on the nucleation potential of reaction products. If particle number, as opposed to mass, is also associated with adverse health effects (Harrison and Yin, 2000), then ozone reactions with single terpenoids with high nucleation potential (e.g. d-limonene) may be more harmful to human health than with mixtures with lower nucleation potential. Since consumer products contain other reactive compounds besides terpenoids, other formation trends may exist, and caution should be used when extrapolating mixture results directly for consumer products.

4.5. The influence on SOA formation of heterogeneous reactions on building surfaces between ozone and d-limonene

This section summarizes the experimental methods and results for the research presented in full in the article in Appendix E, which explored the SOA formation due to heterogeneous reactions of ozone with surface-adsorbed terpenoids. Terpenoids have vapor pressures that lead to modest adsorption to real building materials from the gas-phase (Won et al., 2001; Singer et al., 2004), and they are also applied directly to interior surfaces in the form of consumer products (Singer et al., 2006). Since the primary loss mechanism of ozone indoors is reaction with interior surfaces (Sabersky et al., 1973; Weschler, 2000), and adsorbed terpenoids and ozone react on surfaces (Fick et al., 2005; Flemmer et al., 2007; Springs and Morrison, 2008), an investigation of the potential SOA formation from these reactions was warranted.

The specific research objectives were to develop a model framework to describe SOA formation due to ozone/terpenoid surface reactions; to conduct experiments on ideal surfaces to quantify the yield to gas-phase SOA of surface reactions between ozone and adsorbed d-limonene; to estimate the potential effects for a variety of indoor materials;

and to model surface effects observed in the field study described in Section 4.2 and Appendix B. The monoterpene d-limonene was used in the experiments because it adsorbs to surfaces (Singer et al., 2004), is the primary terpenoid constituent of many consumer products (including the field study discussed herein) (Singer et al., 2006b), has been shown to react with ozone on surfaces (Fick et al., 2005; Springs and Morrison, 2008), and has high SOA yield potential (Ng et al., 2006).

The model framework envisions a three-step mechanism by which ozone reactions with terpenoids adsorbed to surfaces increase gas-phase SOA concentrations. (1) Ozone either (a) adsorbs to the surface and then collides with the terpenoid molecule or (b) collides directly from the gas-phase with the adsorbed terpenoid molecule. (2) Some collisions cause the ozone and terpenoid molecules to react and form products. (3) The reaction products partition between the surface-, the SOA- and/or the gas-phases at fractions that depend on the product vapor pressures and polarity (Kamens et al., 1999; Leungsakul et al., 2005).

The model framework is described in full in Appendix E and is only briefly described here. Steps (1) and (2) are incorporated into one mass transfer coefficient, the ozone deposition velocity to the adsorbed terpenoid, $v_{d,terp}$ (m/h). The $v_{d,terp}$ is rate-controlled by the inverse sum of two resistances in series, the rate of transport through the boundary layer and the rate of surface reactions (Cano-Ruiz et al., 1993). The full expression for $v_{d,terp}$ is in Appendix E, but when $v_{d,terp}$ is rate-limited by reactions, it is:

$$v_{d,terp} = r_{terp}\gamma_{terp}\frac{<v>}{4} \quad (2)$$

where r_{terp} (m^2 terpenoid/m^2 intrinsic surface area) is the fractional coverage of a surface with the adsorbed terpenoid, γ_{terp} (-) is the reaction probability (defined as the ratio of the reaction and collision rates of ozone) of the adsorbed terpenoid, and ‹v› is the Boltzmann velocity (1.296×10^6 m/h for O_3 at 296 K). Therefore, for surfaces for which ozone deposition is reaction rate-limited, $v_{d,terp}$ depends only on r_{terp} (for the same γ_{terp}).

The $v_{d,terp}$ can be used to calculate the SOA emission rate due to ozone/terpenoid surface reactions, E_s (μg/h), as in Equation 3:

$$E_s = Y_{s,m} v_{d,terp} A C_{O3} \left(\frac{MW_{SOA}}{MW_{O3}} \right) \quad (3)$$

where A (m^2) is the nominal surface area; C_{O3} ($\mu g/m^3$) is the mass concentration of ozone, and MW_{SOA} (g/mol) and MW_{O3} (g/mol) are the molecular weights of SOA and ozone, respectively (MW_{SOA} is assumed as 180 g/mol as in Weschler and Shields, 1999). $Y_{s,m}$ (moles SOA formed/moles ozone consumed), the yield to SOA of reactions of ozone with surface-adsorbed terpenoids, represents step (3) in the model framework.

Experiments were performed to determine the magnitude of $Y_{s,m}$ due to ozone reactions with adsorbed d-limonene, in a 283 L stainless-steel chamber in which ozone and d-limonene were combined. The basic premise of the experiments was to hold parameters that influence gas-phase formation of SOA constant while varying the surface area, A, in the chamber. Since Equation 3 shows that E_s is a function of A, any observed difference in SOA formation in chambers with varying values for A is due to surface reaction effects. Thus, chamber experiments were conducted with the air exchange rate, ozone, and d-limonene concentrations at approximately constant conditions, while A was varied for two different chamber conditions, Chamber 1 and 2, where Chamber 1 = the empty stainless-steel chamber, and Chamber 2 = the chamber plus 14 stainless-steel woven wire screens. The addition of the stainless-steel screens increased the A by 460% and decreased V by 2%, respectively, which changed the total A/V by 469%.

The experimental method used to determine and results for $Y_{s,m}$ are in Appendix E. Experiments in Chamber 2 led to higher SOA formation, particularly in number. For the experiments in Chamber 2 versus Chamber 1 at RH = 50%, the mass concentration increase was 19% and the number concentration increase was 56%. The calculated $Y_{s,m}$ values at RH = 20, 50, and 70% RH are in Figure 11(a). The $Y_{s,m}$ values ranged from 0.14 to 0.16, which is approximately two-thirds of the gas-phase yield used in the calculations. Also shown in Figure 11(b) is the ratio of the SOA number concentration formed ($\#/cm^3$) and the mass concentration formed ($\mu g/m^3$) for the gas-phase (χ_g) and

surface-phase (χ_s) reactions, at the three different experimental RH values. The χ_s ranged from 126–339 (#/cm^3)/(μg/m^3) and χ_g ranged from 51.1–60.2 (#/cm^3)/(μg/m^3).

Both $Y_{s,m}$ and χ_s decreased as RH increased. The $Y_{s,m}$ was only slightly higher at the lower RH values, which is consistent with observations from other SOA formation experiments with gas-phase reactions of ozone and d-limonene (Leungsakul et al., 2005). However, χ_s was much higher at the lower RH values, indicating that more SOA particle formation occurred for ozone/d-limonene reactions at lower RH.

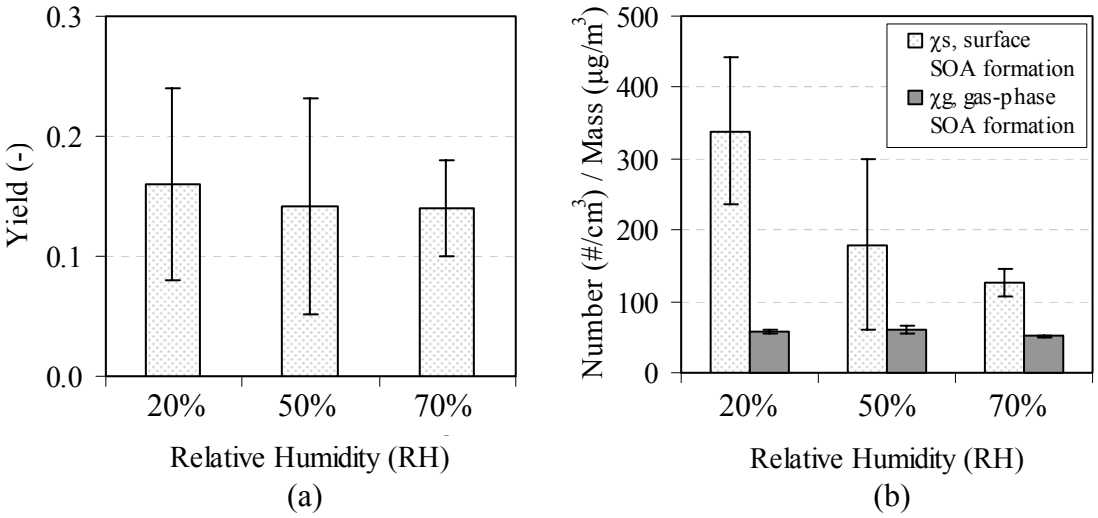

Figure 11. The (a) SOA yields ($Y_{s,m}$) due to surface reactions of ozone with surface-adsorbed d-limonene and (b) the ratio of the SOA number concentration formed (#/cm^3) and the mass concentration formed (μg/m^3) for gas-phase (χ_g) and surface-phase (χ_s) reactions, at RH = 20, 50, and 70%. Linear dependence to RH for χ_s is y = -4.34x + 417 (R^2 = 0.97) and for χ_g is y = -0.115x + 62.0 (R^2 = 0.37).

The model framework and the results for $Y_{s,m}$, χ_s and χ_g were used to explore the SOA formation from ozone/d-limonene surface reactions on surfaces of different levels of initial ozone reactivity. The original reactivity of a material with ozone can be described with its reaction probability without terpenoid adsorption, γ_o (-), and values of γ_o for common building materials range from approximately 10^{-8} to 10^{-4}. Figure 12 plots $v_{d,terp}$ versus r_{terp} for different surfaces with this range of γ_o, using $\gamma_{terp} = 3\times10^{-4}$ for d-

limonene (Springs and Morrison, 2008) and other parameters described in Appendix E. The thick black line is the reaction rate limited $v_{d,terp}$ (Equation 2).

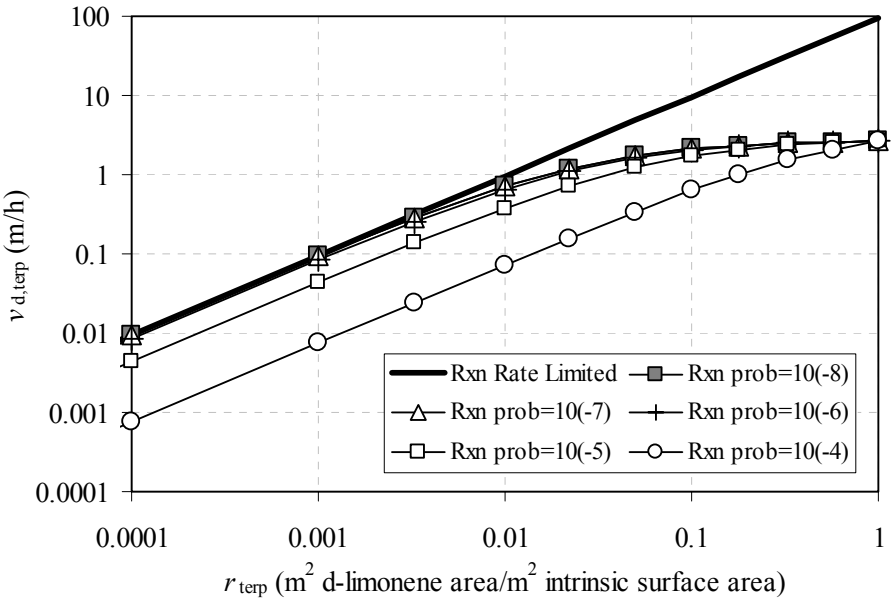

Figure 12. Plot of $v_{d,terp}$ versus r_{terp} for a range of different γ_o that represent those common for building materials, using $\gamma_{terp} = 3\times10^{-4}$ for d-limonene. The reaction probabilities listed in the legend are the γ_o.

Figure 12 shows that the $v_{d,terp}$ calculated for the surfaces with $\gamma_o \leq 10^{-6}$ are quite similar to each other. Also, for values of $r_{terp} \leq 0.01$, the $v_{d,terp}$ for those surfaces are well-approximated with Equation 2. For $r_{terp} > 0.01$, $v_{d,terp}$ for those surfaces deviate from the reaction rate limited approximation and $v_{d,terp}$ approaches a maximum transport-limited value that is controlled by the rate of ozone transport through the boundary layer. The surfaces with $\gamma_o \geq 10^{-5}$ are never in the reaction rate limited regime, and $v_{d,terp}$ for those surfaces is less that that calculated for surfaces with $\gamma_o \leq 10^{-6}$. For instance, when $v_{d,terp}$ for materials with $\gamma_o \leq 10^{-6}$ are fully in the reaction rate limited regime (i.e., $r_{terp} \leq 0.001$), the $v_{d,terp}$ for a surface with $\gamma_o = 10^{-5}$ is a factor of 2.2 less and for $\gamma_o = 10^{-4}$ is a factor of 13 less than those surfaces with $\gamma_o \leq 10^{-6}$. These results imply that contribution to SOA

formation of ozone/d-limonene surface reactions is more important on surfaces with low initial reactivity than on surfaces with high initial reactivity.

This analysis was extended to $v_{d,terp}$ for real building materials. Material parameters were gathered from Cano-Ruiz et al. (1993), Morrison and Nazaroff (2000), Won et al., (2001), or estimated, and the full analysis is presented in full in Appendix E. In summary, for adsorption of d-limonene from the gas-phase at a concentration of 50 ppb, $v_{d,terp}$ is expected to range from 0.00039 m/h for ceiling tile to 0.10 m/h for glass. The largest $v_{d,terp}$ are about an order of magnitude below those measured for indoor surfaces (Wang and Morrison, 2006), and the smallest $v_{d,terp}$ are nearly inconsequential. Building materials with the largest $v_{d,terp}$ were glass, sealed surfaces, stainless-steel, aluminum, apples, and vinyl flooring. Also, the $v_{d,terp}$ for these materials fell within 85% of the value estimated by the reaction rate limited approach, indicating that at this d-limonene concentration, materials with $v_{d,terp}$ that will influence SOA concentrations can have their $v_{d,terp}$ estimated with Equation 2. The potential SOA contribution for ozone/d-limonene reactions on six common building materials are further explored in Figure 13.

Figure 13 displays the predicted steady-state SOA number formation rates (#/cm^3·h) from ozone deposition to d-limonene adsorbed to glass (Gl), stainless-steel (SS), aluminum (Al), painted gypsum board (PGB), vinyl flooring (VF), and carpet (Carp). Contributions for these surfaces are determined for two surface areas, 10 m^2 or 45 m^2, in a 27 m^3 indoor space with concentrations of 10 ppb and 50 ppb for ozone and d-limonene, respectively. The SOA number formation rates (#/cm^3·h) for surface and gas-phase reactions were determined as described in Appendix E. The SOA formation rate from the gas-phase reactions was 401 #/cm^3·h. For the low surface area (10 m^2) in the room, the surface contributions are a small fraction of the total SOA number formation, and the largest contributor, glass, was responsible for 7%. For the high surface area (45 m^2), the surface contributions are a larger fraction, and glass was responsible for 27% of the total number formation. For the 10 m^2 and 45 m^2 of glass, surface reactions were only responsible for 0.7 and 3% of the SOA mass formed.

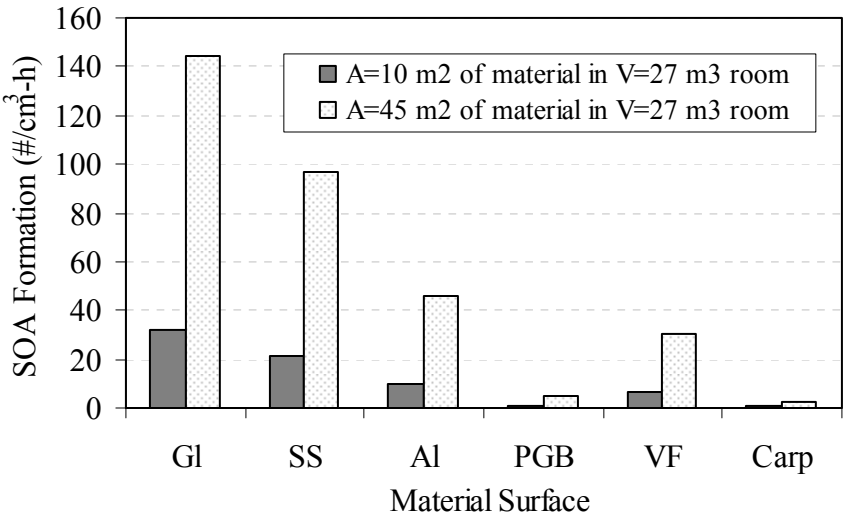

Figure 13. The (a) predicted steady-state SOA number formation from ozone deposition to d-limonene adsorbed to (Gl) glass, (SS) stainless steel, (Al) aluminum, (PGB) painted gypsum board, (VF) vinyl flooring, and (Carp) carpet, for two surface areas of 10 m^2 or 45 m^2, in a 27 m^3 indoor space with $C_{terp,m}$ = 50 ppb and $C_{O3,m}$ = 10 ppb.

As a screening exercise, the model framework was applied to results with transient SOA formation for the field study described in Section 4.2 and Appendix B, which determined the SOA formation in a residential room with an ozone-emitting ion generator and a terpene-emitting air freshener. Tests at similar air exchange rates and ozone and d-limonene concentrations were conducted with different flooring surfaces in the room. Four tests used the original flooring of sealed/stained concrete, and two tests used carpet with padding that was installed over the original flooring. Figure 14(a) shows the change in average concentrations for each floor surface for ten hours of testing.

At time zero in Figure 14(a), the air exchange rate in the room decreased from approximately 1.3 h^{-1} to 0.4 h^{-1}, corresponding to the shutting off of the HVAC system supplying the room. After the air exchange rate decreased, the residence time of reactant concentrations increased and the loss rate of SOA due to ventilation decreased, resulting in increased formation of SOA particles. The tests with carpet exhibited approximately one-third the SOA number formation than tests with stained/sealed concrete.

The ozone and d-limonene concentrations in all tests were on the order of 10 ppb and 40 ppb, respectively (both were approximately constant due to their emissions in the

room). The main variable that changed was the floor surface. The effect of this variable change on SOA formation was explored with a numerically-solved transient version of the model framework, along with equations that describe d-limonene sorption (Tichenor et al., 1991) that were modified to account for loss on the surface due to ozone reactions.

The modeled results at the field investigation conditions are shown in Figure 14(b). The time-resolved model predicted the SOA number concentrations reasonably well, with the modeled final number concentrations falling near the observed final concentrations. For the modeled results, the contribution from the ozone reactions with d-limonene adsorbed to the sealed/stained concrete floor was responsible for approximately one-half of the final SOA number concentration.

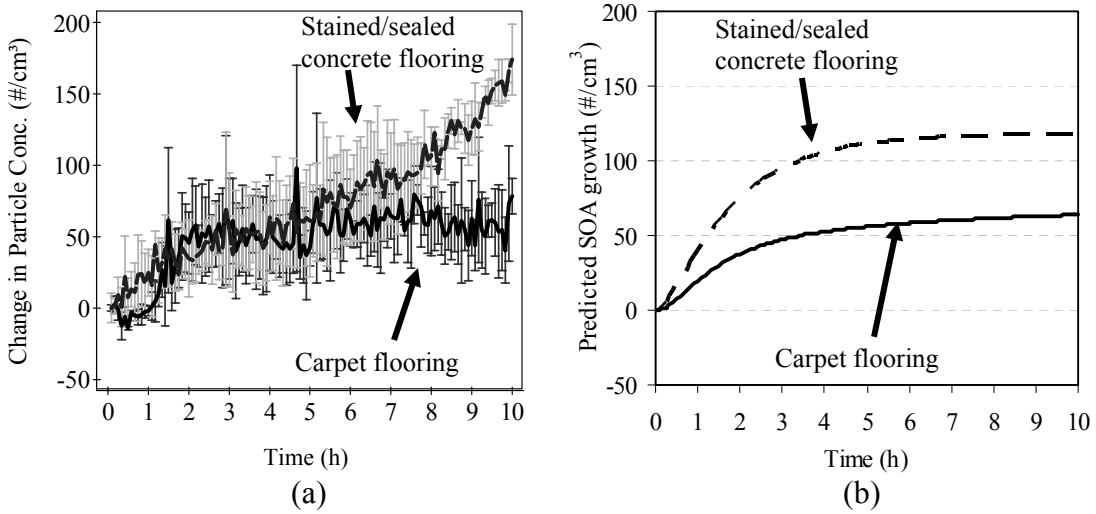

Figure 14. (a) Change in mean particle concentrations (0.015–0.53 μm) vs. time for four nights of testing with stained/sealed concrete flooring and for two nights with carpet flooring, in the same 27 m^3 room. Error bars represent one standard deviation from the mean value. An operating ion generator and energized air freshener were present during all tests. (b) Modeled results. (See text for more information.)

This study was the first that I know of that investigated SOA formation due to ozone reactions with terpenoids adsorbed to surfaces. The chamber experiments determined that yields of SOA due to ozone/terpenoid surface reactions are influenced little by RH, but that SOA number formation is enhanced at lower RH. The analysis with

the model framework indicates that in certain types of indoor spaces, surface reactions may be responsible for a substantial fraction of SOA number formation, which has implications for health effects due to exposure to particle number concentrations. Further attention should be focused on designing experiments that allow observation of this effect indoors, as well as validating the model framework as ideal with a more controlled data set than was available with the field study results, which were used as a screening test.

5. CONCLUSIONS

The work in this dissertation explored novel ways that ozone reacts with terpenoids indoors to yield secondary organic aerosol (SOA). Five different research studies were conducted, which were summarized in this Research Summary and are presented in full in Appendices A–E. The research fell into two distinct categories:

(i) Exploration of the primary and secondary impacts of particle controls on indoor SOA formation (the research in Appendices A–C), and

(ii) Investigation of two fundamental aspects of SOA formation indoors (the research in Appendices D and E).

Objectives A and B were to investigate the net effects of ozone-emitting ion generators on SOA formation. Objective C was to investigate the influence of heating, ventilating, and air conditioning (HVAC) systems on SOA formation and concentrations. Objective D was to investigate the SOA number and mass formation due to ozone reactions with single versus mixtures of pure terpenoids. Objective E was to examine the SOA formation potential of ozone reactions with terpenoids adsorbed to building surfaces. The major findings from the five research objectives are summarized below.

- (A) Ion generators are an order of magnitude less effective than other types of portable air cleaners at removing particles in the size range of SOA particles, when compared with the Clean Air Delivery Rate (CADR).
- (A) Ion generators emit ozone at rates that influence indoor ozone concentrations (this work found 3.3–4.3 mg/h). During the test to determine the CADR of an ion generator, this ozone could react with unsaturated organics to form SOA and invalidate the CADR test, necessitating a modified CADR test that scavenges as much ozone as possible from the test chamber.
- (A and B) Ion generators can act as steady-state net SOA producers (in the size range of < 250 nm in diameter), in the presence of terpenoid source (e.g. an air freshener), both in a laboratory setting and in a residential room. Multiple ion generators and air fresheners were tested, and all exhibited net SOA formation.

- (C) Heating, ventilating, and air-conditioning (HVAC) system design and operation can influence concentrations of SOA. Specifically:
    - Residential SOA concentrations are most influenced by the particle filtration efficiency, whether the HVAC system cycles on and off or runs continuously, and the indoor set-point temperature.
    - Commercial SOA concentrations are most influenced by the particle filtration efficiency, whether ozone is removed by HVAC filters or other ozone sinks, the fraction of ventilation versus recirculated air, and the indoor set-point temperature.
    - The particle removal capability of an in-duct electrostatic precipitator (ESP) can be substantially dampened by its ozone generation and consequent SOA formation. The relative effect of the ozone emissions of an ESP on SOA formation are larger in a rural area than an urban area since ambient ozone concentrations are typically lower in rural areas.
    - The filtration of ozone by an HVAC component is an effective way to reduce indoor SOA concentrations. To reduce indoor SOA, methods that lead to the lowest formation of gaseous byproducts, such as ozone filtration by activated carbon, are preferable.
- (D) At low initial ozone concentrations, $[O_{3,i}]$, ozone reactions with pure d-limonene produced larger peak total number concentrations than ozone reactions with mixtures of terpenoids, even if those mixtures contained d-limonene.
- (D) For experiments where the product of $[O_{3,i}]$ and the initial pseudo first-order loss rate of ozone with terpenoid(s), $k_{pseudo,i}$, is greater than 45 ppb/h, the peak total number concentration is linearly related to $([O_{3,i}] \times k_{pseudo,i})$.
- (D) The yield of SOA from ozone reactions with single terpenoids can be used to approximate mass formation in a mixed terpenoid environment reasonably well.
- (E) Yields for SOA mass from surface reactions were observed as 0.14–0.16 and changed little with varying relative humidity, though SOA number formation increased with lower relative humidity.

- (E) Indoor SOA number concentrations are likely to be affected by ozone reactions with surface-adsorbed terpenoids, but mass concentrations are not.
- (E) Building materials that affect SOA concentrations depend primarily on γ_o (-), which is the original reaction probability of the material. Materials that contribute are those with low γ_o (i.e., $< 10^{-6}$) such as glass, metals, sealed surfaces, etc.
- (E) For these materials with a low γ_o, $v_{d,terp}$ (m/h), the deposition velocity of ozone to surface-adsorbed terpenoids, is primarily reaction rate limited.

This research provides a more complete picture of the phenomenon of indoor SOA formation. Objectives A and B reveal that the use of ion generators indoors should likely be avoided, as they tend to generate more pollution than they remove. Objective C illustrates that HVAC systems can be strategically used to reduce concentrations of SOA indoors. Objective D showed that which terpenoids are present in a reactive mixture is important to the number of particles that nucleate initially. Objective E determined that SOA number formation due to ozone/d-limonene surface reactions can be important for indoor spaces with large surface areas of materials with low surface reactivity. Also, though applied to ozone/d-limonene surface reactions that yield SOA, the framework in Appendix E can be used to model any chemical that adsorbs to a surface from the gas-phase and undergoes surface reactions to yield gas-phase products.

Appendix A

PAPER I

Ultrafine Particle Removal and Generation by Portable Air Cleaners

(Published in *Atmospheric Environment*)

ABSTRACT

Portable air cleaners can both remove and generate pollutants indoors. To investigate these phenomena, we conducted a two-phase investigation in a 14.75 m^3 stainless steel chamber. In the first phase, particle size-resolved (12.6–514 nm diameter) clean air delivery rates (CADR) and efficiencies were determined, as were ozone emission rates, for two high efficiency particulate air (HEPA) filters, one electrostatic precipitator with a fan, and two ion generators without fans. The two HEPA air cleaners had count average CADR (± one standard deviation) of 188 (30) and 324 (44) $m^3\ h^{-1}$; the electrostatic precipitator 284 (62) $m^3\ h^{-1}$; and the two ion generators 41 (11) and 35 (13) $m^3\ h^{-1}$. The electrostatic precipitator emitted ozone at a rate of 3.8 ± 0.2 mg h^{-1}, and the two ion generators 3.3 ± 0.2 and 4.3 ± 0.2 mg h^{-1}. Ozone initiates reactions with certain unsaturated organic compounds that produce ultrafine and fine particles, carbonyls, other oxidized products, and free radicals. During the second phase, five different ion generators were operated separately in the presence of a plug-in liquid or solid air freshener, representing a strong terpene source. For air exchange rates of between 0.49 and 0.96 h^{-1}, three ion generators acted as steady-state net particle generators in the entire measured range of 4.61–157 nm, and two generated particles in the range of approximately 10 to 39–55 nm. Aldehyde and terpene concentrations were also sampled for one ion generator, and concentrations of terpenes decreased and formaldehyde increased. Given these results, the pollutant removal benefits of ozone generating air cleaners may be outweighed by the generation of indoor pollution.

INTRODUCTION

As more Americans realize the importance of indoor air quality, there is increased interest in air cleaning devices. Shaughnessy and Sextro (2006) report that 3 of 10 American households own one type of air cleaning device. The California Air Resources Board (2007) reports that 14% of California households own an air cleaner, and 10% own an air cleaner that produces ozone intentionally or as a byproduct. Common portable air cleaners designed to remove indoor airborne particles include: (1) high-efficiency particle arresting (HEPA) filters, which force air with a fan through filter media, and (2) ionizers, which charge incoming particles with a corona, removing them to oppositely charged collector plates and/or building surfaces. One type of ionizer, electrostatic precipitators (ESP), have a fan and collection plates, and tend to have higher flow rates than smaller ion generators, which often do not have a fan and may or may not have collection plates.

Researchers have developed performance metrics to uniformly evaluate portable air cleaners so that direct performance comparisons are possible. One such metric is the clean air delivery rate (CADR), which is the effective volumetric flow rate of clean (i.e., particle free) air delivered by the air cleaners. The CADR is a function of particle diameter, and it is the best available metric to compare portable air cleaners because it takes into account (and is the product of) the flow rate through the air cleaner and the particle removal efficiency (Shaughnessy et al., 1994; Offermann et al., 1985; Shaughnessy and Sextro, 2006). Additionally, the CADR is more independent of the testing environment than other metrics that have been used to evaluate air cleaners, such as the air cleaning factor (ACF) (e.g., Lee et al., 2004), which is dependent on the volume and air exchange rate of the experimental chamber. Typical measured CADRs for particles associated with environmental tobacco smoke (ETS) range from 277–407 $m^3 h^{-1}$ for HEPA air cleaners, 197–499 $m^3 h^{-1}$ for electrostatic precipitators, and 2–51 $m^3 h^{-1}$ for ion generators (Shaughnessy et al., 1994; Offermann et al., 1985). Most reported CADRs are not size-resolved and were determined with fine (100 nm–2.5 μm diameter) or larger particles, rather than the ultrafine (<100 nm) particle size range.

Size-resolved ultrafine particle removal by portable air cleaners is important to quantify because elevated exposure to ultrafine particles is associated with effects on human health, including cardiopulmonary diseases (Pekkanen et al. 2002). Further, indoor peak concentrations of ultrafine particles can be several times outdoor concentrations (Wallace, 2006), and the typical American spends 18 hours indoors for every hour outdoors (Robinson and Nelson, 1995), so most exposure to ultrafine particles is likely indoors. Typical indoor sources of ultrafine particles are gas stoves (Wallace et al., 2004), vented gas clothes dryers (Wallace, 2005), electric ovens (Dennekamp et al., 2001), and candles (Wallace, 2000). Additionally, chemical reactions between ozone and unsaturated organic compounds, such as the terpenes d-limonene or α-pinene (both commonly found indoors), can result in significant formation of oxygenated gases (e.g., aldehydes) and secondary organic aerosol (SOA) in the ultrafine and fine range due to nucleation or partitioning of semi-volatile reaction products to smaller seed particles (e.g., Weschler and Shields, 1999). Studies on mice suggest that the health effects due to SOA may be different and more deleterious than those from primary aerosols (e.g., Rohr et al., 2002).

The potential to generate particles indoors due to reactions between ozone and terpenes is of particular concern with respect to ionizers because they influence indoor ozone concentrations. Measured ozone emission rates from portable ion generators range from 0.056–2.757 mg h^{-1} (Niu et al., 2005), 0.234–2.144 mg h^{-1} (Tung et al., 2005), 0.74–4.04 mg h^{-1} (Mullen et al., 2005), and 0.16–2.2 mg h^{-1} (Britigan et al., 2006). In typical indoor environments with a significant terpene source (such as an air freshener), an ozone emission rate of this magnitude might lead to increases in ultrafine and fine particles. It follows that if an ion generator had a low CADR for ultrafine and fine particles, it might operate as a net particle emission source, rather than a removal device, in certain size ranges. For instance, Alshawa et al. (2007) showed that injections of 15 and 45 mg of d-limonene into an office with an energized ion generator led to a transient elevation in ultrafine particle concentrations. It is clear that more research is necessary to understand the total impact of portable air cleaners on ultrafine and fine particle concentrations.

METHODOLOGY

A two-phase investigation was performed. During the first phase, five different portable air cleaners were characterized according to their power draw, airflow rate, particle size-resolved (12.6–514 nm diameter) CADR and single pass efficiency, and ozone emission rate. During the second phase, a set of screening experiments were conducted in which five portable ion generators were operated in the presence of a terpene source (either a plug-in or solid air freshener) to determine the impact of SOA formation on steady-state particle concentrations (in the range of 4.61–157 nm diameter). All tests were conducted in a 14.75 m^3 stainless steel chamber. Nylon sampling lines were installed approximately 1.5 m from the floor in the center of the chamber to measure particles and ozone. The 6 mm OD tube lengths were approximately 3.5 m for the particle measurements and 3 m for the ozone measurements. Three oscillating fans were operated in the chamber to ensure that the air was well-mixed. The chamber air exchange rate (h^{-1}) during all of the tests was measured by releasing approximately 3 L of CO_2 into the chamber and monitoring its continuous decay with a TSI model 8551 Q-Trak.

Phase 1: Characterization of portable air cleaners

During the first phase, five different portable air cleaners were tested: two different HEPA air cleaners (HEPA 1 and 2), one electrostatic precipitator (ESP), and two different ion generators (IG 1 and 2). The ESP had collector plates, a high-flow fan, a pre-filter for removal of large diameter particles, and an activated carbon post-filter for removal of generated ozone. Neither IG 1 nor IG 2 used a fan, and IG 1 was a common tower model and IG 2 a common table-top model. The air cleaners were cleaned as per the manufacturers instructions before all testing. The electrical power draw, airflow rate, particle size-resolved (12.6–514 nm diameter) clean air delivery rate (CADR) and single-pass removal efficiency, and ozone emission rate were determined for each air cleaner.

The electrical power drawn by the highest setting of each air cleaner was monitored with a Brand Custom Power Meter. The airflow rate through each of the air

cleaners at their highest setting was determined by attaching to the inlet of the air cleaner an airtight capture hood that was also connected to an Energy Conservatory Duct Blaster calibrated fan (uncertainty 3% of volumetric flow). When the air cleaner was energized and the flow rate of the fan was such that the pressure difference was zero between the air inside and outside of the capture hood, the flow rate of the air cleaner equaled that of the fan (Offermann et al., 1985).

For the CADR tests, the chamber was operated so that the inlet air was as free of particles, ozone, and organic compounds as possible. To this end, all chamber openings were closed and/or taped and inlet air was filtered through HEPA and activated carbon filters. The inlet chamber fan also positively pressurized the chamber (at ~1 Pa pressure difference from the laboratory) and prevented unfiltered air from entering the chamber due to infiltration. Additionally, since the ozone emitted by the ionizers could react with any remaining terpenes in the chamber air to produce particles, 4 m^2 of activated carbon strips were hung on chamber surfaces during the CADR tests to remove the ozone emitted, thus removing this potential particle source from the CADR test environment.

Particles were generated in the chamber by burning three sticks of incense for approximately 15 minutes. Once the incense was extinguished, the size-resolved natural decay constant of particles, k_n (h^{-1}), due to air exchange and deposition on the chamber walls and activated carbon was measured using a TSI model 3936 scanning mobility particle sizer (SMPS) with a TSI model 3080 electrostatic classifier (EC) and a TSI model 3785 water-based condensation particle counter (WCPC). The SMPS was equipped with a TSI model 3081 long-differential mobility analyzer (long-DMA) and was set to measure particles in the range of 12.6–514 nm over 104 particle size bins, every three minutes. Then, three more sticks of incense were burned for 15 minutes, and the size-resolved particle decay was measured with the air cleaner energized at its highest setting, k_{ac} (h^{-1}). The size-resolved decay constants (k_n and k_{ac}) were calculated by fitting a linear regression line to the slope of $-\ln(C(t)/C_0)$, which is the negative of the natural log of the time-varying concentration ($C(t)$) normalized by the initial concentration at the time the incense was extinguished (C_0), versus time (h). The particle size-resolved CADR

($m^3\ h^{-1}$) was calculated by applying a mass balance to the chamber and subtracting the background decay of particles from the decay when the air cleaner was energized: CADR = $V(k_{ac} - k_n)$ where V is the volume of the chamber (m^3) (Shaughnessy et al., 1994). It should be noted that this equation may not be valid for air cleaners that generate ozone, because of the potential source term associated with SOA formation. Thus, the use of activated carbon strips or other removal of ozone and unsaturated compounds are required to use this expression for calculating the CADR of an ozone-generating air cleaner.

The CADR for each of the 104 size bins was based on the maximum number of data points to calculate the decay slopes without (k_n) and with (k_{ac}) the air cleaner in operation for which the R^2 value for that decay slope remained above 0.975, with a minimum of four data points (12 minutes of decay). In addition, calculated CADR values were discarded if they did not meet the following quality control criteria: (1) the first data points during the natural and air cleaner decay periods both had a number concentration of at least 100 cm^{-3}, and the first four data points during each of the two decay periods were (2) non-zero and (3) decreasing in number as time increased. These quality control criteria were necessary because the incense burning did not always generate enough particles in a particular size bin to yield meaningful results. The CADR uncertainty was calculated as the quadratic sum of the standard error of each decay slope. The ESP was tested twice and IG 1 three times, and their CADRs are the averages of those single-test CADRs that met the three criteria.

The CADR equals the product of the flow rate through the air cleaner and the single-pass removal efficiency. The size-resolved single pass removal efficiency, η (--), for each air cleaner was calculated as the ratio of CADR to air flow rate.

To measure the ozone emission rates for each of the air cleaners, all ozone from the incoming air into the chamber was removed with an activated carbon filter, and the ozone concentrations inside the chamber were measured every minute with a calibrated 2B Technologies model 205 dual beam ozone monitor (±1 ppb or 2%). The air cleaner was placed in the chamber and energized, and the increase in chamber ozone

concentrations over time was measured. Once a steady-state was reached for ten minutes, the air cleaner was switched off, and the ozone decay with time was measured. Then a mass balance was used to determine the ozone emission rate for each air cleaner, using the decay period to determine the deposition loss of ozone to the chamber surfaces, following the work of Niu et al. (2001). To avoid artificially inflating both the loss rate during the decay period and thus the ozone emission rate for the ESP, the activated carbon filter on the outlet of the ESP was removed during the decay period.

Phase 2: Ion generators in the presence of a terpene source

During the second phase, five different tower-variety ion generators from two popular manufacturers were tested in the chamber. Three units of different models of one brand were tested: IG 1, 3, and 4. Two units of the same model of a different brand were also tested: IG 5A and 5B. IG 4 was operated with a UV lamp intended to neutralize bioaerosols. All five ion generators were brand new units and were cleaned according to the instructions of the manufacturer before testing. Screening chamber experiments were performed to determine the change in steady-state particle concentrations (4.61–157 nm diameter) resulting from the operation of an ion generator in an environment with high terpene concentrations (due to a plug-in or liquid air freshener).

The chamber was cleaned with tap water (i.e., no terpene containing cleanser) and allowed to dry overnight initially before testing and once again halfway through testing. It was treated to remove ozone reaction sites by operating two ion generators in it overnight before each test. Each test took place over an approximate one-day period. During each test, continuous measurements of ozone and particle concentrations of the air in the chamber were taken. The ozone concentrations were measured every minute with a calibrated UV absorbance ozone analyzer (2B Technologies model 205). The particle concentrations were measured with the same SMPS used in the first-phase. However, during the second phase it was equipped with a TSI model 3085 nano-differential mobility analyzer (nano-DMA) and configured to measure particles in the

diameter range of 4.61–157 nm over 99 particle size bins, with a scan-time of three minutes for all tests except IG 5B, which had a scan-time of five minutes.

The test for IG 1 had four distinct periods of testing: the Background (BG) period, the Air Cleaner (AC) only period, the Air Cleaner/Air Freshener (AC/AF) period, and the Air Freshener (AF) only period. The tests for IG 3, 4, 5A, and 5B did not include the AF period as no particle formation was seen during this phase. During the BG period, the ion generator was not energized and there was no terpene source. During the AC period, the ion generator was energized but there was also no terpene source. During the AC/AF period, the ion generator was energized and a new plug-in air freshener for IG 1 or solid air freshener for IG 3, 4, 5A, and 5B was located approximately 1.5 m from the floor in the center of the chamber. The plug-in air freshener was "Hawaiian" scented and emitted a total mass of 1.5 g day^{-1}, and the solid air fresheners were made to be hung (e.g., in an automobile) and were "country fresh" and "pine" scented. During the AF period, the ion generator was not energized and the air freshener was in the chamber. Each period of the test was conducted for at least four hours to ensure that a steady-state condition was obtained. Additionally, for the IG 1 test, the chamber was operated under the positively pressurized conditions described above for the CADR and ozone emission tests.

For each of the five tests, the resulting steady-state particle concentrations during each period were compared. The steady-state concentrations were calculated as the mean concentrations for the last 20 scans (one hour) during each of the test periods for all but IG 5B, for which the last 12 scans were used. Due to the small sample size and non-equal variance, a modified t-test (Hines and Montgomery, 1990) was used to evaluate if there were statistically significant changes ($\alpha < 0.05$) in steady-state concentrations among the different periods.

Additionally, for the IG 1 experiment, terpene and light aldehyde samples were taken during the last hour of the steady-state periods. Terpenes were sampled onto two Atas glass focus liners packed with Tenax-GR 60/80 mesh sorbent connected in series, at flow rates of between 21.9–23.1 cm^3 min^{-1} for between 33–43 minutes. The terpenes were analyzed by thermal desorption, gas chromatography, with mass spectrometry

(HP5890 GC equipped with Atas Optic 2 thermal desorber and HP5971A mass selective detector), for a total run time of 21 minutes. The focus liners were thermally desorbed by ramping at 10 °C/s from an initial temperature of 45 °C up to a holding temperature of 280 °C. The split ratio for the thermal desorber was 10:1, and a sample transfer pressure of 15 psi was held for 3 minutes before dropping to 7 psi and linearly increasing to 25 psi over the remainder of the run time. A Restek Rtx 5SilMS capillary column was used (30 m length, 0.25 mm internal diameter, 0.5 μm film thickness). The GC oven was held at the initial temperature of 40 °C for 2.5 minutes, after which it was ramped at 10 °C/min up to 150 °C and then 25 °C/min from 150 to 310 °C, at which it was held for 1.1 minutes until the end of the run time. The terpenes were quantified with an internal standard of 1-bromo-4-fluorobenzene. The measurement uncertainty was calculated as the percentage ratio of one standard deviation over the mean of the internal standard variation and was 12%. The light aldehydes were sampled onto dinitrophenylhydrazone (DNPH)-coated silica cartridges preceded by a KI ozone scrubber, at flow rates of between 488–503 cm^3 min^{-1} for between 60–65 min. Batches of DNPH-coated cartridges were prepared based on EPA method TO-11A (US EPA, 1999). Analytes were identified and quantified using dinitrophenylhydrazone standards.

RESULTS AND DISCUSSION

Phase 1: Characterization of portable air cleaners

The electrical power draw (W), air flow rates (m^3 h^{-1}), and a summary of CADR (m^3 h^{-1}) for the five portable air cleaners tested during the first experimental phase are listed in Table 1. The flow rate for IG 2 was not determined because it was below the detection limit of the Duct Blaster calibrated fan (30 m^3 h^{-1}). The ESP had the highest tested flow rate of 850 m^3 h^{-1}, and IG 1 the lowest measurable value of 51 m^3 h^{-1}. The ESP and HEPA 1 and 2 each had flow rates an order of magnitude higher than IG 1, which is expected since they all employ a fan to move air through the unit. These electrical power draw and air flow results are on the same order as others reported in the

literature for similar portable air cleaners (Shaughnessy et al., 1994; Offermann et al., 1995; Mullen et al., 2005).

The reported CADRs, including the minimum, maximum, count average (and standard deviation), and median values, are summarized in Table 1. Reported CADRs for the particle diameter range of 12.6–514 nm are displayed in Figure 1. Both axes of Figure 1 are plotted on a logarithmic scale, and the whiskers represent the calculated uncertainty of the CADR for each size bin.

Table 1. Electrical power draw, air flow rates, and summary of size-resolved (12.6–514 nm diameter) reported CADR values. N is the number of the 104 size bins that met the three CADR reporting criteria described in the Methodology Section.

	Electrical power draw	Air flow rate	Summary of CADR ($m^3 h^{-1}$)				
Air cleaner	(W)	($m^3 h^{-1}$)	Min	Max	Mean	Median	N
ESP	102.2	850 ± 26	111.9	454.7	283.5 ± 61.6	283.1	83
HEPA 1	205.6	309 ± 9.3	92.4	259.3	188.1 ± 30.4	187.9	76
HEPA 2	102.6	571 ± 17	203.4	480.8	324.4 ± 43.7	339.9	75
IG 1	8.4	51 ± 1.5	16.2	75.8	40.7 ± 11.0	39.3	85
IG 2	4.9	< 30	17.0	74.0	35.0 ± 12.7	30.9	71

ESP or HEPA 2 had the highest CADR, depending on the particle size. Overall, the HEPA 2 exhibited the largest count average CADR (± one standard deviation) of 324 (44) $m^3 h^{-1}$. The ESP followed with a count average CADR of 284 (62) $m^3 h^{-1}$, and the ESP also exhibited the largest range of CADR from 112 $m^3 h^{-1}$ for 23.3 nm particles to 455 $m^3 h^{-1}$ for 359 nm particles. The HEPA 1 had higher CADR than both IG 1 and 2, and it exhibited a count average CADR of 188 (30) $m^3 h^{-1}$, which is approximately 100 to 150 $m^3 h^{-1}$ lower than both the ESP and HEPA 2, commensurate with its lower flow rate than the ESP and HEPA 2. IG 1 and 2 both generally had a CADR an order of magnitude lower than the other tested air cleaners, and IG 1 had a count average CADR of 41 (11) $m^3 h^{-1}$ and IG 2 had 35 (13) $m^3 h^{-1}$. Thus, the ESP and HEPA air cleaners removed particles better than ion generators by an order of magnitude.

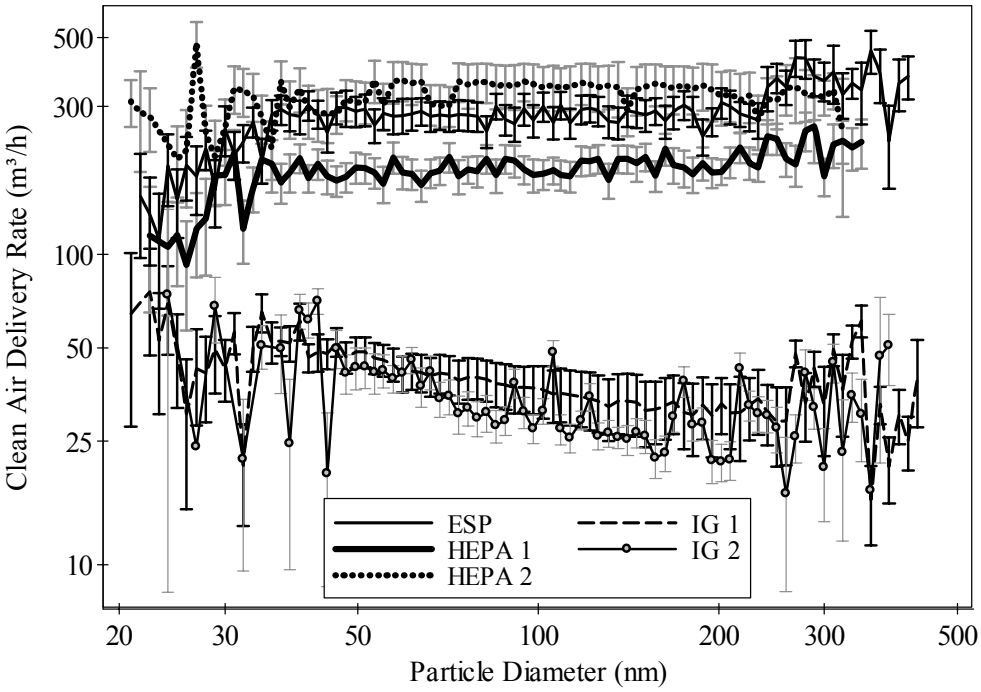

Figure 1. CADR as a function of particle diameter, with both axes plotted on log-scales.

The single-pass efficiency, η (--), of the air cleaners is plotted in Figure 2. These efficiency curves are the efficiencies of the air cleaners, not the filtration media. The HEPA air cleaners and ESP each have efficiencies of approximately less than 0.6 (60%) for particle sizes of less than 200 nm and start to increase slightly above 200 nm. These low efficiencies are perhaps unexpected for the HEPA air cleaners, which have filter efficiencies of at least 99.97% for all particle sizes. This reduced air cleaner efficiency is likely due to bypass of air around the filter media or the unit itself. It could also be due to short-circuiting of air flow in the chamber (i.e., it is not well-mixed), but we attempted to reduce this effect by operating three fans on their highest setting in the chamber. IG 1 exhibited efficiencies of greater than one for some particle sizes, potentially because ions emitted into the space can lead to particle reductions greater than the air flow capacity of the device. However, the CADRs, one of two components in the efficiency calculation, have large uncertainty in the upper and particularly lower size bins of the measured range

(Figure 1). The efficiency for IG 2 was not determined since its flow rate could not be measured.

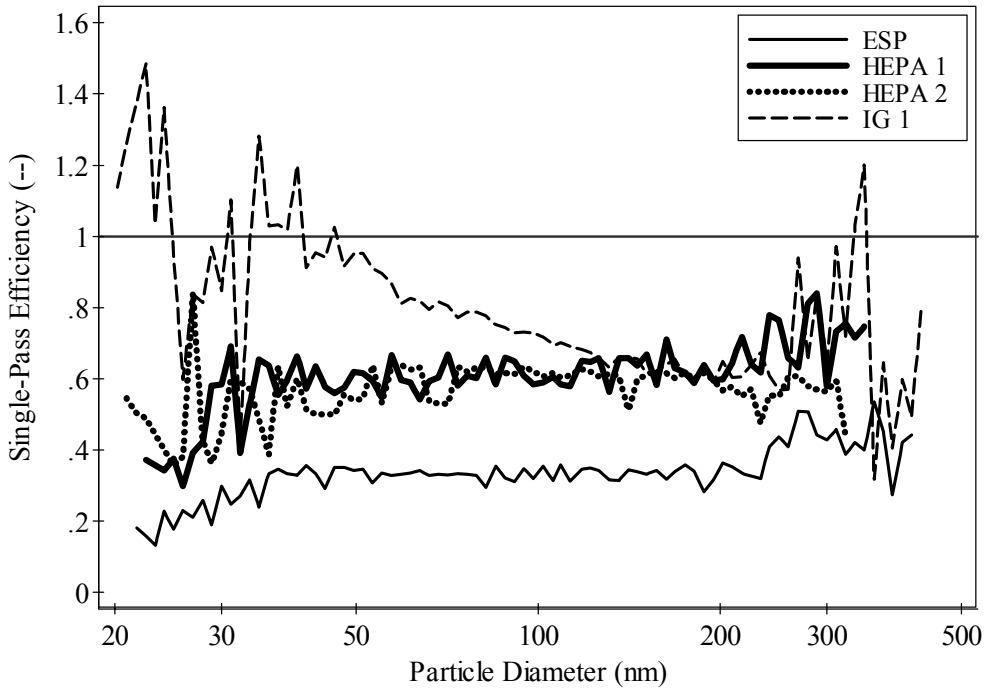

Figure 2. Efficiency as a function of particle diameter, with the x-axis plotted on a log-scale. The efficiency for IG 2 was not determined because its flow rate was below the detectable limit (30 m^3 h^{-1}).

The influence of a particular air cleaner on particle concentrations in a given space may be quantified by the air cleaner effectiveness. Miller-Leiden et al. (1996) defined the air cleaner effectiveness, H (--), as one minus the ratio of the indoor particle concentration with an operating air cleaner (C_{AC}) to the indoor concentration with no air cleaner operating ($C_{No\,AC}$), as in Equation 1:

$$H = 1 - \frac{C_{AC}}{C_{No\,AC}} = 1 - \frac{\lambda + \beta_P}{\lambda + \beta_P + \frac{CADR}{V}} \quad (1)$$

where λ is the air exchange rate of the space (h^{-1}), and β_p is the size-resolved particle deposition loss rate (h^{-1}). The air cleaner effectiveness is bounded by zero and one, with zero indicating a completely ineffective air cleaner (0% of the particles are removed) and one indicating a perfectly effective air cleaner (100% of the particles are removed). The air cleaner effectiveness assumes steady-state and a well-mixed space, neglects removal by the HVAC system, is independent of indoor sources (so long as they are the same for both C_{AC} and $C_{No\,AC}$), and is highly dependent on the volume of the space. For Equation 1, we assumed an air exchange rate of 0.5 h^{-1}, which is the median air exchange rate of 2,844 residences reported in Murray and Burmaster (1995), and used the predicted fit to experimental values for β_P as summarized by Riley et al. (2002). Figure 3 displays the air cleaner effectiveness of each of the five tested air cleaners as a function of particle diameter, for a typical (a) 50 m^3 room and (b) 392 m^3 residential house. The room volume of 50 m^3 was assumed, and the residential house volume of 392 m^3 is the median floor area from the U.S. Bureau of the Census (2005) of 163.3 m^2 multiplied by an assumed ceiling height of 2.4 m.

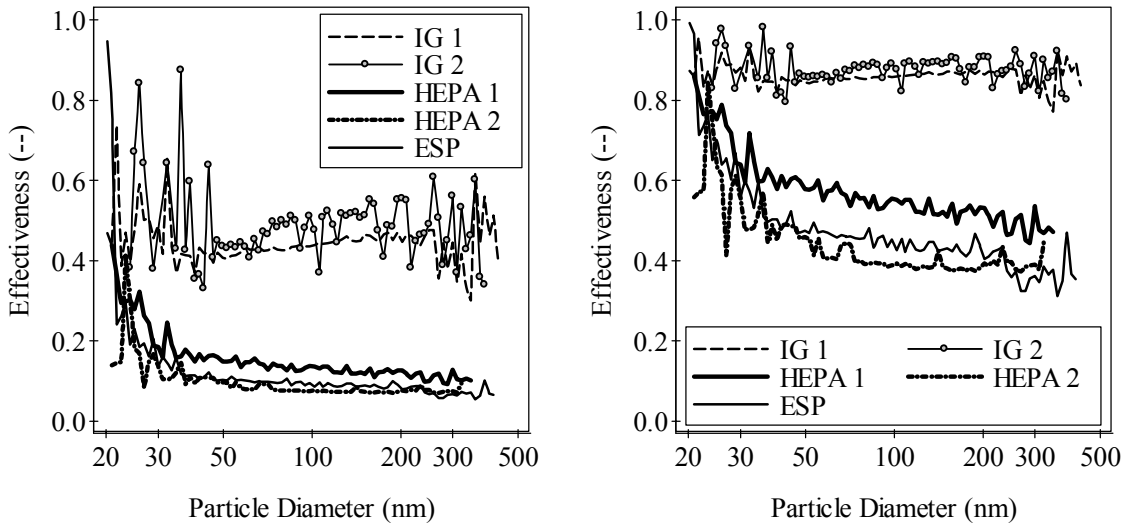

Figure 3. Air cleaner effectiveness, Γ, as a function of particle diameter, with the x-axes on log-scales, for a hypothetical (a) 50 m^3 room and (b) 392 m^3 residential building.

The HEPA air cleaners and the ESP are more effective at removing particles in the tested range than either IG 1 or 2, as indicated in Figure 3. In the typical 50 m^3 room, the HEPA air cleaners and the ESP remove approximately 80–90% of particles with diameters above 50 nm. The IG 1 and 2 only remove 40–60% of the same size particles. In the 392 m^3 residential home, the HEPA air cleaners and the ESP remove approximately 40–60% of particles with diameters above 50 nm. However, the IG 1 and 2 have little effect on particle concentrations in the median-sized home, removing only 10–20% of particles in the same size range.

Results from the ozone emission tests for the three portable air cleaners found to emit ozone, the ESP and IG 1 and 2, are listed in Table 2. The ozone emission rates ranged from 3.3–4.3 mg h^{-1}. This range is comparable to the emission rates reported by Niu et al. (2001) and Tung et al. (2005) for portable ionizers. Overall, no clear relationship between CADR and ozone emission was observed, as IG 2 emitted the most ozone but had the lowest CADR, and the ESP emitted nearly the same amount and had the highest CADR. However, the ESP also utilized an activated carbon filter which removed some of the ozone it generated.

One way to quantify the impact of these ozone emissions, E, on the previously discussed hypothetical spaces with volumes, V, of 50 and 392 m^3, respectively, is with the predicted indoor ozone concentration increase due to the device, C^* (ppb), as in Equation 2:

$$C^* = \frac{E/V}{\lambda + \beta_{O3}} \tag{2}$$

where the air exchange rate, λ, was again assumed as 0.5 h^{-1} (Murray and Burmaster, 1995), and the ozone deposition loss rate, β_{O3}, was assumed as 4.0 h^{-1}, which is an experimentally determined value for offices and bedrooms (Weschler, 2000). The indoor ozone concentration increases for each volume are also listed in Table 2. These predicted increases are significant, particularly for the smaller room, given that a recent epidemiological study found that a 10 ppb increase in the outdoor ozone concentration of the previous week was associated with a 0.52% increase in daily mortality (Bell et al.,

2004). Moreover, 89% of the ozone removal ($\lambda + \beta_{O3}$) is due to surface reactions (β_{O3}), which may yield byproducts more harmful than the ozone itself (Weschler, 2004).

The equivalent outdoor ozone concentration increase, ΔC_{out} (ppb), is the amount the outdoor concentration of ozone would need to increase to equal the predicted indoor ozone concentration increase due to the ozone emitting device, as in Equation 3:

$$\Delta C_{out} = \frac{E/V}{p\lambda} \tag{3}$$

where p, the ozone penetration factor (dimensionless), was assumed as unity due to the lack of values for this parameter in the literature. The equivalent outdoor ozone increases for the two hypothetical spaces are also listed in Table 2. Caution must be used in interpreting C^* and ΔC_{out} for the 50 m^3 volume, since a volume of this size would likely be connected to other parts of the building.

Table 2. Ozone emission rates for the ionizers in phase one, as well as predicted ozone concentration increases, C^*, and equivalent outdoor ozone increases, ΔC_{out}, for a hypothetical residential 50 m^3 room and 392 m^3 home.

		V = 50 m^3		V = 392 m^3	
Air cleaner	Ozone emission rate (mg h^{-1})	C^* (ppb)	ΔC_{out} (ppb)	C^* (ppb)	ΔC_{out} (ppb)
ESP	3.8 ± 0.19	8.6	150	1.1	19
IG 1	3.3 ± 0.16	7.5	130	1.0	16
IG 2	4.3 ± 0.20	9.7	170	1.2	21

Phase 2: Ion generators in the presence of a terpene source

A summary of chamber conditions and results from the second phase are listed in Table 3. The air exchange rates were 0.49–0.96 h^{-1}. The mean steady-state ozone concentration for IG 1 during the BG period of 0.1 ppb is near zero since ozone was intentionally removed from the chamber supply air by activated carbon. The five energized ion generators during the AC period elevated the ozone concentrations significantly ($\alpha < 0.05$) over the corresponding BG period concentration. The reactions between the ozone and the terpenes during the AC/AF period each resulted in a

significant ($\alpha < 0.05$) reduction from the corresponding AC period ozone concentration. During the AF period for IG 1, the ozone-emitting ion generator was not energized, so the chamber returned to a low ozone concentration. The concentration during the AF period did not return completely to the BG period concentration likely due to interference between compounds emitted by the air freshener and the ozone monitor. Because of this effect, there is likely a small bias in the AC/AF period ozone concentration results as well.

Table 3. Summary of air exchange rates (λ), mean (s.d.) temperature and relative humidity (RH) over all periods, as well as steady-state ozone and total (measured range of 4.61–157 nm diameter) particle number concentrations, for the second phase. BG is Background period, AC is Air Cleaner only period, AC/AF is Air Cleaner/Air Freshener period, AF is Air Freshener only period. The "size range with net formation" is the range of particles over which there was a statistically significant ($P < 0.05$) increase in concentrations of the AC/AF period over the BG period.

Air Cleaner	λ (h^{-1})	Temp. (°C)	RH (%)	Ozone (O_3) and total particle (PM) steady-state concentrations	BG	AC	AC/AF	AF	Size range with net formation (nm)
IG 1	0.87	25.9 ± 0.5	46.4 ± 1.7	O_3 (ppb)	0.1[b]	92.3	16.6	4.8	21.7–157
Liquid plug-in, "Hawaiian" scent				PM (cm^{-3})	114.5	145.4	1135	140.4	
IG 3[a]	0.91	26.2 ± 0.2	54.3 ± 1.5	O_3 (ppb)	22.7	46.2	9.9	n/a	4.6–157
Solid hanging, "pine" scent				PM (cm^{-3})	213.0	136.7	2545	n/a	
IG 4	0.96	27.3 ± 0.3	52.1 ± 1.3	O_3 (ppb)	10.5	44.8	11.7	n/a	20.9–157
Solid hanging, "country fresh" scent				PM (cm^{-3})	305.2	130.5	650.3	n/a	
IG 5A	0.54	26.9 ± 2.6	49.1 ± 1.6	O_3 (ppb)	10.7	117.7	19.2	n/a	9.5–55.2
Solid hanging, "pine" scent				PM (cm^{-3})	501.8	152.3	1569	n/a	
IG 5B[a]	0.49	27.0 ± 0.4	47.1 ± 2.0	O_3 (ppb)	10.0	115.7	18.2	n/a	9.47–38.5
Solid hanging, "pine" scent				PM (cm^{-3})	250.8	200.1	886.6	n/a	

[a]Temperature and RH were measured during BG period only.
[b]Ozone monitor uncertainty was the greater of 1 ppb or 2%.

The resulting particle total (4.61–157 nm diameter) number concentrations measured during the steady-state periods for all five ion generator tests are listed in Table 3. For every test but IG 1, the steady-state particle concentrations were higher during the

BG period than the AC period when the ion generator was energized. Steady-state particle concentrations during the AC/AF period were much higher than either the BG or AC period for all five ion generators, higher than the BG period by a factor of 2–12 and the AC period by a factor of 4–19. For IG 1, the steady-state particle concentration during the AF period was much lower than the AC/AF period by a factor of eight and on the same order as those during the BG and AC periods. Thus, our screening experiments demonstrate a *net increase* in steady-state particle concentrations due to the use of an ion generator in the presence of a terpene source.

Additionally, the particle size range with net formation, which is the range of measured particle size bins for which there was a statistically significant ($\alpha < 0.05$) increase in the particle number concentration of the AC/AF period over the BG period, is presented in Table 3. IG 1, 3, and 4 showed significant increases in nearly the entire range of investigated particles, and IG 5A and 5B showed significant increases in the range of approximately 10 nm to between 39–55 nm.

The steady-state particle number concentrations as a function of particle diameter during the BG, AC, AC/AF, and AF periods for the IG 1 test are displayed in Figure 4a. Results for IG 3 and 4 exhibit similar trends, but results for IG 5A and 5B display elevated concentrations during the AC/AF period for the narrower particle size range. The change in concentrations for five particle size bins as a function of time is displayed in Figure 4b. After the air freshener was introduced to the chamber (the vertical line on the plot), the particle concentrations initially increased sharply and then declined to their steady-state values. Similar growth patterns were also seen for the other experiments, as well as those of other researchers (e.g., Weschler and Shields, 1999). The final steady-state concentrations are controlled principally by the competition between the source of particles due to ozone/terpene reactions and the loss of particles due to removal by the ion generator and air exchange.

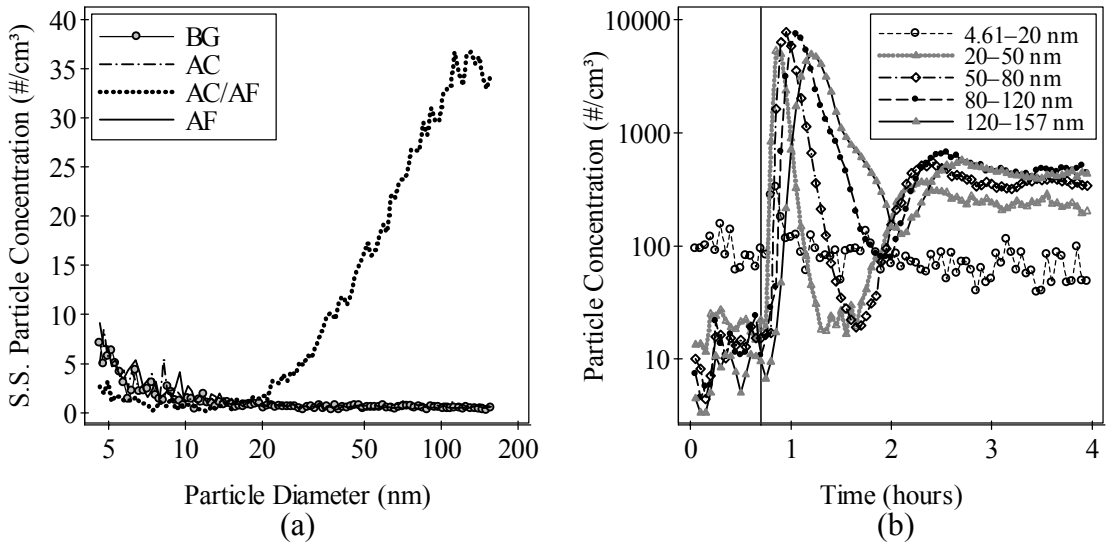

Figure 4. For IG 1 during the second phase, (a) steady-state particle concentrations as a function of particle diameter (x-axis on a log-scale), and (b) particle concentrations as a function of time (y-axis on a log-scale) after the plug-in liquid air freshener was energized (represented by the vertical line on the plot). BG is Background period, AC is Air Cleaner only period, AC/AF is Air Cleaner/Air Freshener period, AF is Air Freshener only period.

The resulting steady-state concentrations of terpenes and light aldehydes during the steady-state periods for the IG 1 test are listed in Table 4. The d-limonene measured during the BG period was likely reduced to below the detection limit during the AC period because it reacted with the ozone emitted by IG 1. This SOA forming reaction may be why for IG 1 the total number of particles for the AC period was elevated over the BG period (see Table 3). The chief terpene emitted by the plug-in liquid air freshener was also d-limonene, and its concentration was elevated during the AC/AF period and then further increased during the AF period. β-Myrcene was also emitted by the air freshener, though at a much lower rate, and this terpene was only detectable during the AF period. The ozone/d-limonene reaction is likely primarily responsible for particle formation observed during the IG 1 test. d-Limonene is a common terpene found indoors (Brown et al., 1994), is a citrus scent in commercial products and an active ingredient in some organic solvents, and readily reacts with ozone to yield particles (Weschler and Shields, 1999).

Table 4. Steady-state light aldehyde and terpene concentrations during the IG 1 test. BG is Background period, AC is Air Cleaner only period, AC/AF is Air Cleaner/Air Freshener period, AF is Air Freshener only period. b.d. represents below the detectable limit of the GC/MS

	Steady-state concentrations ($\mu g/m^3$)			
Compound	BG	AC	AC/AF	AF
Terpenes				
d-Limonene	1.4 ± 0.2	b.d.	81.9 ± 9.8	94.6 ± 11.4
β-Myrcene	b.d.	b.d.	b.d.	2.7 ± 0.3
Light aldehydes				
Formaldehyde	17.6 ± 2.8	19.3 ± 2.8	49.3 ± 3.9	45.9 ± 2.7
Acetaldehyde	14.4 ± 0.5	22.4 ± 0.4	14.6 ± 0.4	9.4 ± 0.5

Without the air freshener, the use of the ion generator increased the formaldehyde concentration during the AC period. In the presence of the air freshener, the use of the ion generator during the AC/AF period increased formaldehyde concentrations slightly over that during the AF period. The high formaldehyde concentration observed during the AF period could be the result of ozone or formaldehyde diffusion into the liquid air freshener during the AC/AF period. No clear trend was observed for acetaldehyde, as observed by others conducting research on the products of ozone and air fresheners (Singer et al., 2006).

One limitation regarding the second phase screening experiments is that the application of these results to real indoor environments is dependent on there being similar ozone and terpene concentrations, which might differ for the following reasons. Indoor volumes are typically larger, diluting the influence of the ozone and terpene emissions. There is a much larger surface-to-volume ratio (S/V) indoors than in the chamber, and the multitude of indoor surfaces, including carpeting and other furnishings, compete with terpenes as ozone reaction sites (e.g., Weschler et al., 1992). Additionally, there may be indoor particle sources that compete in magnitude with the secondary emissions due to the use of an ion generator, diminishing the effect of the SOA formation. Large indoor sources of formaldehyde might have the same effect. Additional tests are being conducted in real indoor settings to address these concerns.

However, these results do demonstrate that ozone-emitting ion generators can generate ultrafine and fine particles, as well as gas-phase byproducts, when operated in the presence of a terpene source.

CONCLUSIONS

A two-phase investigation was performed to assess the magnitude of indoor pollutant removal and generation due to the use of a portable air cleaner. The tested HEPA filters and ESP remove particles much more effectively than the ion generators. For the measured particle diameter range of 12.6–514 nm, the two HEPA air cleaners had count average CADR (± one standard deviation) of 188 (30) and 324 (44) $m^3\ h^{-1}$; the electrostatic precipitator 284 (62) $m^3\ h^{-1}$; and the two ion generators 41 (11) and 35 (13) $m^3\ h^{-1}$. The three tested ionizers, the ESP and the two ion generators, emitted ozone at rates of 3.3–4.3 mg h^{-1}.

Ozone emitted by ion generators can react with terpenes to produce secondary organic aerosol (SOA) in the ultrafine and fine size ranges. The five tested ion generators acted as *steady-state net particle generators* under the experimental conditions in the test chamber. The measured range of particle diameters was 4.61–157 nm, and three of the five ion generators acted as steady-state net particle generators in nearly the entire measured range, and two ion generators in the range of approximately 10 to 39–55 nm. The benefits of using an ozone-emitting ion generator indoors may be outweighed by its particle, ozone, and aldehyde generation.

In summary, this investigation suggests caution in the use of ozone-emitting ion generators in indoor environments. Furthermore, technologies do exist, such as the portable HEPA filters tested here, that are effective at particle removal and do not generate ozone or other harmful byproducts.

ACKNOWLEDGEMENTS

This research was funded by the International Society for Exposure Assessment (ISEA)/American Chemistry Council (ACC) Early Career Award and by Consumers Union. Michael S. Waring's contribution was also funded by an NSF IGERT traineeship (Award #0549428).

Appendix B

PAPER II

The Effect of an Ion Generator on Indoor Air Quality in a Residential Room

(Submitted to *Environmental Science and Technology*)

ABSTRACT

Portable air cleaners are popular devices that are often used to improve indoor air quality. Ion generators, one prominent air cleaning technology, emit ozone as a byproduct of their operation. Ozone emitted by ion generators can react with terpenes and other unsaturated organic compounds to yield ultrafine and fine particles, carbonyls, carboxylic acids, and free radicals. This investigation experimentally characterizes the indoor air quality implications of operating an ion generator in a 27 m^3 residential room, with four different test room configurations. Two of the room configurations had carpet (a likely ozone sink) overlaying the original floor of stained/sealed concrete, and for one configuration with and without carpet, a plug-in air freshener was used as a source of terpenes. Measurements included airborne sampling of size-resolved particulate matter (0.015–20 μm), terpenes and C_1–C_4 and C_6–C_{10} aldehydes, ozone concentrations, and air exchange rates. The use of ion generators in the presence of the air freshener lead to a net increase in ultrafine particles (< 0.1 μm). Increased concentrations of ozone, formaldehyde, and nonanal were also byproducts of ion generator use, whether or not the air freshener was present. Carpet increased the surface reactivity of the room with ozone. This research suggests that the operation of ion generators can degrade indoor air quality, and that their use in occupied environments should likely be avoided.

INTRODUCTION

Exposures to ultrafine (< 0.1 μm) and fine (0.1–2.5 μm) particles have been associated with adverse health effects (Pope and Dockery, 2006; Pekkanen et al., 2002). Portable air cleaners are designed to remove particles from the indoor air, where a

significant portion of exposure may occur because the average American spends 18 hours indoors for every hour outdoors (Klepeis et al., 2001). Portable ion generators are marketed as air cleaners, and their intended purpose is to clean the air of particles by charging them with a corona before removal to collector plates or indoor surfaces. Portable ion generators can be set on a floor or table-top and are meant to clean a room-sized space. The particle removal capability of an ion generator can be quantified with the clean air delivery rate (CADR), which is the effective volumetric flow rate of particle-free air delivered by an air cleaner (m^3/h). CADR for portable ion generators range 0–90 m^3/h (Offermann et al., 1985; Niu et al., 2001a; Mullen et al., 2005; Waring et al., 2008), an order of magnitude less than high efficiency particulate air (HEPA) cleaners (Offermann et al., 1985, Mullen et al., 2005; Waring et al., 2008).

The use of a corona causes ion generators to emit ozone as a byproduct of operation, at measured rates of 0.056–13.4 mg/h (Niu et al., 2001a, 2001b; Mullen et al., 2005; Tung et al., 2005; Britigan et al., 2006; Waring et al., 2008). These rates are lower than dedicated ozone generators but still affect indoor ozone concentrations (Waring et al., 2008; Britigan et al., 2006). Ozone is deleterious to human health (Bell et al., 2004; Weschler, 2006), and it is also a primary driver of indoor chemistry (Weschler, 2000). The largest loss mechanism of ozone indoors is by surface reactions (Sabersky et al., 1973), which can lead to secondary emissions of carbonyls (Wang and Morrison, 2006). For instance, ozone reacts with unsaturated fatty acids in carpets to form nonanal (Morrison and Nazaroff, 2000). Ozone can also react in the gas-phase with terpenes and other unsaturated organics to form secondary organic aerosol (SOA) in the ultrafine and fine particle size ranges (Weschler and Shields, 1999, 2003 ; Wainman et al., 2000; Rohr et al., 2003; Sarwar et al., 2003, 2004; Hubbard et al., 2005; Sarwar and Corsi, 2007; Vartiainen et al., 2006; Destaillats et al., 2006; Singer et al., 2006; Alshawa et al., 2007; Zuraimi et al., 2007; Coleman et al., 2008; Langer et al., 2008), as well as carbonyls, carboxylic acids, and free radicals. Terpenes are common indoor hydrocarbons and are emitted indoors from wood materials (Baumann et al., 1999a; Saarela, 1999) and

consumer products such as air fresheners, surface cleaners, and perfumes (Nazaroff and Weschler, 2004; Singer et al., 2006; Corsi et al., 2007).

Since ion generators are generally not very effective at removing particles and emit ozone during operation, they can operate as net producers of particles and gaseous pollutants in the presence of terpenes. Alshawa et al. (2007) operated an ion generator in an office, injected d-limonene into the air, and observed transient elevations of ultrafine particle concentrations. Other studies report the particle forming effects of dedicated ozone generators, which often emit more than 30 mg/h of ozone, in real environments with terpenes (e.g. Weschler and Shields, 1999, 2003; Hubbard et al., 2005). Also, we observed steady-state net particle and formaldehyde formation when ion generators were operated in a 14.75 m^3 stainless steel chamber with terpene-emitting air fresheners (Waring et al., 2008). The purpose of this study was to extend this chamber investigation to a residential space, since real indoor spaces have larger volumes and surface-to-volume ratios, as well as other sources and sinks of particles, ozone, and carbonyls. The goal of this study was to determine the impact of using a portable ion generator on indoor air quality in a room, and to explore the role of ozone sinks and elevated terpene concentrations.

METHODS

Experimental room configurations and setup

Field experiments were performed in a 27 m^3 unoccupied room, located in an approximately 475 m^3 three-floor duplex town home in Austin, Texas. The room was furnished with a futon, bookshelf, desk with a computer, television, and curtains covering a sliding glass door to outdoors. The walls and ceiling were painted with flat latex paint, and the flooring was sealed/stained concrete. A single heating, ventilating, and air-conditioning (HVAC) supply duct conditioned the room. The HVAC system was operated for two different periods each day. The HVAC system cycled normally from 9

a.m. to 11 p.m. and was turned off overnight from 11 p.m. to 9 a.m.. A ceiling fan was operated continuously throughout the testing on its lowest setting to aid in air mixing.

The room air was sampled in four different Room Configurations (RC).

- RC 1: Original flooring of sealed/stained concrete, without air freshener
- RC 2: Installed flooring of carpet with padding, without air freshener
- RC 3: Original flooring of sealed/stained concrete, with air freshener
- RC 4: Installed flooring of carpet with padding, with air freshener

Tests were conducted for two-day-long test periods, starting and stopping at approximately 12 p.m. At least one two-day-long test was conducted per room configuration without and with an ion generator operating on its highest setting, located in the center of the room. At least one full day occurred between each test configuration, and during that rest period, extra fans were used to help flush the room. The air freshener served as a terpene source and was a "Hawaiian" scented plug-in liquid air freshener operated on its highest setting. One liquid cartridge was used for each room configuration, and the total emission rate was 1.5 g/day, which was determined by mass difference between each test. The ion generator was a tower model with collector plates and no fan and was cleaned according to manufacturer instructions between each test. It had an ozone emission rate of 3.3 ± 0.2 mg/h, a mean CADR (± one s.d.) for particles 12.6–514 nm diameter of 41 (11) m^3/h, and was IG 1 in our previous work (Waring et al., 2008).

Continuous measurements

Instruments were located within the room itself, and all samples were taken near the center of the room, 2 m from the floor. Indoor temperature and relative humidity (RH) were monitored (TSI Q-Trak 8551) as well as the temperature (Onset HOBO U12) at the supply duct register, which indicated when conditioned air was supplied to the room. Air exchange rates (h^{-1}) were measured (Lagus Autotrac ATGM) by the decay of sulfur hexafluoride (SF_6), and were calculated as the best fit slope of the negative of the natural log of the ratio of the time-varying concentration of SF_6 to the initial

concentration versus time. The ozone monitor (2B Technologies 205) drew indoor samples through 3 m of 6 mm OD Teflon tubing, averaged over one minute. Hourly outdoor ozone concentrations were taken from a monitoring station approximately 9 km from the residence. Indoor size-resolved particle concentrations were measured in the range of 0.015–0.661 μm diameter with a scanning mobility particle sizer (TSI SMPS 3936L85) and in the range of 0.542–20 μm diameter with an aerodynamic particle sizer (TSI APS 3321), both every five minutes.

VOC sampling and analysis

Integrated gas-phase samples were taken early each morning, between 1 and 3 a.m. Light aldehydes (C_1–C_4) were sampled onto focus liners packed with dinitrophenylhydrazine (DNPH) coated silica gel, with a potassium iodide (KI) ozone trap (SKC 226-120). Sample flow rates were 0.5 L/min and sample volumes 30 L. The DNPH-filled focus liners were prepared based on EPA method TO-11A (U.S. EPA) and analyzed with high pressure liquid chromatography (Waters 600). Heavy aldehydes (C_6–C_{10}) and terpenes were sampled onto Tenax-GR-filled focus liners (Atas A100094). Samples were collected without ozone scrubbers, since indoor ozone concentrations were always below 15 ppb and ozone scrubbers can degrade measurement quality. Sample flow rates were 21 mL/min and sample volumes 1.3 L. Heavy aldehydes and terpenes were analyzed with thermal desorption followed by gas chromatography with mass spectrometry (HP5890, HP5971A), and quantified using an internal standard of 1-bromo-4-fluorobenzene, with an experimental uncertainty of 10%. The method is further outlined in our previous work (Waring et al., 2008).

RESULTS

Test information and environmental conditions

Test information and a summary of the room environmental conditions for each test is presented in Table 1. Twelve two-day-long tests were completed, with four of the

twelve tests as experimental replicates. Each two-day-long test was assigned a unique test ID: the first number corresponds to the room configuration, the second letter corresponds to no ion generator (N) or ion generator (I) present, and the last number the test iteration. Mean temperature and RH while the HVAC was cucle across all tests were 28.0 (0.8) °C and 46 (2)%, respectively. Mean temperature and RH during the HVAC Off period across all tests were 28.7 (0.9) °C and 49 (2)%, respectively.

Table 1. Room environmental conditions for each two-day test. Italicized air exchange rates were calculated with less than 10 data points and are estimates.

						HVAC Cycle (9am-11pm)		HVAC Off (11pm-9am)			
Room Config.	Floor	Terpene Source	IG[a]	Test ID[b]	Dates of Test[c]	T[d](sd) [°C]	RH[e](sd) [%]	T[d](sd) [°C]	RH[e](sd) [%]	λ_{cycle}[f] [h^{-1}]	λ_{off}[g] [h^{-1}]
RC 1	Stained/ sealed concrete	None	No	1-N1	May 22-24	-	-	27.9 (0.8)	55 (2)	-	0.62, 0.65
				1-N2	June 14-16	27.4 (0.6)	47 (3)	28.0 (0.4)	51 (3)	1.5	0.55, *0.58*
			Yes	1-I1	June 5-7	27.4 (0.7)	51 (3)	27.7 (0.2)	48 (1)	1.2	*0.75*
				1-I2	June 18-20	27.9 (0.5)	47 (3)	28.7 (0.3)	48 (2)	1.4	0.51, *0.55*
RC 2	Carpet	None	No	2-N1	June 27-29	27.6 (0.7)	48 (2)	28.6 (0.5)	52 (2)	1.1	*0.52*
			Yes	2-I1	July 1-3	28.4 (0.6)	47 (2)	29.2 (0.2)	49 (1)	1.3	*0.51*
RC 3	Stained/ sealed concrete	Air freshener	No	3-N1	July 31-Aug. 2	27.2 (0.5)	47 (2)	28.1 (0.4)	50 (2)	0.7	*0.18*
				3-N2	Aug. 9-11	27.7 (0.5)	44 (1)	28.7 (0.3)	47 (2)	1.2	0.32, *0.68*
			Yes	3-I1	Aug. 4-6	27.5 (0.6)	46 (2)	28.4 (0.5)	49 (2)	1.2	0.40, *0.66*
				3-I2	Aug. 6-8	28.0 (0.4)	44 (1)	28.8 (0.4)	47 (1)	1.5	0.51, *0.66*
RC 4	Carpet	Air freshener	No	4-N1	July 7-9	29.3 (0.6)	46 (2)	30.1 (0.4)	48 (2)	1.4	*0.69*
			Yes	4-N2	July 10-12	29.5 (0.5)	42 (1)	30.6 (0.5)	45 (1)	1.9	0.44, *0.63*

[a]Ion generator; [b]Test ID: the first number = Room Configuration, the second letter = ion generator (N) or ion generator (I), and the last number = experimental iteration. [c]Experiments started and stopped at approximately 12 p.m.; [d]Temperature; [e]Relative humidity; [f]Air exchange rate during HVAC Off duration; [g]Air exchange rate during HVAC Cycle duration.

Air exchange rates were measured while the HVAC system was cycling (λ_{cycle}) and turned off (λ_{off}). At least one type of air exchange rate was measured for each two-day-long test except 1-N1, during which the HVAC system remained off. Italicized air exchange rates were calculated with less than 10 data points and should be regarded as

approximations. For all experiments, the mean λ_{cycle} was 1.3 (0.3) h^{-1} and λ_{off} was 0.5 (0.1) h^{-1}. The predominate terpene emitted from the air freshener was d-limonene. Mean d-limonene concentrations without and with an ion generator, respectively, for RC 1 were 10 (9.1) and 8.7 (8.1) ppb, for RC 2 were 2.6 (0.56) and 6.7 (3.7) ppb, for RC 3 were 53 (10) and 39 (4.4) ppb, and for RC 4 were 46 (5.4) and 38 (3.3) ppb.

Typical results

As an example of typical results, Figure 1 displays the continuous particle and ozone concentrations for (a) day-one of test 3-N1 and (b) day-one of test 3-I2. These results represent typical days of testing in RC 3, which had sealed/stained concrete flooring and an air freshener. The particle concentrations are on a log-scale and on the left side of the y-axis, and the ozone concentrations are on a linear scale and on the right side of the y-axis. Particle concentrations are plotted in four bins, in the ranges of 0.015–0.05, 0.05–0.1, 0.1–0.533, and 0.542–2.5 μm. The first three bins were measured by the SMPS and the fourth bin by the APS. The first two bins display ultrafine concentrations, which are the size range most affected by SOA formation in this study (discussed below), and the third and fourth bins display fine particle concentrations. Particles greater than 2.5 μm typically had concentrations on the order of 0.01–0.1 #/cm^3 and are not reported. Since ozone concentrations were taken from a monitoring station 9 km away, they should be regarded as an estimate of the outdoor concentration. The HVAC Off time (11 p.m. to 9 a.m.) is labeled and demarcated by vertical lines on the plots.

In RC 3, the air freshener is a source of d-limonene, and Figure 1 shows SOA formation, (a) without and (b) with the ion generator present. In Figure 1a, the highest particle concentrations occur at approximately 3 p.m. when the HVAC system was cycling. These higher particle concentrations occur concurrently with elevated outdoor and indoor ozone concentrations, and their source is likely both SOA formation and infiltration of outdoor particles. The lowest particle concentrations are at night while the HVAC system was off. However, Figure 1b shows that with the ozone-emitting ion generator present, the trend is reversed. At approximately 6 p.m., particle concentrations

for particles of less than 0.1 µm began to rise. Then right after 11 p.m., near the start of the HVAC Off period, concentrations rose more sharply and continued to climb, not reaching steady-state by the time the HVAC system switched on at 9 a.m.

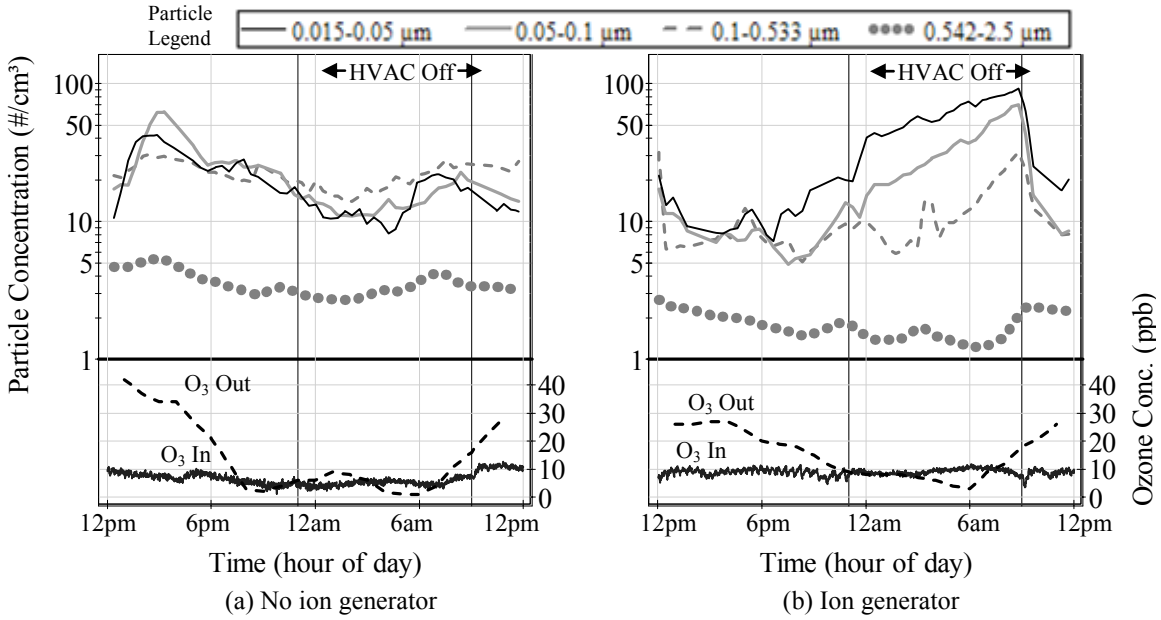

Figure 8. Typical indoor particle number and indoor and outdoor ozone concentrations versus time in a 27 m^3 test room, (a) without and (b) with an ozone-emitting ion generator operating (ozone emission rate = 3.3 ± 0.2 mg/h). The test room door was closed, and the room had a sealed/stained concrete floor and an air freshener present (Room Configuration 3). The HVAC system cycled on/off from 9 a.m. to 11 p.m. and was off from 11 p.m. to 9 a.m. (labeled on the plot).

These particle increases are most likely due to SOA formation from ozone emitted by the ion generator reacting with d-limonene. The size range of 0.1–0.533 µm are the most likely particles to penetrate the building envelope (Liu and Nazaroff, 2001; Long et al., 2001), but this size range increased less than smaller size ranges, indicating the particles are unlikely of outdoor origin. The SOA formation is not likely due to terpene/ozone reactions with ozone of outdoor origin, since outdoor concentrations approached zero during the HVAC Off period. The measured concentrations of d-limonene for (a) day-one of test 3-N1 was 49 ppb and (b) day-one of test 3-I2 was 36

ppb, implying that on the order of 10 ppb of d-limonene reacted with ozone emitted by the ion generator. Detectable SOA formation occurred while the HVAC system was off because the air exchange rate decreased from λ_{cycle} to λ_{off}, increasing the residence time of ozone, terpenes, and their reaction products. After the air exchange rate decreased, the SOA formation rate was high enough relative to the particle loss rate (removal by air exchange, deposition, and the ion generator) to yield SOA formation.

Summary of all results

Figure 2 displays a summary of the effects of operating an ion generator in all room conditions. The solid lines separate the mean results into the four different room configurations, and within those, the dashed lines separate the results into no operation (N) and operation (IG) of an ion generator. Figure 2 shows the means for particle, ozone, formaldehyde, and nonanal room concentrations, for results during periods when the HVAC system was turned off. The ion generator had a negligible effect on concentrations of other sampled compounds. It is most appropriate to compare the effect of the ion generator while the HVAC was off as this coincided with the periods of lowest outdoor ozone concentrations, lowest air exchange rates, and least occupant activity in the home. Displayed particle concentrations are the mean of all results from 4 to 6 a.m., which was chosen to be as near the end of the HVAC Off period as possible before particles associated with the morning rush hour may have influenced concentrations on some test days. Ozone concentrations are the mean of results for all experiments at a given room condition with the HVAC system off, since ozone reached steady-state within about an hour of the change from λ_{cycle} to λ_{off}. Formaldehyde and nonanal concentrations are the integrated results from the sample times (1 to 3 a.m.) averaged across all measurements at a given room configuration.

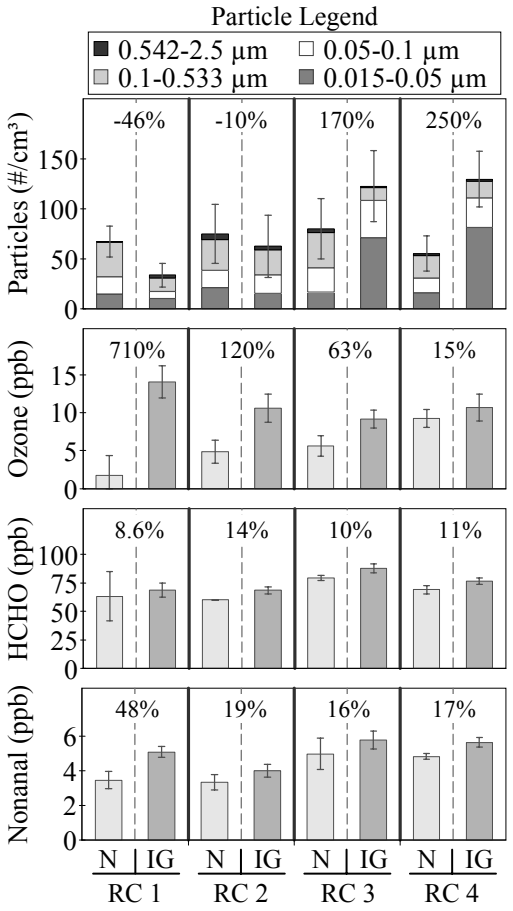

Figure 9. Summary particle, ozone, formaldehyde (HCHO), and nonanal concentrations in the four Room Configurations (RC 1–4), for tests without (N) and with (IG) an operating ion generator. Error bars represent one standard deviation from the mean. Percentages are % differences for each room configuration, and positive % differences indicate the ion generator increased concentrations.

The data displayed in Figure 2 were chosen as follows. For all pollutants, the second day of the 1-N1 experiment was discarded because the HVAC system was not shut off as intended. For particle samples, the first day of the 1-N2 experiment was discarded because a car was pulled into the attached garage right before the HVAC system was turned off, which coincided in time with a large increase of particles that persisted throughout the averaging time. To establish meaningful background concentrations with which to evaluate the ion generator effect on pollutants, Chauvenet's criterion (Holman, 1989) was applied to each day of testing without the ion generator.

Two outliers were discarded, one high unexplained particle concentration for the second day of the 2-N1 experiment and one low unexplained formaldehyde concentration for the first day of the 1-N1 experiment. Also listed on Figure 2 are the percent differences of the pollutants that are associated with operating the ion generator in RC 1–4, calculated with the mean concentrations as (no ion generator – ion generator)/(no ion generator). A positive difference indicates that the ion generator increased the concentration in that room configuration.

Generally, Figure 2 shows that particle number concentrations decreased with the operation of the ion generator in RC 1 and 2 but increased with the operation of the ion generator in RC 3 and 4. The majority of the particle number increase was in the ultrafine range, and the increases on Figure 2 are for ultrafine particles only. The ozone-emitting ion generator led to a decrease in d-limonene mean concentrations in RC 3 of 14 ppb and in RC 4 of 8 ppb, indicating that the particle number increases were likely SOA formed from ozone/d-limonene reactions. The particle generation due to the ion generator operation in RC 3 and 4, with the d-limonene source, was larger in magnitude than its removal by the ion generator in RC 1 and 2. According to the summary results in Figure 2, particles larger than the ultrafine range are either decreased or unaffected by the use of the ion generator.

Since the ion generator emitted ozone at a rate of 3.3 mg/h, it increased ozone concentrations in all room configurations. Ozone concentration increases were largest in RC 1, the second largest in RC 2, the third largest in RC 3, and were the smallest in RC 4. The successive decreases in the ozone concentration increases likely reflect the increasing reactivity of each room configuration with ozone. With the sealed/stained concrete flooring and no terpene source, RC 1 results in the fewest reactions of ozone with surfaces and gas-phase compounds. With the addition of the carpet in RC 2 the surface reactivity of the room with ozone increased (Morrison and Nazaroff, 2000). The reactive air freshener in RC 3 increased the gas-phase reactivity of the room with ozone. Finally, the carpet and the air freshener in RC 4 yielded the most reactive room configuration, and the ozone concentration difference in RC 4 without and with the ion

generator was very small. The fact that the ozone concentration difference is smaller for RC 3 than RC 2 implies that the addition of the air freshener increased the reactivity of the room more than the addition of the carpet.

Concentrations of two aldehydes, formaldehyde and nonanal, also increased due to the operation of the ion generator in every room configuration. These aldehyde increases are products of reactions initiated by the ozone. Though we measured C_1–C_4 and C_6–C_{10} aldehydes, only formaldehyde and nonanal were affected by the use of the ion generator. In RC 1 and 2, most of the increases in aldehyde concentrations are likely due to ozone interactions with surfaces in the room since there was not a source of gas-phase unsaturated organics in the room. In RC 3 and 4, however, ozone also reacted with unsaturated organics emitted from the air freshener, likely leading to formaldehyde production as well (Singer et al., 2006a). Nonanal production is associated with ozone reactions with interior residential surfaces such as carpets, walls, floors, and countertops (Morrison and Nazaroff, 2000; Wang and Morrison, 2006). The largest nonanal increase is in RC 1, which coincides with its large ozone concentration increase. It was expected that the addition of carpet would lead to higher nonanal concentrations, but we did not observe this phenomenon. However, Wang and Morrison (2006) also observed that carpet does not necessarily produce secondary emissions of nonanal.

Because our experiments were carried out in a real environment, the summary results shown in Figure 2 exhibit both the net effect of the ion generator in each room configuration and fluctuations in background conditions, which included fluctuations in background concentrations of all measured pollutants and air exchange rates. The exclusion of the one particle and one formaldehyde data point from the background results using Chauvenet's criterion was in an effort to deemphasize background fluctuations and/or experimental error. Air exchange rates are a function of both the house geometry and outdoor weather conditions, and λ_{off} were similar but fluctuated among experiments over a range of 0.32–0.65 h^{-1}. However, in spite of any background concentration and air exchange rate fluctuations that may be represented in the data, the

emergent trend is that the ion generator can increase concentrations of particles, ozone, formaldehyde, and nonanal.

DISCUSSION

Impact of the different flooring on ozone reactions.

One goal of this research was to explore the impact of adding the carpet (an ozone sink). The addition of another ozone sink, the air freshener, affected gas-phase reactions of ozone with d-limonene, which are apparent in the SOA formation in RC 3 and 4 versus the lack of formation in RC 1 and 2. However, by varying the flooring surface in the room, we were also able to observe the impact of adding carpeting by comparing RC 1 and 2.

The ozone decay rates, β_{O3} (h^{-1}), for RC 1 and 2 were calculated. β_{O3} (h^{-1}) is defined as $v_d \cdot A/V$ (Sabersky et al., 1973; Klenø et al., 2001), where v_d (m/h) is the ozone deposition velocity to all room surfaces, A (m^2) is the total surface area of all room surfaces, and V (m^3) is the room volume. There was a constant ozone emission source with the operating ion generator. When outdoor-to-indoor transport of ozone is negligible, β_{O3} can be determined with Equation 1, which assumes steady-state, well-mixed conditions, and that gas-phase ozone reactions are negligible:

$$\beta_{O3} = \frac{E_{O3}/V}{C_{O3}} - \lambda_{off} \quad (1)$$

where C_{O3} (mg/m^3) is the mean ozone concentration in the room during 4 to 6 a.m. and E_{O3} (mg/h) is the ozone emission rate of the ion generator (3.3 mg/h). The ozone decay rates were calculated with the mean λ_{off} during tests in RC 1 and 2. Ozone decay rates were only calculated for RC 1 and 2 because Equation 1 neglects gas-phase reactions of ozone, and the air freshener in RC 3 and 4 renders this assumption invalid. The calculated ozone decay rates were 2.6 h^{-1} for RC 1 and 3.9 h^{-1} for RC 2, which are comparable to other reported ozone decay rates (Sabersky et al., 1973; Lee et al., 1999; Weschler, 2000;

Klenø et al., 2001). The larger decay in RC 2 over RC 1 likely reflects increased ozone deposition to the added carpet.

Knowing the decay rates for RC 1 and 2 allows the estimation of their whole-room formaldehyde and nonanal yields due to the use of the ion generator. The yield, Y (-), is defined as the ratio of the molar increase in the aldehyde to the molar reduction of ozone and is Equation 2, which makes the same assumptions as Equation 1:

$$Y = \frac{\lambda_{\text{off}} \Delta C_{\text{aldehyde}}}{\beta_{\text{O3}} \Delta C_{\text{O3}}} \tag{2}$$

where $\Delta C_{\text{aldehyde}}$ and ΔC_{O3} are the concentration differences (in ppb) of the aldehyde and ozone for that particular room configuration due to the use of the ion generator. The whole-room yields for formaldehyde are 0.10 for RC 1 and 0.19 for RC 2, with the higher yield likely due to the presence of carpet. The whole-room yields for nonanal are 0.031 for RC 1 and 0.015 for RC 2. We are not aware of any other whole-room yields in the literature.

Impact of air exchange rate

We also varied the air exchange rate in each room configuration. Assuming comparable outdoor concentrations of a pollutant, emissions cause higher room concentrations as the air exchange rate decreases. Thus, concentrations of ozone from the ion generator and d-limonene from the air freshener increase once the air exchange rate in the room decreases from λ_{cycle} to λ_{off}. SOA formation also increased with decreasing air exchange rate, which is consistent with the literature (Weschler and Shields, 2003; Sarwar et al., 2003; Sarwar and Corsi, 2007). The resulting concentrations of d-limonene in the room and values of λ_{cycle} to λ_{off} provided an opportunity to see the importance of the air exchange rate on SOA formation. For a reaction to be important indoors, it must proceed at a fast enough rate to compete with air exchange loss (Weschler and Shields, 2000). For the reaction of d-limonene and ozone, the pseudo first-order loss rate can be approximated as the product of the second order reaction rate

constant of ozone and d-limonene (0.018 ppb^{-1} h^{-1}) and the d-limonene concentration. Using the mean concentrations of d-limonene, this loss rate was 0.70 h^{-1} for RC 3 and 0.68 h^{-1} for RC 4. Thus, it was not until the HVAC system was turned off and the mean room air exchange rate lowered from λ_{cycle} = 1.3 h^{-1} to λ_{off} = 0.5 h^{-1} that the reaction loss rate could effectively compete with the air exchange loss rate. During the HVAC Off period, the SOA from this reaction was formed at a high enough rate relative to particle loss rates in the room to yield detectable SOA concentration increases.

Impact of indoor temperature

The average room temperature approached 30 °C at all conditions because of the heat from the instrumentation. However, typical room temperatures in the U.S. are often between 18 to 27 °C, depending on the season and thermostat operation. The total mass of SOA formed from ozone and d-limonene reactions increases as temperature decreases (Leungsakul et al., 2005; Sarwar and Corsi, 2007). Though the reaction rate of ozone and terpenes decreases, this decrease is surpassed by the increase in gas-to-particle partitioning that occurs as the vapor pressures of condensing products decrease. For reactions between ozone and d-limonene, Leungsakul et al. (2005) report that the mass of SOA formed changes at a rate of -0.016 $°C^{-1}$ and Sarwar and Corsi (2007) report a rate of -0.04 $°C^{-1}$. However, for gas-phase ozone reaction products, such as formaldehyde or nonanal, lowering the ambient temperature would likely decrease concentrations because of reduced homogeneous reaction rates. These effects indicate that our results may underestimate SOA formation and overestimate aldehyde byproducts when compared to a similar indoor environment at a lower temperature.

Impact of ion generators on indoor air quality

The ion generator used in our study increased concentrations of ultrafine particles, ozone, formaldehyde, and nonanal. It also slightly decreased concentrations of larger particle sizes of particles. Portable ion generators are common in the U.S. (Shaughnessy and Sextro, 2006), and other brands and models may lead to different results. For

instance, IG 2 in our previous work had a CADR of 35 (13) m^3/h and an ozone emission rate of 4.3 ± 0.2 mg/h (Waring et al., 2008). The lower CADR and higher ozone emission rate would likely increase concentrations of particles, ozone, formaldehyde, and nonanal than we found here. However, the electrostatic precipitator (ESP) in our previous work had a much higher CADR of 284 (62) m^3/h and a slightly higher ozone emission rate of 3.8 ± 0.2 mg/h (Waring et al., 2008). Thus, the ESP would likely lead to decreased particle concentrations in all room configurations because the CADR is approximately an order of magnitude greater than the other loss mechanisms. The ESP would, however, still likely increase concentrations of ozone, formaldehyde, and nonanal.

The pollutants increased by the ion generator have consequences for human exposure and health. Ozone exposure is harmful to human health, and an outdoor increases of ozone have been associated with a increase in mortality (Bell et al., 2004; Ito et al. 2005; Levy et al. 2005). Reaction products of ozone and d-limonene have been shown to increase respiratory burden in mice (Rohr et al., 2002). However, newer research has shown that not the SOA but gas-phase products, such as formaldehyde, more complex aldehydes, carboxylic acids, and free radicals, that may be responsible for acute effects (Wolkoff et al., 2008). We know of no investigation into the chronic effects of SOA exposure. Formaldehyde is a known human carcinogen, having been associated with naso-pharyngeal cancer (Cogliano et al., 2005), and nonanal is an odorous and irritating compound (Morrison and Nazaroff, 2000). Thus, given the results in this investigation as well previous laboratory research on ion generators (Alshawa et al., 2007; Waring et al., 2008), the operation of ion generators can degrade indoor air quality and their use indoors should likely be avoided.

ACKNOWLEDGEMENTS

This research was funded by the International Society for Exposure Assessment (ISEA), the American Society of Heating, Refrigerating and Air-Conditioning Engineers (ASHRAE) and by Consumers Union. The lead author's contribution was also funded by an NSF IGERT traineeship (Award 0549428). Dr. Glenn Morrison and students at

Missouri University of Science and Technology performed the light aldehyde analysis. Dr. Richard Corsi and Donghyun Rim from the University of Texas at Austin provided a careful review of this manuscript.

Appendix C

PAPER III

The Influence of HVAC Systems on Indoor Secondary Organic Aerosol Formation

(Accepted to *ASHRAE Transactions*)

ABSTRACT

Chemical reactions between ozone and terpenoids can yield secondary organic aerosol (SOA), which are potentially a large source of indoor particles that are harmful to human health. The mass of SOA formed in a building is influenced by the operation of the heating, ventilation, and air-conditioning (HVAC) system. This investigation models the influence of HVAC systems on SOA concentrations in residential and commercial buildings. A parametric analysis explores the role of ventilation and recirculation rates, filtration efficiency and loading, and the operation of heat exchangers. In a rural setting, the median residential and commercial SOA concentrations for all simulations were 17.4 $\mu g/m^3$, with a range of 2.47–27.0 $\mu g/m^3$, and 10.6 $\mu g/m^3$, with a range of 1.81–26.3 $\mu g/m^3$, respectively. In an urban setting, the median predicted residential and commercial SOA concentrations were 68.0 $\mu g/m^3$, with a range of 14.7–108 $\mu g/m^3$, and 44.8 $\mu g/m^3$, with a range of 11.6–105 $\mu g/m^3$, respectively. The most influential HVAC parameters are the flow rates through the system, particle filtration efficiency, and indoor temperature for the residential and commercial models, as well as ozone removal on used filters for the commercial model. The results presented herein can be used to estimate the effects of altering HVAC system components and operation strategies on indoor SOA concentrations and subsequent exposure.

INTRODUCTION

Particulate matter (PM) diameter spans many orders of magnitude, from a few nanometers to tens of micrometers, and exposure to particles has been associated with harmful effects on human health. Fine particles (< 2.5 μm in diameter) can penetrate deep into the alveolar regions of the lung (Hinds, 1999). In a review of studies in the last

20 years on associations between exposure to particles and increased human mortality, Pope and Dockery (2006) conclude that fine particles have adverse effects on cardiopulmonary health. Also, exposure to ultrafine particles (< 0.1 μm in diameter) have an adverse effect on cardiopulmonary function that is independent of fine particle exposure (Pekkanen et al., 2002). Most epidemiological research on the influence of particle exposure on human health has focused on the outdoor environment. However, the average American spends 18 hours indoors for every hour outdoors (Klepeis et al., 2001), and particle concentrations indoors are often much higher than outdoors, due to the strong influence of indoor sources (Wallace, 2006). Common indoor sources of fine particles include cooking (Wallace et al., 2004), cigarettes (e.g. Waring and Siegel, 2007), and vented clothes dryers (Wallace, 2005).

Another source of indoor fine particles are chemical reactions. Weschler and Shields (1999) and other researchers (e.g. Wainman et al., 2000; Long et al., 2000; Rohr et al., 2003; Sarwar et al., 2003; Sarwar and Corsi, 2007) showed that gas-phase reactions between ozone (O_3) and various terpenoids yield particles in the form of secondary organic aerosol (SOA). The reactions proceed at fast enough reaction rates to compete with loss due to air exchange (Weschler and Shields, 1996), and the reactants both commonly occur indoors. Ozone infiltrates the indoors from the outdoors (Weschler, 2000), and is directly emitted indoors from office electronics (Lee et al., 2001), portable ionizers (e.g. Waring et al., 2008) or in-duct electrostatic precipitators (ESPs) (Viner et al., 1992). Also, terpenoids are commonly emitted indoors from consumer products, cleaners, and fragrances (Wallace et al., 1991; Singer et al., 2006; Corsi et al., 2007). The SOA is composed of condensed products that either nucleated or partitioned onto preexisting seed particles, and SOA is in the ultrafine and lower portion of the fine particle size ranges. Further, the health effects due to SOA may be different and more deleterious than those from primary aerosols (Rohr et al., 2002 and 2003).

The heating, ventilation, and air-conditioning (HVAC) system of a building can affect the concentration of SOA formed by influencing the reactant and seed particle concentrations, as well as the indoor air temperature and relative humidity (RH). For

example, ventilation rates influence indoor ozone (Weschler, 2000) and seed particle concentrations (Riley et al., 2002) by affecting the rate of transport between the indoors and outdoors. Recirculation rates affect ozone, seed particle, and SOA concentrations by altering both the removal to filters in the recirculation air stream and the deposition to indoor surfaces (Sabersky et al., 1973; Lai and Nazaroff, 2000; Zuraimi et al., 2007). Seed particle and SOA concentrations are reduced by HVAC filters (Hanley et al., 1994) and in-duct ESPs (Wallace et al., 2004). Ozone is either removed by particle-laden filters (Zhao et al., 2007) or can be generated by in-duct ESPs (Viner et al., 1992). The HVAC heat exchanger (or coil) alters both the temperature and RH in the space, and the temperature affects the chemical reaction rates and resulting product vapor pressures and the RH the mass of SOA yielded (Leungsakul et al., 2005). Since the HVAC system design and operation can affect the mass of SOA formed, we explore its effects by developing a simulation that predicts the size-resolved mass of SOA formed in typical residential and commercial spaces with HVAC systems. In both the residential and commercial models, we vary the (i) ventilation and recirculation rates, (ii) the HVAC filter efficiency, (iii) the ozone removal on HVAC filters due to particle loading, and the indoor (iv) temperature and (v) relative humidity. A parametric analysis is used to explore each of these factors on SOA formation.

METHODOLOGY

The residential and commercial models are similar to models in Riley et al. (2002) and Waring and Siegel (2008), with the addition of gaseous transport and emission and SOA formation. For size-resolved parameters, including the mass of SOA formed, a particle diameter (d_p) range of 0.01–10 μm was considered. Residential and commercial spaces were modeled separately because of differences in values of input parameters and HVAC system operation.

The Residential and Commercial Models

Figure 1 shows the schematic that was used to account for pollutant fate and transport. The residential model does not have ventilation air intake, as most U.S. residential spaces get fresh air only from infiltration.

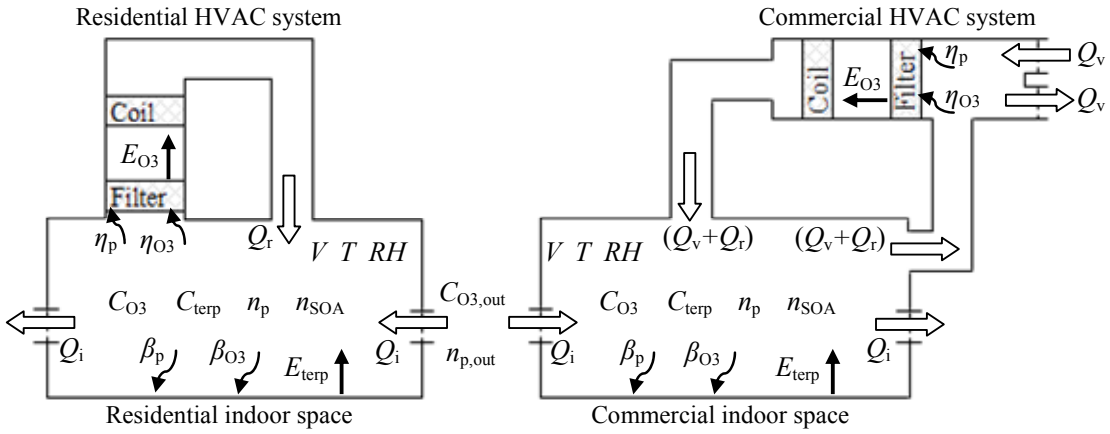

Figure. 1. Schematic for the (a) residential and (b) commercial models. Block arrows represent airflows and line arrows represent species losses or gains. (Symbols are defined in text.)

V (m^3) is the volume of the space. T (°C) and RH (%) are the indoor temperature and relative humidity, respectively. Q_i, Q_v, and Q_r (m^3/h) are the infiltration, ventilation, and recirculation volumetric flow rates, respectively. The ratio of a particular flow rate to the building volume is the air exchange rate, λ (h^{-1}). β_p and β_{O3} (h^{-1}) are the loss rates of particles, including SOA, and ozone to indoor surfaces, respectively. Both loss rates are equal to the terms $v_d S$, where v_d (m/h) is a mass transfer coefficient that is often called the deposition velocity and S (m^{-1}) is the surface area to volume ratio in the space. η_p and η_{O3} (-) are the removal of particles, including SOA, and ozone by the HVAC filter, respectively. Particle removal by HVAC filters is intentional, but ozone removal is unintentional and occurs due to reactions with particle-laden filters. E_{O3} and E_{terp} (μg/h) are mass emission rates of ozone by an ESP or of terpenoids by building contents (e.g., consumer products), respectively. C_{O3}, $C_{O3,out}$, C_{terp} (μg/m^3) are mass concentrations of

indoor ozone, outdoor ozone, and indoor terpenoids, respectively, and $C_{O3,m}$, $C_{O3,m,out}$, and $C_{terp,m}$ (ppb) are molar concentrations of those compounds, respectively. n_{seed}, $n_{seed,out}$, and n_{SOA} (μg/μm·m^3) are mass distributions of indoor and outdoor seed particles, and indoor SOA, respectively.

The models assume steady-state, well-mixed conditions, constant air density, and no indoor sources of particles other than SOA formation. These assumptions are not realistic over all indoor conditions, but this is an appropriate approach to compare the relative influence of HVAC system parameters on SOA formation. The steady-state indoor mass concentration of SOA, C_{SOA} (μg/m^3), may be calculated as the ratio of the mass formation rate of SOA and the loss rate of SOA, and C_{SOA} is calculated with Equation 1:

$$C_{SOA} = \int_{d_p} n_{SOA} \mathrm{d}d_p = \left(F_T F_{RH}\right)\left(\Gamma C_{terp,m}\left(kC_{O3,m}\right)\right)\int_{d_p} \frac{Y_{g,sr}}{\beta_p + \lambda_i + \lambda_v + \lambda_r \eta_p} \mathrm{d}d_p \quad (1)$$

where F_T (-) and F_{RH} (-) are formation factors that adjust for changes in T and RH, respectively; k (ppb^{-1} h^{-1}) is the reaction rate constant of terpenoids and ozone; $Y_{g,sr}$ (μm^{-1}) is the size-resolved mass distribution yield of SOA formed by gas-phase reactions between ozone and the terpenoid, which is the ratio of the change in mass of SOA formed to the change in mass of terpenoid consumed; Γ (-) is a conversion factor to change units of ppb/h to μg/m^3·h; and λ_i, λ_v, and λ_r (h^{-1}) are air exchange rates due to infiltration, ventilation, and recirculation, respectively. Equation 1 is integrated over the modeled range of d_p = 0.01–10 μm. All terms in Equation 1 except k are influenced by the HVAC system and varied in the parametric analysis. In reality, k is a function of indoor temperature and is also thus affected by the HVAC system, but our model incorporates this effect in the F_T term. $Y_{g,sr}$ is a function of the seed particle concentration that infiltrates indoors from outdoors. The indoor steady-state seed particle concentration of outdoor origin, C_{seed} (μg/m^3), is calculated with Equation 2, which also contains an integral since n_{seed}, $n_{seed,out}$, p_p, η_p, and β_p are particle size-resolved:

$$C_{\text{seed}} = \int_{d_p} n_{\text{seed}} \mathrm{d}d_p = \int_{d_p} n_{\text{seed,out}} \frac{p_p \lambda_i + \lambda_v (1-\eta_p)}{\beta_p + \lambda_i + \lambda_v + \lambda_r \eta_p} \mathrm{d}d_p \quad (2)$$

where p_p (-) is the size-resolved penetration of particles through the building envelope. The steady-state indoor terpenoid mass concentration, C_{terp}, is calculated with Equation 3 and was considered to be independent of the indoor ozone concentration. In reality, some amount of terpenoid would react with the ozone and thus decrease, but we assume that this decrease is small compared to the amount of reacted ozone and is thus neglected.

$$C_{\text{terp}} = \frac{E_{\text{terp}} / V}{\lambda_i + \lambda_v} \quad (3)$$

The steady-state indoor ozone mass concentration, C_{O3}, is calculated with Equation 4:

$$C_{O3} = C_{O3,\text{out}} \frac{\lambda_i + \lambda_v (1-\eta_{O3}) + \dfrac{E_{O3}}{C_{O3,\text{out}} V}}{\beta_{O3} + \lambda_i + \lambda_v + \lambda_r \eta_{O3} + k C_{\text{terp}}} \quad (4)$$

All integration was performed numerically. Particle size-resolved parameters were divided into 80 different bins, with 20 to 30 bins for each order of magnitude range. The HVAC parameters in Equations 1–4 were varied to parametrically explore their influence on C_{SOA}.

Building Model Parameters

The volume, V, for the residential model was 392 m^3, which is based on the typical floor area from the U.S. Bureau of the Census (2005) of 163.3 m^2 multiplied by an assumed ceiling height of 2.4 m. The volume, V, for the commercial model was assumed as 1,000 m^3, which was arbitrarily chosen because commercial buildings span a wide range of volumes, depending on their use. The commercial floor area is 416.7 m^2, which assumes the same ceiling height of 2.4 m. Using the methods and parameter values of Riley et al. (2002), the size-resolved penetration of particles through the building envelope (p_p) was calculated according to the theory of Liu and Nazaroff (2001). These calculated penetration factors closely resemble the measured penetration factors

reported in Long et al. (2001) for all but the very largest of particle diameters. Because of the lack of commercial penetration factors in the literature, identical penetration factors were used for both models.

Ambient Parameters

For both models, a Rural and an Urban ambient case were modeled to compare how the HVAC system affects SOA formation in different climates. Two parameters were varied for each ambient case, the outdoor ozone concentration and the outdoor particle distribution. An outdoor ozone molar concentration, $C_{O3,m,out}$, was assumed as 25 ppb for the Rural case and 100 ppb for the Urban case. The Urban case had higher ozone because automobile pollution often leads to ozone in the form of photochemical smog (Seinfeld and Pandis, 1998). The outdoor and indoor seed particle mass distribution functions, $n_{seed,out}$ and n_{seed}, respectively, both depend on the size-resolved outdoor particle number distribution, $n_{seed,N,out}$ (#/μm·m^3). For the outdoor distribution in both the residential and commercial models, we used Rural and Urban number distributions from Jaenicke (1993), which are synthesized distribution from various sources. These are described as tri-modal lognormal distributions, and the number, geometric mean diameter (GM), and log of the geometric standard deviation (GSD) that describe the three modes are listed in Table 1. These same distributions were used in Riley et al. (2002) and Waring and Siegel (2008). Each $n_{seed,N,out}$ was converted to $n_{seed,out}$ by assuming the particles are spherical and multiplying the volume of the geometric mean of each size bin by an assumed particle density of 1 g/cm^3. The resulting Rural $PM_{2.5}$ and PM_{10} concentrations are 7.3 and 15 μg/m^3, respectively, and the Urban $PM_{2.5}$ and PM_{10} concentrations are 43 and 60 μg/m^3, respectively.

Table 1. For the Rural and Urban ambient cases, the outdoor ozone concentrations and particle distributions, including the total number concentrations and geometric mean diameters (GM) and log of geometric standard deviations [log(GSD)] for each mode.

		Particle Distributions								
		Mode 1			Mode 2			Mode 3		
Ambient Case	Ozone Conc. (ppb)	Number (#/cm^3)	GM (μm)	log(GSD) (-)	Number (#/cm^3)	GM (μm)	log(GSD) (-)	Number (#/cm^3)	GM (μm)	log(GSD) (-)
Rural[a]	25	6,650	0.015	0.225	147	0.054	0.557	1,990	0.084	0.266
Urban[a]	100	99,300	0.013	0.245	1,100	0.014	0.666	36,400	0.05	0.337

[a]Ozone concentrations were assumed and particle number distributions are from Jaenicke (1993).

Terpenoid Reactant Parameters

The parameters E_{terp}, $Y_{g,sr}$, and k were derived from a series of papers that reported SOA formation from ozone reactions with a set of common consumer products (Destaillats et al., 2006; Singer et al., 2006a and 2006b; Coleman et al., 2008). The results for a pine-oil cleaner (POC) are used to determine E_{terp}, $Y_{g,sr}$, and k in both the residential and commercial models, since its use in both settings is realistic. The pine-oil cleaner labeled GPC-1 in Singer et al. (2006b) and POC in Coleman et al. (2008) are the same consumer product, and E_{terp} is derived from Singer et al. (2006b) and $Y_{g,sr}$ and k from Coleman et al. (2008).

The modeled emission, E_{terp}, is a floor-mopping event based off a technique described in Singer et al. (2006b). Floor-mopping with the POC emits 7.26 mg of terpenoids/g POC and the mopping technique uses 3.3 g POC/m^2·h. In the residential model, the emission is a floor-mopping of one-fourth the total floor area, so E_{terp} = 978 mg/h of terpenoids. In the commercial model, the emission is a floor-mopping of one-half the total floor area, so E_{terp} = 3,743 mg/h of terpenoids. Of these emissions, 78.5% are due to two terpenes, d-limonene and terpinolene, and one terpene-alcohol, α-terpineol. Of these, d-limonene has the largest SOA formation potential (Weschler and Shields, 1999; Ng et al., 2006).

Three experiments in Coleman et al. (2008) were conducted under nearly identical conditions, except two had deliberately low seed particle concentrations and one used

laboratory air with seed particles, with $PM_{1.1} = 4\ \mu g/m^3$. $Y_{g,sr}$ was modeled as depending on the seed particle concentrations and was calculated with results for the average of the low seed particle experiments (0.111) and for the seed particle experiment (0.197). The following linear relationship was determined: $Y_{g,sr} = 0.0213(C_{seed,PM1.1}) + 0.1107$, where $C_{seed,PM1.1}$ ($\mu g/m^3$) is the concentration of indoor seed particles less than 1.1 μm in our models. This relationship is only used in our residential and commercial models if $C_{seed,PM1.1} \leq 4\ \mu g/m^3$. If $C_{seed,PM1.1} > 4\ \mu g/m^3$ then $Y_{g,sr}$ is constant at 0.197. The size-resolved mass yield, $Y_{g,sr}$, is modeled as a lognormal distribution, and its parameters were fitted to the POC-Seed experiment by converting the tri-modal lognormal distribution of the steady-state SOA number concentration into a uni-modal lognormal mass distribution, with GM = 0.37 μm and GSD = 1.52. The ozone and terpenoid reaction rate constant, k, was calculated as follows. Neglecting ozone decay due to irreversible wall deposition (experiments were in Teflon-lined chamber), a steady-state mass balance with ozone and terpenoid concentrations yields $k = 0.05\ ppb^{-1}\ h^{-1}$. $Y_{g,sr}$ and k are identical in both models.

HVAC Parameter (i): HVAC Flow

The air exchange rates used in the models are listed in Table 2. The HVAC system directly controls the ventilation and recirculation rates, and these were varied to explore their influence on SOA formation. The Flow cases used infiltration and recirculation air exchange rates from Riley et al. (2002) and Waring and Siegel (2008). The residential Duty case assumed cycling of conditioning equipment, and therefore recirculation for one-sixth of the total time, and the Continuous case considered the air handler fan to be running the entire time. For the commercial HVAC Flow cases, all operation was continuous and three air makeup cases were considered, with assumed air exchange rates based on engineering judgment that were also used in Waring and Siegel (2008). The 100% outside air (OA) case represents a building for which air recirculation is undesirable. The 50% OA/50% recirculated air (RA) case represents a heavily occupied building, and the 10% OA/90% RA case represents a lightly occupied building.

Table 2. Summary of air exchange rates used in the residential and commercial models.

Air exchange rate (h^{-1})	Residential		Commercial		
	Duty	Continuous	100% OA	50% OA / 50% RA	10% OA / 90% RA
λ_i	0.75	0.75	0.25	0.25	0.25
λ_v	0	0	4	2	0.4
λ_r	0.67	4	0	2	3.6

In the residential model, the Duty and Continuous flow cases also cause different airflow regimes in the modeled indoor space. Indoor spaces without continuous recirculation are assumed to have average air flows of lower velocity than those indoor spaces with continuous recirculation. Since higher velocity flows lead to a decreased thickness of the boundary layers adjacent to surfaces, the deposition parameters of β_p and β_{O3} are expected to increase with higher velocity flows. Thus, the residential model uses different values of β_p and β_{O3} for the Duty and Continuous cases. The commercial model has continuous flow for all cases, so it uses one constant value for both β_p and β_{O3}.

Similar to in Riley et al. (2002) and Waring and Siegel (2008), we used the model of Lai and Nazaroff (2000) to determine specific values of β_p. One input in their model for β_p is the friction velocity, u^* (cm/s), which is an empirical parameter that describes the level of turbulence intensity near a surface. This parameter thus represents the air flow conditions in a space, with higher values for u^* associated with higher velocity flows. Typical values of u^* for indoor environments are 0.3–3 cm/s (Lai and Nazaroff, 2000). For the residential model, the Duty case was assigned the β_p for $u^* = 1$ cm/s and the Continuous case for $u^* = 3$ cm/s. For the commercial model, all three flow cases were assigned β_p for $u^* = 3$ cm/s.

Sabersky et al. (1973) described β_{O3} for two residential cases in the same home, without and with the forced air system operating, at 2.9 and 5.4 h^{-1}, respectively. In the residential model, our Continuous case assumes the forced air system is always on, so it was assigned as $\beta_{O3} = 5.4$ h^{-1}. For the Duty case, we assumed a value of 5.4 h^{-1} when the system was on and a value of 2.9 h^{-1} when the system was off, for an overall value of β_{O3}

= 3.3 h^{-1}. For the commercial model, β_{O3} was assigned for all flow cases as 4.2 h^{-1}, which is an average of the office ozone deposition loss rates summarized in Weschler (2000).

HVAC Parameter (ii): PM Filtration

Five removal devices were used in the residential and commercial models: four porous-media filters and one electrostatic precipitator (ESP). The efficiency curves for all five filters are displayed in Figure 2. We assumed that each filter retains the efficiency shown in Figure 2 and is constant over time, though filter removal efficiency typically changes with loading (Hanley et al., 1994; Wallace et al., 2004). Filter efficiency data for the four porous-media HVAC filters were obtained from ASHRAE Standard 52.2 tests (ASHRAE, 2007) provided by filter manufacturers. The ASHRAE Standard 52.2 procedure challenges filters with particles from 0.3 to 10 μm, so the fibrous filtration theory described by Hinds (1999) was used to extend the data into the full range used in this study, following the procedure in Riley et al. (2002). These are the same filter curves used in Waring and Siegel (2008).

The fifth filter used in our models was an in-duct ESP, and its efficiency curve was derived from Wallace et al. (2004), who reported size-resolved mean deposition rates in a townhome with the central house fan operating continuously, both without and with an in-duct ESP operating. The size-resolved efficiency of the in-duct ESP was calculated for each reported particle diameter in Wallace et al. (2004) with the relationship, $\Delta\beta_{ESP} = (\lambda_{r,townhome})(\eta_{ESP})$, where $\Delta\beta_{ESP}$ is the difference in deposition loss rates with and without the ESP operating, $\lambda_{r,townhome}$ is the rate of recirculated air in the townhome (reported by the authors as 5.4 h^{-1}), and η_{ESP} is the calculated size-resolved efficiency of the in-duct ESP. Wallace et al. (2004) reported size-resolved deposition rates for the particle diameter range of 0.0181 to 1.843 μm, so the efficiencies of modeled particle diameters that were lower than this range were assigned the η_{ESP} for the particle diameter of 0.0181 μm and those higher were assigned the η_{ESP} for the particle diameter of 1.843 μm. The same efficiency curve for η_{ESP} was used in the residential and commercial models due to the lack of efficiencies reported for ESPs in commercial systems. The use of an in-duct

ESP produces ozone, so our models coupled an indoor ozone emission rate, E_{O3}, to the residential and commercial scenarios that employed the ESP. Wallace et al. (2004) did not report ozone emission rates for the studied ESP, so our residential and commercial models used the rate of a commercially available unit in Viner et al. (1992) of E_{O3} = 21.6 mg/h for the continuous HVAC Flow cases in the residential and commercial models. For the Duty case in the residential model, the ozone emission rate is one-sixth the Continuous case and is E_{O3} = 3.6 mg/h.

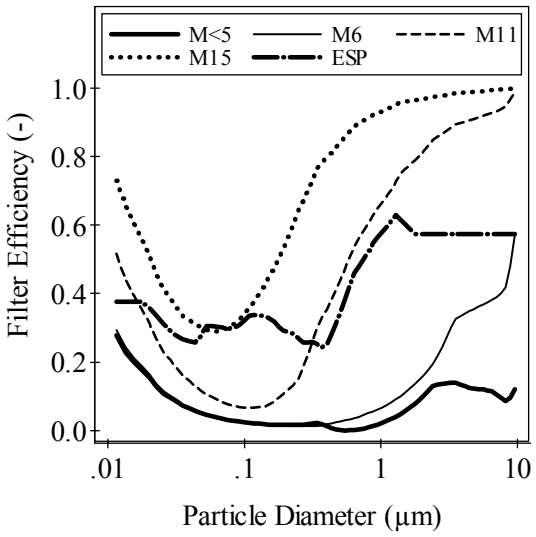

Figure 2. Filter efficiency curves for the MERV <5, 6, 11, and 15 filters (M<5, M6, M11, and M15) and the electrostatic precipitator (ESP) used in this modeling study.

HVAC Parameter (iii): O_3 Filtration

As ozone-laden air passes through a porous-media HVAC filter, ozone can be removed by the filter, predominately due to reactions with loaded particles (Hyttinen et al., 2003; Bekö et al., 2006, 2007; Zhao et al., 2007). We modeled New and Used filter cases for ozone removal. Both models assumed that η_{O3} = 0% for their New cases. The models assumed Used values of η_{O3} = 10% and 41% for residential and commercial buildings, respectively (Zhao et al., 2007). The residential value of 10% is the mean of

eight particle-laden filters taken from actual residences, and the commercial value of 41% is the mean of five particle-laden filters from commercial environments. Though the ozone removal efficiency of a porous-media filter is likely associated with its particle removal efficiency, our model does not link the two since there are insufficient data to make such an association. All scenarios with an ESP are assigned the ozone removal value of $\eta_{O3} = 0\%$.

HVAC Parameter (iv): Temperature

The heating or cooling coil operation influences the air temperature in a modeled space. Three different indoor temperatures, 18.3, 23.9, and 29.4 °C were considered. The total mass of SOA formed increases as temperature decreases (Leungsakul et al., 2005; Sarwar and Corsi, 2007). Though the reaction rate of ozone and terpenoids decreases, this decrease is surpassed by the increase in gas-to-particle partitioning that occurs as the vapor pressures of condensing products decrease. For reactions between ozone and d-limonene (the primary SOA forming reactant in the POC), Leungsakul et al. (2005) report that the mass of SOA formed changes at a rate of -0.016 $°C^{-1}$ and Sarwar and Corsi (2007) report a rate of -0.04 $°C^{-1}$. The experiments reported in Coleman et al. (2008) were conducted at a temperature of 23 °C, and temperature formation factors, F_T, were calculated with the averages of the two rates from Leungsakul et al. (2005) and Sarwar and Corsi (2007). These F_T adjust the mass of SOA formed at the experimental temperature to represent that which would occur at the modeled temperatures. For both models, F_T equals 1.13, 0.98, and 0.82 for the cases of 18.3, 23.9, and 29.4 °C, respectively.

HVAC Parameter (v): Relative Humidity

The heating or cooling coil also influences the relative humidity (RH) in a space. Both models utilize three different values for indoor RH of 25, 50, and 75% to model the range of RH that occurs in buildings in different climates. As RH decreases, the water available for reactions becomes limited. Some products of the ozone and d-limonene

reaction (stabilized Criegee intermediates) that can react with water instead react with other products of the ozone and d-limonene reactions (aldehydes) to form less volatile compounds, increasing total SOA mass formed (Leungsakul et al., 2005). Leungsakul et al. (2005) report that the mass of SOA formed changes at a rate of -0.0009 $\%^{-1}$. The experiments reported in Coleman et al. (2008) were conducted at an RH of 50%, and RH formation factors, F_{RH}, were calculated with the rate from Leungsakul et al. (2005). These F_{RH} adjust the mass of SOA formed at the experimental RH to represent that which would occur at the modeled RH. For the residential and commercial models, F_{RH} equals 1.02, 1.0, and 0.98 for the cases of 25, 50, and 75%, respectively.

Base Case Definitions and Number of Reported Scenarios

For the residential and commercial models, the varied HVAC parameters, as well as the literature sources used for input values, are summarized in Table 3. A Rural and Urban base case for both the residential and commercial models was selected based on typical values for each parameter. Within the Rural and Urban distributions, the residential base case consisted of a Duty flow cycle, a MERV 6 filter (the requirement for new homes in ASHRAE Standard 62.2 (ASHRAE, 2004)), a Used filter with an ozone removal efficiency of 10%, and indoor temperature of 23.9 °C and an RH of 50%. Within the Rural and Urban distributions, the commercial base case consisted of a 10% OA/90% RA flow cycle, a MERV 6 filter, a Used filter with an ozone removal efficiency of 41%, and indoor temperature of 23.9 °C and an RH of 50%. Each combination of the parameters was modeled. The residential model had 324 unique scenarios (162 each of Rural and Urban) and the commercial model had 486 unique scenarios (243 each of Rural and Urban).

Table 3. Summary of varied HVAC parameters for the residential and commercial models. The base cases are listed in bold. Literature sources are listed below.

Parameter	Model	Cases (Base cases in bold)
HVAC Flow[a]	Residential	**Duty**, Continuous
	Commercial	100% OA, 50% OA/50% RA, **10% OA/90% RA**
PM Filtration[b]	Residential, Commercial	MERV <5, **6,** 11, 15; ESP
O_3 Filtration[c]	Residential, Commercial	New, **Used**
Temperature[d]	Residential, Commercial	18.3, **23.9**, 29.4 °C (65, **75**, 85 °F)
Relative Humidity[d]	Residential, Commercial	25, **50**, 75%

[a]Riley et al. (2002), Waring and Siegel (2008); [b]Waring and Siegel (2008), Hinds (1999), and Wallace et al. (2004); [c]Zhao et al (2007); [d]Leungsakul et al. (2005).

RESULTS AND DISCUSSION

Using Equations 1–4, the resulting SOA concentrations, C_{SOA}, varied over an order of magnitude, depending on the HVAC input parameters. SOA yield and other size-resolved parameters are lognormally distributed, so the median was used as a descriptive statistic. For the residential model, the median C_{SOA} over all 162 Rural scenarios was 17.4 μg/m^3, with a range of 2.47–27.0 μg/m^3, and over all 162 Urban scenarios was 68.0 μg/m^3, with a range of 14.7–108 μg/m^3. The residential base case C_{SOA} for the Rural case was 22.8 μg/m^3 and for the Urban case was 90.9 μg/m^3. For the commercial model, the median C_{SOA} over all 243 Rural scenarios was 10.6 μg/m^3, with a range of 1.81–26.3 μg/m^3, and over all 243 Urban scenarios was 44.8 μg/m^3, with a range of 11.6–105 μg/m^3. The commercial base case C_{SOA} for the Rural case was 15.4 μg/m^3 and for the Urban case was 62.9 μg/m^3. These ranges are of the same order as reported in real buildings under a variety of experimental conditions (Weschler and Shields, 1999; Hubbard et al., 2005). The size-resolved distributions of SOA for these base cases, as well as the outdoor and indoor seed, SOA, and total indoor particle distributions are in Figure 3.

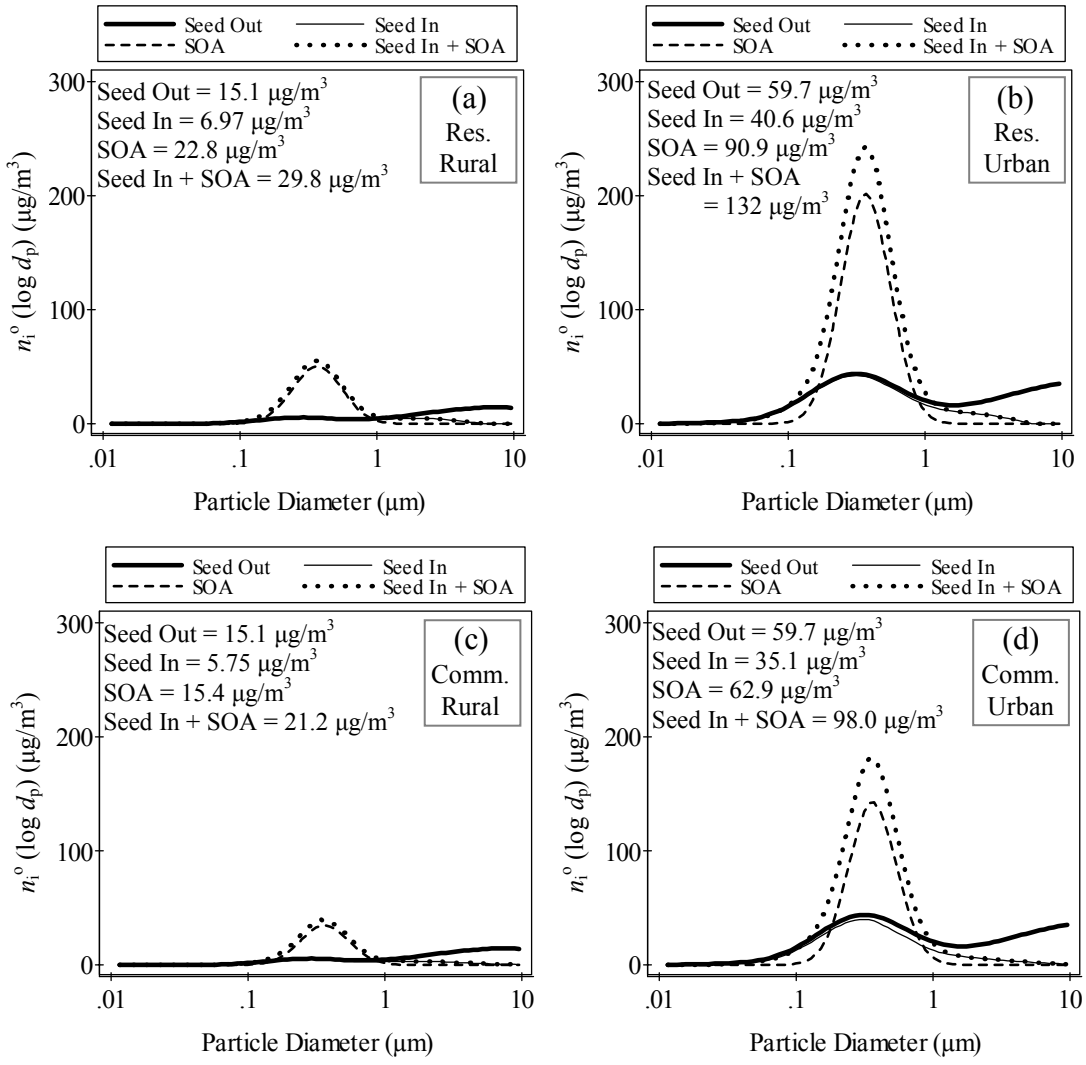

Figure 3. Outdoor seed, indoor seed, SOA, and indoor seed + SOA particle distributions (µg/m^3) for residential (a) Rural and (b) Urban base cases and commercial (c) Rural and (d) Urban base cases.

The median C_{SOA}, the ranges of formation, and the base case results for C_{SOA} illustrate that much more SOA is formed in the Urban than the Rural area, in both models. The indoor terpenoid concentrations, C_{terp}, were the same in both areas, and the higher formation is due to the greater urban outdoor ozone concentration, $C_{O3,m,out}$, of 100 ppb over the rural concentration of 25 ppb. The integrated concentrations for each of the

four plotted particle mass distributions are also displayed in Figure 3. For the base cases in both models, the C_{SOA} in the Rural environment was a higher fraction of the total indoor particles than in the Urban environment, at 76.5% versus 68.9% for the residential base cases and 72.6% versus 64.2% for the commercial base cases. Figure 3 shows for all bases cases, most of the resulting SOA distribution is in the 0.1–1 μm diameter size range, consistent with the findings of other researchers (Weschler and Shields, 1999; Coleman et al., 2008).

The parametric influence of each of the HVAC parameters on the base cases was determined with the SOA Change Ratio (SCR), which is listed in Table 4. The SCR equals the *adjusted* C_{SOA} divided by the *base case* C_{SOA}, and the adjusted C_{SOA} is the result of holding all parameters in the base case constant except for the varied parameter. Thus, the SCR is a measure of how sensitive C_{SOA} is to a change of a given HVAC parameter, relative to the base case. Non-influential parameters have SCRs at or near unity. Parameter changes that lead to lower C_{SOA} have an SCR less than unity, and parameter changes that lead to higher C_{SOA} have an SCR greater than unity. The product of the SCR and the base case C_{SOA} yields the adjusted C_{SOA}.

Table 4 shows that there was little change in the SCR for the same case in the Rural versus the Urban environments. The different $C_{O3,m,out}$ of 25 ppb and 100 ppb affect the absolute C_{SOA} formed for the different ambient cases. However, these different $C_{O3,m,out}$ do not affect the SCR since it is a measure of change relative to the base case. The differences that are observed in SCRs for the Rural versus the Urban cases are due to the different seed particle concentrations, C_{seed}, for the two ambient conditions, since lower seed particle concentrations lead to a lower $Y_{g,sr}$. However, this effect is small because of limitations in available input parameters. The experimental data in Coleman et al. (2008) that were used to generate the linear relationship between $Y_{g,sr}$ and $C_{seed,PM1.1}$ were only for the particle mass range of $C_{seed,PM1.1} \leq 4$ μg/m^3. For most of the modeled scenarios, $C_{seed,PM1.1}$ was greater than 4 μg/m^3, so $Y_{g,sr}$ was at a constant value that did not change with the indoor seed particle concentration. In reality, the SOA yield could

increase further with higher seed particle concentrations, but there is limited data in the literature on the subject to more fully model this effect.

The SCRs in Table 4 show that the most influential HVAC parameters are those in the cases of Flow, PM Filtration, and Temperature for the residential and commercial models, as well as O_3 Filtration for the commercial model. In the residential model, changing flow cases from Duty to Continuous decreases the SCR since continuous air flow allows the HVAC filter to remove more of the SOA formed. The different Flow cases have a larger relative effect in the commercial building, since volumetric air flow is larger and always continuous with an air exchange rate through the HVAC system of ($\lambda_r + \lambda_v$) = 4 h^{-1}. For the changes to the two different flow strategies, the 100% OA case causes the largest relative decrease in the SCR since no air is recirculated and both the terpenoids emitted indoors and the SOA formed indoors is completely ventilated (though the C_{O3} of outdoor origin is higher in this case). The 50% OA/50% RA case also yields a smaller C_{SOA} than the base case, but it has a larger C_{SOA} than the 100% OA case since some of the air is recirculated. Filtration affects the results with the SCR generally increasing with lower efficiency filters and decreasing with higher efficiency filters. The SCR for going to a MERV <5 filter is near unity since the MERV <5 and 6 filters have similar removal for the size range of SOA formation of 0.1–1 μm (see Figure 2). An increase in filter efficiency has a larger relative effect on the SCR within the commercial than the residential model due to its continuous flow and larger volumetric flow rates through the HVAC filter. In the residential model, the O_3 Filtration had little effect on the SCR since there was ozone removal by the Used filter, η_{O3}, of 10% and duty air flow. However, the commercial model exhibited a large SCR since it had a Used η_{O3} of 41% within a continuous flow case with as much as 90% recirculated air. The Temperature and RH cases affect C_{SOA} with F_T and F_{RH} in Equation 1, and their SCRs vary by approximately 15% over the temperature range considered and about 2% over the relative humidity range.

Table 4. SOA Change Ratios (SCR = adjusted C_{SOA}/base case C_{SOA}) for Rural and Urban base cases in the residential and commercial models.

				SOA Change Ratio (SCR)	
Parameter	**Model**	**Base Case**	**Going To**	**Residential**	**Commercial**
Rural Base Case					
Flow	Residential	Duty	Continuous	0.84	
	Commercial	10% OA/90% RA	50% OA/50% RA		0.73
			100% OA		0.52
Filtration (PM)	Residential, Commercial	MERV 6	MERV <5	1.01	1.06
			MERV 11	0.76	0.34
			MERV 15	0.53	0.14
			ESP	0.94	0.70
Filtration (O_3)	Residential, Commercial	Loaded	New	1.00	1.37
Temperature	Residential, Commercial	T75	T65	1.15	1.15
			T85	0.84	0.84
RH	Residential, Commercial	R50	R25	1.02	1.02
			R50	0.98	0.98
Urban Base Case					
Flow	Residential	Duty	Continuous	0.86	
	Commercial	10% OA/90% RA	50% OA/50% RA		0.71
			100% OA		0.51
Filtration (PM)	Residential, Commercial	MERV 6	MERV <5	1.01	1.04
			MERV 11	0.80	0.44
			MERV 15	0.62	0.22
			ESP	0.85	0.68
Filtration (O_3)	Residential, Commercial	Loaded	New	1.00	1.37
Temperature	Residential, Commercial	T75	T65	1.15	1.15
			T85	0.84	0.84
RH	Residential, Commercial	R50	R25	1.02	1.02
			R50	0.98	0.98

Rural base case: residential model = 22.8 μg/m^3; commercial model = 15.4 μg/m^3.
Urban base case: residential model = 90.9 μg/m^3; commercial model = 62.9 μg/m^3.

Table 4 displays results derived from the integrated C_{SOA} results. More nuanced trends in the SOA formation can be determined by examining summary results from a size-resolved perspective, also within the context of parametric influence on C_{SOA}. Figure 4 displays the median particle size-resolved residential Rural (a) C_{SOA} and (b) C_{seed} and residential Urban (c) C_{SOA} and (d) C_{seed}, for PM Filtration parameters within each Flow case. Each bar summarizes the results that use the two parameters listed below it as inputs, with the fraction of C_{SOA} and C_{seed} attributed to each size bin demarcated by a different shade within the bar. In Figure 4a, for example, the size-

resolved bar for the MERV <5 filter within the Duty case was created by summing the median size-resolved geometric means of C_{SOA} and C_{seed} for any modeled result that had MERV <5 and Duty parameters as inputs. The total number of Rural and Urban scenarios were each 162, and each bar is the result of 18 scenarios except the ESP, which is the result of 9 scenarios (since the ESP does not have a Used case for O_3 Filtration).

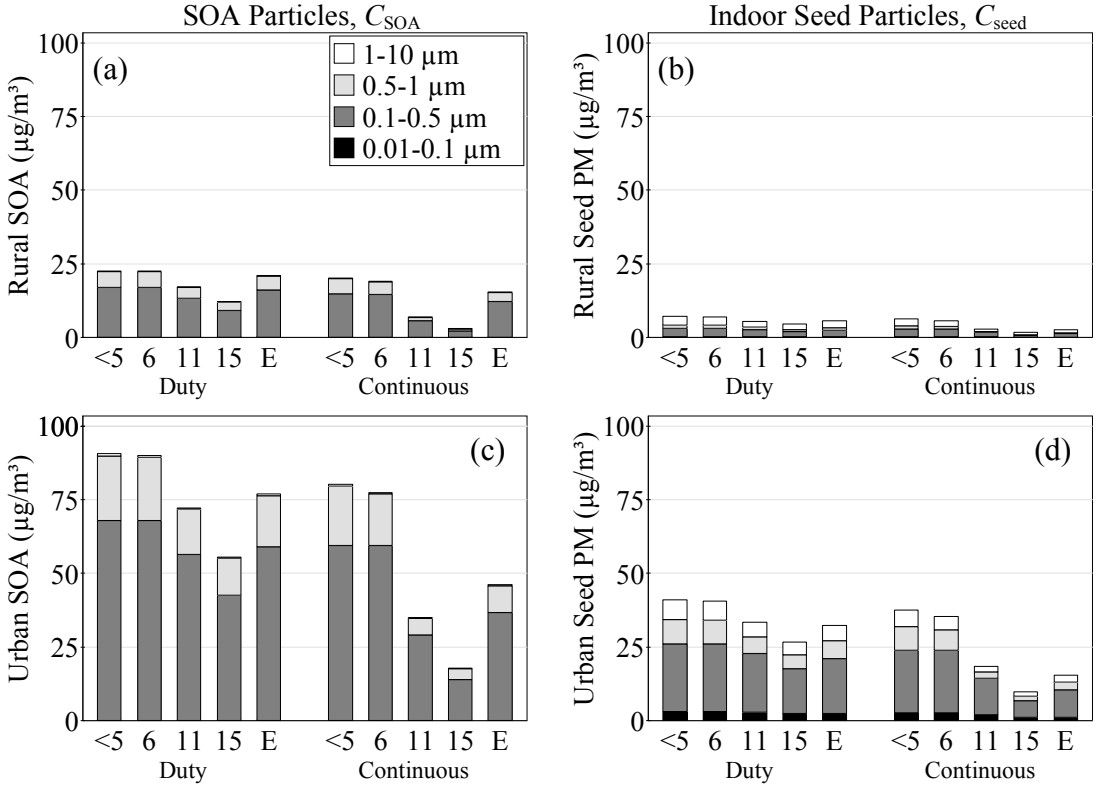

Figure 4. Size-bin-resolved residential Rural (a) C_{SOA} and (b) C_{seed} and residential Urban (c) C_{SOA} and (d) C_{seed} (µg/m^3), for PM Filtration parameters within each Flow case.

As with the base cases, the Rural cases yielded lower C_{SOA} than the Urban cases, due to the lower rural $C_{O3,out}$. Indoor seed particles, C_{seed}, were higher for the Urban than the Rural cases, since the outdoor mass concentrations were higher, particularly for particles within the range of 0.1–1 µm. This size range readily penetrates through the building envelope with the infiltration air exchange, which is the only source of outdoor particles in the residential model. Most of the resulting C_{SOA} mass were particles in the

size range of 0.1–0.5 μm, with the rest in the range of 0.5–1 μm. This particle size range also tends to have the longest residence time in the air, since it has the lowest values for removal by both filtration and deposition to indoor surfaces. The fact that the C_{SOA} are larger than C_{seed} and most of the C_{SOA} is in the range of 0.1–1 μm implies the following about particle source apportionment in indoor environments with substantial SOA formation. Particles in the range of 0.1–1 μm are likely to be SOA products of chemical reactions, and particles in the size ranges smaller than or larger than 0.1–1 μm are likely to be of outdoor origin, assuming no other indoor sources of particles.

This result has implications for applying density assumptions to concentrations of indoor particles with a substantial fraction of SOA, implying that one density assumption for all sizes may not be ideal. Our models and Coleman et al. (2008) assumed a density of 1 g/cm^3 for all SOA and particles of outdoor origin, but other researchers have assumed different values. SOA density assumptions in the literature commonly fall into the range of 1–1.4 g/cm^3. Our SOA density assumption did not affect the GM or the GSD of the lognormal yield of SOA that was calculated from Coleman et al. (2008), but only the magnitude of formation. Outdoor particles are often assigned a density of 1 g/cm^3, but sometimes they are assigned a density of 2.5 g/cm^3 for particles over 2.5 um, since this size range may be more likely to contain crustal material (Seinfeld and Pandis, 1998). However, our density assumptions do not affect the utility of the results of our model. To adjust any reported C_{SOA} or C_{seed} to the value it would have with a different density assumption, multiply that C_{SOA} or C_{seed} by the factor change of density (e.g. multiply C_{SOA} by 1.2 to change the C_{SOA} results to those for a density of 1.2 g/cm^3).

Figure 4 also shows that higher efficiency filters lead both to reduced C_{SOA} and C_{seed}. Furthermore, the higher efficiency filters have a larger effect for the residential scenarios with continuous HVAC operation. Continuously recirculated air moves through the HVAC system with an air exchange rate of 4 h^{-1} versus 0.67 h^{-1} for the cyclical duty flow, which allows the filter to remove six times more mass in the Continuous versus the Duty cases. The ESP removes particles much better than the MERV <5 or 6 filters and better than or similarly to the MERV 11 filter for the size range

of 0.1–1 μm (see Figure 2). However, the ESP leads to approximately equal C_{SOA} when compared to the MERV <5 or 6 filters for Duty or Continuous flow within the Rural cases and for Duty flow within the Urban cases. These comparable resulting C_{SOA} values are because the indoor ozone concentration, C_{O3}, increases due to the ozone emission of the ESP, E_{O3}. The relative effect of E_{O3} on C_{SOA} is larger in the rural environment since $C_{O3,out}$ is lower. Though not included in this model, filter bypass would have a relatively large affect on reducing the effect of changing filtration efficiency, since the range of SOA formation is the size range of particles very likely to follow fluid streamlines and flow around the filter with the bypass air (Ward and Siegel, 2005; Waring and Siegel, 2008). Our models also assumed a constant filter removal efficiency, though filter loading over time will likely change the removal efficiency of the porous-media filters (Hanley et al., 1994) and decrease the removal efficiency of the ESP (Wallace et al, 2004).

Figure 5 is similar to Figure 4, but for the commercial Rural (a) C_{SOA} and (b) C_{seed} and commercial Urban (c) C_{SOA} and (d) C_{seed}, for PM Filtration parameters within each Flow case. Figure 5 does not display the MERV < 5 and 11 filters for brevity and since their trends may be inferred from the results of the MERV 6 and 15 filters. The total number of Rural and Urban scenarios were each 243, and each bar is the result of 36 scenarios except the ESP, which is the result of 18 scenarios (since the ESP does not have a Used case for O_3 Filtration). As with the base cases, there are smaller C_{SOA} in the commercial versus the residential model. Similar to the residential model, in the commercial model the effect of PM Filtration depends on the Flow case. However, in contrast to the residential model, all flow is continuous in the commercial model, and higher filtration efficiency leads to lower C_{SOA} in cases with higher fractions of recirculated air. For the 100% OA case, more efficient filtration had no effect on SOA concentrations since all indoor air was continuously ventilated. The ESP led to a higher C_{SOA} for the 100% OA cases due to its emission of ozone, E_{O3}. The C_{SOA} for scenarios with the ESP changed little for different Flow cases, since the filtration of SOA by the

ESP is challenged by the extra SOA that is formed due to the increased influence of the E_{O3} within recirculated air.

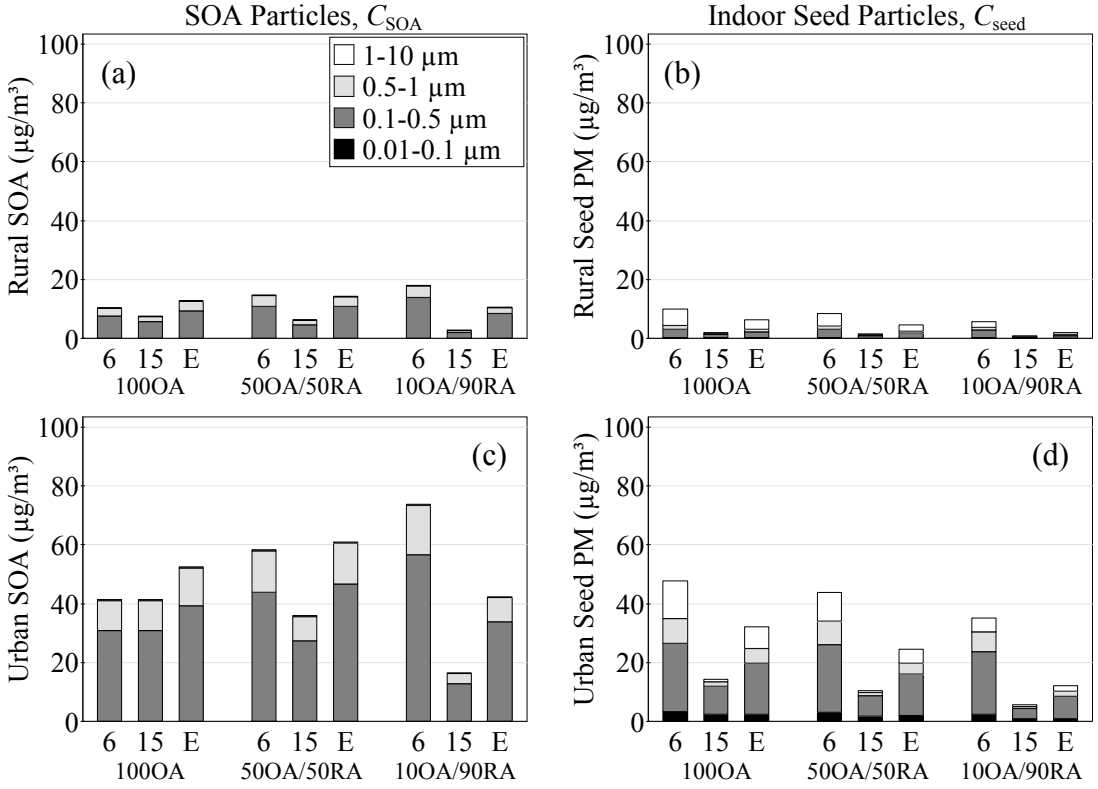

Figure 5. Size-bin-resolved commercial Rural (a) C_{SOA} and (b) C_{seed} and commercial Urban (c) C_{SOA} and (d) C_{seed} (µg/m^3), for PM Filtration parameters within each Flow case.

The parametric analysis with the SCRs demonstrates that the O_3 Filtration parameter influences C_{SOA} in the commercial model. Figure 6 is similar to Figures 4 and 5, and it shows the size-bin-resolved commercial (a) Rural and (a) Urban C_{SOA}, for O_3 Filtration parameters within each Flow case. Figure 6 does not display C_{seed} since it is not dependent on η_{O3}. The total number of Rural and Urban scenarios were each 243, and each of the New bars are the result of 45 scenarios and the Used bars the result of 36 scenarios (since the ESP does not have a Used case for O_3 Filtration). The Rural and Urban cases exhibit similar trends, but with different magnitudes of C_{SOA} since $C_{O3,out}$ is different. The change in C_{SOA} going from a New to a Used case is the smallest within the

10% OA/90% RA case since these cases have the lowest C_{O3} due to their having the lowest fraction of outdoor air. The differences in New versus Used cases are very similar within the other two flow cases of 100% OA and 50% OA/50% RA. This similarity is because going from the 100% OA case to the 50% OA/50% RA increases C_{terp} (due to indoor emission) but decreases the C_{O3} (due to outdoor-to-indoor transport) at amounts that result both in comparable values of absolute C_{SOA} and comparable differences in New versus Used cases.

In general, the η_{O3} parameter has less of an effect on C_{SOA} in the residential than the commercial model, for two reasons. The first is that the Used value for η_{O3} is much less in the residential than the commercial model. The second reason for the reduced relative influence of η_{O3} in the residential model is because ozone-laden air is only introduced indoors from outdoors in the residential model through infiltration. In the commercial model, ozone is introduced indoors from outdoors via both infiltration and ventilation (see Equation 4), so η_{O3} has an effect on source as well as removal mechanisms. One potential limitation of our approach is that the values for η_{O3} from Zhao et al. (2007) were determined with ozone removal tests at face velocities of 0.4 cm/s, which is much lower than would likely occur in most HVAC systems. However, their mean residential value of 10% is comparable to values reported in two other studies conducted at larger face velocities (Hyttinen et al., 2003; Bekö et al., 2007). Their mean commercial value of 41% from Zhao et al. (2007) is somewhat higher than other reported commercial values, but these larger values could reflect a choice of venue from which used filters were procured (e.g. a filter from an office would likely have a lower value of η_{O3} than a restaurant because of unsaturated cooking oils that would settle on the particle-cake on a used filter from a restaurant).

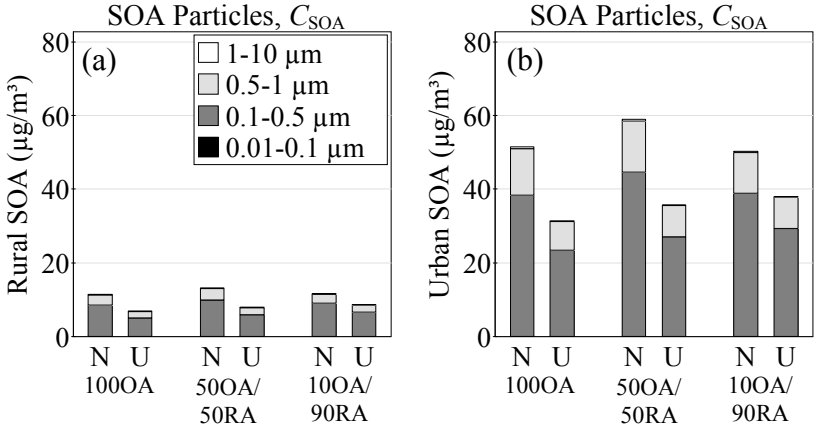

Figure 6. Size-bin-resolved commercial (a) Rural and (a) Urban C_{SOA} (µg/m^3), for O_3 Filtration parameters within each Flow case.

To compare the influence of HVAC system components and operation on SOA concentrations, we developed a steady-state model. In reality, one or both reactant sources and resulting concentrations are likely to be transient in nature. Outdoor ozone concentrations rise and fall according to a diurnal cycle, and indoor ozone concentrations due to outdoor-to-indoor transport thus also fluctuate diurnally, albeit at lower concentrations than and lagging slightly in time behind those outdoors (Weschler, 2000). However, indoor emissions of ozone, such as from in-duct ESPs (Viner et al., 1992), portable ion generators (e.g. Waring et al., 2008), or office equipment (Lee et al., 2001), can produce either a steady-state or time-averaged indoor emission, which leads to a portion of the indoor ozone concentration having a steady or nearly steady baseline with the influence of the diurnal outdoor ozone concentration added over it. Also, most terpenoid emissions indoors are likely to be nearly pulse emissions, such as the floor mopping event used here, or the application of a surface cleaner (Singer et al., 2006b) or consumer product (Corsi et al., 2007). However, plug-in air fresheners emit terpenoids at a nearly steady rate over a time-scale of days (Singer et al., 2006b). Thus, the resulting C_{SOA} from our models should not necessarily be interpreted as those to which occupants would be exposed over long periods of time. Nevertheless, this modeling effort effectively illustrates the relative effects that HVAC components and operation strategies can have on indoor SOA concentrations.

It is important to revisit other assumptions of our approach. The assumptions that have the largest impacts on SOA formation are those related to the input parameters of the models. Where possible we used values from the literature, but there are numerous gaps in the research as well as assumptions and limitations described in the text. Therefore, we suggest caution in applying the results to a real building without sufficient knowledge of parameter values and without validation of the results presented here. Another important assumption is that the entire building was well-mixed, despite the fact that the emission of the terpenoids and the removal of ozone on HVAC components are likely to occur in a single zone in the buildings. However, given the relatively small losses of SOA due to deposition onto surfaces as compared to air exchange and filtration losses, this assumption will likely have a small impact on the final results. A further assumption is that this entire analysis considered particles as spheres. This assumption is better for SOA than particles of outdoor origin, since SOA are formed from gas-phase products that condense into spheres, the form that results in the lowest free energy of the aerosol. Finally, we assumed one volume, V, each for the residential and commercial model. For the model Equations 1–4, V occurs in Equations 3 and 4, which include indoor emissions of terpenoids and ozone, respectively. Equation 3, however, is unaffected by a change in V, since the terpenoid emission is function of the floor area, which changes linearly with V, since the ceiling height is fixed. Only Equation 4 when it includes an indoor emission of ozone by the ESP, E_{O3}, is affected by a change in V. As V decreases, the influence of E_{O3} on C_{O3} increases, and vice versa. Thus, for all scenarios without an ESP, C_{SOA} is independent of V.

The terpenoid emission and reaction assumptions deserve their own discussion. The floor mopping emission in the residential model led to a $C_{terp,m}$ of 592.9 ppb for all scenarios. The floor mopping emission in the commercial model led to different $C_{terp,m}$ values, depending on the ventilation rate, and the range of $C_{terp,m}$ was 157.0–1026 ppb, the median 296.5 ppb, and the mean 493.3 ppb. These concentrations are largely on the same order as those in Singer et al. (2006) for the floor mopping emission in a 50 m^3 test chamber with an air exchange rate of 0.5 h^{-1}. For reference, the odor threshold of d-

limonene is 440 ppb (Devos et al., 1990). We also assumed that the only loss of terpenoids was by ventilation and that there was no change in terpenoid concentrations due to the reaction with ozone (see Equation 3), which is a reasonable assumption because we focus on the relative effect caused by the HVAC system operation. Moreover, in Coleman et al. (2008), the reacted ozone changed much more than the reacted terpenoids, at 90% decrease versus a 25% decrease, respectively. Terpenoids do adsorb to building surfaces (Singer et al., 2004) and HVAC system components (Fick et al., 2005), but adsorption was neglected since it does not affect steady-state concentrations. The terpenoid emission in our model and its SOA yield was based on a pine-oil cleaner with d-limonene as one of its major constituents. The terpene d-limonene has the highest SOA mass formation potential of common indoor terpenoids (Weschler and Shields, 1999; Ng et al., 2006), so different consumer products with other reactive terpenes or terpene alcohols would likely result in lower SOA concentrations.

Using the HVAC system to reduce the amount of SOA that forms in buildings is a worthwhile goal. To cause the biggest reduction in SOA exposure, using a high-efficiency filter will have the most impact, followed by ozone control strategies, such as eliminating ozone sources such as an ESP or reducing outdoor-to-indoor transport of ozone with an activated carbon filter. HVAC flow strategies can also have a large effect at reducing SOA concentrations indoors. For instance, at times when ozone concentrations are low outdoors, a commercial HVAC system could deliver 100% ventilation air to dilute concentrations resulting from indoor terpenoid emissions. Conversely, when there are terpenoid emissions that coincide with high outdoor ozone concentrations, the highest allowable level of recirculated air could be used. In a residential home, setting the HVAC system on continuous recirculation will likely reduce SOA concentrations.

As shown in Figures 3–5, the amount of SOA formed has the potential to constitute a large fraction of the total mass concentration of indoor particles, which has implications for particle loading onto HVAC equipment. The deposition of particles onto HVAC filters, coils, and ducts can lead to increased energy use and secondary indoor air

quality problems. The SOA size range of 0.1–1 μm predominately deposits only on HVAC filters and penetrates through coils and ducts (Waring and Siegel, 2008). Filter loading can increase the pressure drop across a filter, which can lead to increased energy use over time in HVAC systems with a variable speed fan. Filter loading also affects indoor air quality, in both positive and negative ways. Positively, removal of SOA by a filter can improve the indoor air by removing the SOA particles themselves as well as potentially increasing the removal efficiency of the filter, which can increase with loading for porous-media filters (Hanley et al., 1994). Negatively, however, filter loading can also reduce indoor air quality by decreasing the efficiency of ESPs (as well as some filters) and increasing the reactivity of porous-media filters with ozone and free radicals, which can react with the particle-cake on used filters to yield gaseous byproducts (Hyttinen et al., 2003; Bekö et al., 2006, 2007; Zhao et al., 2007).

SOA formation also has further implications for human exposure. SOA particles in the size range of 0.1–1 μm have the ability to penetrate the upper airway regions and deposit in the alveolar sacs of the lungs (Hinds, 1999). Additionally, Rohr et al. (2002) exposed mice to the oxidation products (both particle and gas-phase) of limonene and ozone reactions and noted acute upper airway irritation in the mice. However, Wolkoff et al. (2008) later showed that the gaseous elements, rather than the particle phase elements, of the d-limonene/ozone reaction may be responsible for acute upper airway irritation. There has been no research into the chronic effects of exposure to SOA. Since the reactions between terpenoids and ozone lead to both particle-phase SOA and gas-phase products (such as formaldehyde, other more complex aldehydes, and carboxylic acids), for HVAC strategies that lead to the same final concentration of SOA those that reduce the actual formation are preferable to those that remove SOA after formation. Similarly, an SOA reducing strategy of removing ozone in the HVAC stream would preferably be accomplished with an activated carbon filter rather than a used porous-media particle filter, since the activated carbon filter would lead to lower concentrations of gaseous reaction products.

CONCLUSIONS

This paper presented the results of a modeling investigation that predicted the relative influence of a HVAC system components and operation strategies on SOA formation due to ozone reactions with terpenoids. We reported the results for 324 unique residential scenarios (162 each of in a rural and urban climate) and 486 unique commercial scenarios (243 each of in a rural and urban climate). The resulting loading rates varied over a range of an order of magnitude, depending on the inputs of the varied HVAC parameters. For each set of unique parameter combinations, the median and range of resulting SOA concentrations were as follows. In a rural setting, the median residential and commercial SOA concentrations for all simulations were 17.4 $\mu g/m^3$, with a range of 2.47–27.0 $\mu g/m^3$, and 10.6 $\mu g/m^3$, with a range of 1.81–26.3 $\mu g/m^3$, respectively. In an urban setting, the median predicted residential and commercial SOA concentrations were 68.0 $\mu g/m^3$, with a range of 14.7–108 $\mu g/m^3$, and 44.8 $\mu g/m^3$, with a range of 11.6–105 $\mu g/m^3$, respectively. Based on our model and its input parameters, the following further conclusions can be drawn from this work:

- More indoor SOA is formed in urban areas due to higher ambient ozone concentrations. However, SOA concentrations in rural areas may be a higher fraction of the total indoor particles than urban areas.
- Much of the resulting SOA distribution is in the 0.1–1 μm diameter size range, and excluding those from indoor sources, indoor particles above or below this range are likely of outdoor origin.
- Residential SOA concentrations are most influenced by the particle filtration efficiency, whether the HVAC system cycles on and off or runs continuously, and the indoor set-point temperature.
- Commercial SOA concentrations are most influenced by the particle filtration efficiency, whether ozone is removed by HVAC filters or other ozone sinks, the fraction of ventilation versus recirculated air, and the indoor set-point temperature.

- The enhanced particle removal capability of an electrostatic precipitator (ESP) can be substantially dampened by its ozone generation and consequent SOA formation.
- The relative effect of the ozone emissions of an ESP on SOA formation are larger in a rural than an urban area since ambient ozone concentrations are lower.
- The filtration of ozone by an HVAC component is an effective way to reduce indoor SOA concentrations. To reduce indoor SOA, methods that lead to the lowest formation of gaseous byproducts, such as ozone filtration by activated carbon, are preferable.

ACKNOWLEDGMENTS

This work was funded by an ASHRAE Graduate Student Grant-in-Aid, a National Science Foundation IGERT Traineeship (Award DGE 0549428), and a Harrington Dissertation Fellowship from the University of Texas at Austin.

Appendix D

PAPER IV

Secondary Organic Aerosol Formation from Ozone Reactions with Single Terpenoids and Terpenoid Mixtures

(In Preparation for Submission to *Atmospheric Environment*)

ABSTRACT

Ozone reacts with terpenoids indoors to form secondary organic aerosol (SOA). Most SOA research to date has focused on ozone reactions with single terpenoids or with consumer products. To bridge this gap, this paper reports the results from an investigation of SOA formation from ozone reactions with both single terpenoids and mixtures of d-limonene, α-pinene, and α-terpineol. For mixtures, the terpenoids were combined at concentrations that would yield initial equivalent pseudo first-order loss rates, $k_{pseudo,i}$ (h^{-1}), for each terpenoid with ozone, thus eliminating an initial bias of ozone reacting preferentially with one terpenoid over another. For experiments with initial ozone concentrations, $[O_{3,i}]$ = 25 ppb, reactions with only d-limonene yielded larger peak particle number concentrations than for any other experiment with a single terpenoid or mixture, even more than experiments with three times the total combined $k_{pseudo,i}$. For experiments with $[O_{3,i}]$ = 100 ppb, this trend was not observed. When $([O_{3,i}] \times k_{pseudo,i}) \geq$ 45 ppb/h, peak particle formation followed a linear trend for reactions with both single terpenoids and mixtures. These results imply that the nucleation potential for ozone and d-limonene is strong at low ozone conditions when no other reactive compounds are present. From a mass perspective, the SOA formation with $[O_{3,i}]$ = 25 ppb followed linear trend versus $([O_{3,i}] \times k_{pseudo,i})$, but not for $[O_{3,i}]$ = 100 ppb. Also, since yields for many single terpenoids are readily available in the literature, this work suggests that yields for single terpenoids at typical indoor ozone concentrations can reasonably predicted SOA mass formation from ozone reactions with mixtures.

INTRODUCTION

Ozone (O_3) is commonly present indoors and drives a substantial amount of indoor chemistry. Indoor sources of ozone are either due to outdoor-to-indoor transport of ozone-laden air (Sabersky et al., 1973; Weschler, 2000) or indoor emission from devices such as portable ion generators or office equipment (Mullen et al., 2005; Niu et al., 2005; Tung et al., 2005; Britigan et al., 2006). One of the more common and important types of indoor ozone reactions are that with terpenoids. Terpenoids are often at significant concentrations indoors due to their emission from consumer products such as air fresheners, cleaning agents, and perfumes (e.g. Nazaroff and Weschler, 2004; Corsi et al., 2007) or wood products (Baumann et al., 1999; Saarela, 1999). The most common indoor terpenoids are the monoterpenes of d-limonene and α-pinene (Brown et al., 1994). Also, α-terpineol, a monoterpene alcohol, is emitted indoors as component of cleaners and pine oil (Nazaroff and Weschler, 2004). These terpenoids are often present at high enough concentrations indoors that their ozone reaction rates compete with loss due to air exchange (Weschler and Shields, 2000; Wells, 2005).

Ozone/terpenoid reactions lead to the stable products of secondary organic aerosol (SOA), aldehydes, and carboxylic acids (Weschler and Shields, 1999; Kamens et al., 1999; Leungsakul et al., 2005). The SOA is in the ultrafine (< 0.1 μm) and lower fine (0.1–2.5 μm) particle size ranges, and it is composed of low vapor pressure, high molecular weight products that partition to the particle phase. One common parameter used to describe gas-phase SOA formation is the product yield, Y_g (-), which is equal to the ratio of the mass concentration of SOA formed to the mass concentration of terpenoid reacted, $\Delta C_{SOA}/\Delta C_{terp}$ (Odum et al., 1995). Besides producing stable oxidized products, ozone/terpenoid reactions yield unstable reactive intermediates, such as hydroxyl radicals (OH), alkylperoxy radicals (RO_2), and Criegee biradicals (Kamens et al., 1999; Leungsakul et al., 2005).

Previous research on indoor SOA formation due to ozone/terpenoid reactions has focused either on ozone reactions with single terpenoids or with consumer products. Weschler and Shields (1999) first showed that ozone reacted with d-limonene, α-

terpinene, or an α-pinene-based cleaner to form SOA in an office setting. Other research has subsequently investigated SOA formation with single terpenoids at concentrations typical of indoor environments, with most of it focusing on ozone/d-limonene reactions (Wainman et al., 2000; Rohr et al., 2003; Weschler and Shields, 2003; Sarwar and Corsi, 2007; Vartiainen et al., 2006; Alshawa et al., 2007; Zuraimi et al., 2007; Langer et al., 2008) or ozone/α-pinene reactions (Rohr et al., 2003; Sarwar et al., 2003). SOA formed from ozone reactions with consumer products has also been studied. SOA formation has been observed when ozone reacted with lemon- and pine-scented cleaners, air fresheners, and perfumes, both in laboratory chambers or rooms (Sarwar et al., 2004; Destaillats et al., 2006; Singer et al., 2006; Corsi et al., 2007; Coleman et al., 2008; Waring et al., 2008) and in real indoor environments (Long et al., 2000; Hubbard et al., 2005).

Despite this extensive body of research on SOA formation, there has been limited research on ozone reactions with single versus mixtures of terpenoids. In the only investigation of mixtures that I know of, Li et al. (2007) merged separate kinetic models for ozone/d-limonene and ozone/α-pinene reactions and closely simulated the formation and timing for SOA mass concentrations in outdoor air. Investigations of SOA formation due to ozone reactions with single versus mixtures of terpenoids are important because they bridge the gap between research with single terpenoids and with consumer products, allowing further insight into complex indoor oxidative chemistry. To that end, this paper reports the results from a set of experiments investigating the SOA formed from ozone reactions with single terpenoids and mixtures of the terpenoids of d-limonene, α-pinene, and α-terpineol. Reactants were combined in different combinations, at both low and high ozone initial concentrations, and the resulting SOA number and mass concentrations were analyzed. Since SOA yields are readily available in the literature for single terpenoids, this investigation also determined whether single terpenoid SOA yields are additive for SOA formation from ozone reactions with terpenoid mixtures.

METHODOLOGY

Experiments were performed in a 90 L Teflon-film reaction chamber that was operated as a batch reactor with a volume that decreased as samples were withdrawn. Diluent air was introduced to the chamber and was passed through anhydrous $CaSO_4$ and molecular sieves to remove both moisture and organic contaminants. The filling system was equipped with a heated syringe injection port facilitating the introduction of liquid or gaseous reactants into the chambers with the flowing air stream, at amounts that would yield desired initial terpenoid concentrations. Ozone was introduced via a separate injection port at the opposite end of the reactor. Ozone was produced by photolyzing air with a mercury pen lamp in a separate Teflon-film ozone chamber. Ozone concentrations in the ozone chamber were determined with a UV photometric ozone analyzer (Thermo Environmental model 49-C). Aliquots of this ozone/air mixture were added to the reaction chamber using a gas-tight syringe, at amounts that would yield the desired initial ozone concentration in the 90 L reaction chamber.

Particle samples were monitored with a MSP Corporation M1000XP-A Wide-Range Particle Spectrometer (WPS™) equipped with a M1000XP-B Scanning Mobility Spectrometer (SMS™), for a particle size range of 10–500 nm over 40 bins, every two minutes. Terpenoid samples were quantified using an Agilent 6890 gas chromatograph with a 5973 mass selective detector (GC/MS). Gas samples were cryogenically collected employing an Entech 7100 sampling system utilizing the following three-stage trap and temperature parameters: 100 mL of the chamber contents was collected onto Trap 1 (packed with Tenax TA) at −150 °C. Then, Trap 1 was heated to 40 °C, and the sample was transferred under a flow of ultra high-purity helium (UHP He) onto Trap 2 (packed with Tenax TA) cooled to −30 °C. Then, Trap 2 was heated to 180 °C, and the sample was transferred under an UHP He flow onto Trap 3, a silanized 0.53 mm i.d. tube cooled to −160 °C, which then heated to 220 °C to inject the sample onto the GC column (Restek Rtx VRX, 0.25 mm i.d., 30 m long, 1.4 μm film thickness). The GC temperature program used was initial temperature of 45 °C held for 8 min after sample injection, then increased 10 °C/min to 220 °C and held for 4 min. Mass calibration was determined for

the experimental terpenoids by injecting known amounts of terpenes into the reaction chamber and analyzing with GC/MS.

Two experimental phases were conducted, Phase I and II. Phase I consisted of 13 experiments (Experiments 1–13) that monitored the time- and size-resolved formation of SOA due to ozone reactions with single terpenoids and mixtures of terpenoids. Known amounts of a single terpenoid or a mixture of terpenoids were introduced with diluent air into the chamber. Once the chamber was filled, it was then connected to the particle sampler. After one size-resolved particle sample was taken (2 min), a known amount of ozone was introduced into the chamber and 24 more particle samples were taken (48 min), for a total sampling time of 50 min.

The pseudo first-order reaction rate of a terpenoid with ozone, k_{pseudo} (h^{-1}), is the product of the bimolecular reaction rate constant (ppb^{-1} h^{-1}) and terpenoid concentration (ppb). Phase I experimental concentrations were chosen to yield initial pseudo first-order reaction rates of any terpenoid in the experiment with ozone, $k_{pseudo,i}$, that were either equivalent or integer-factors of each other. Mixture experiments with equivalent $k_{pseudo,i}$ eliminates an initial bias of ozone reacting preferentially with one terpenoid over another. The initial terpenoid reactant concentrations, [$terp_i$] (ppb), are referred to as [d-lim_i] for d-limonene, [α-pin_i] for α-pinene, and [α-$terp_i$] for α-terpineol. The reaction rate constants for ozone with d-limonene is 0.018 ppb^{-1} h^{-1}, α-pinene is 0.0076 ppb^{-1} h^{-1} (Atkinson et al., 1992), and α-terpineol is 0.027 ppb^{-1} h^{-1} (Wells, 2005). Thus, reactions of ozone with [d-lim_i] = 50 ppb, [α-pin_i] = 118 ppb, and [α-$terp_i$] = 33 ppb each yield $k_{pseudo,i}$ = 0.9 h^{-1}.

In Phase I, Experiments 1–9 were conducted with [$terp_i$] of between 50 and 118 ppb, depending on the terpenoid, and initial ozone concentrations, [$O_{3,i}$] = 25 ppb. Experiments 10–13 were conducted with identical [$terp_i$] to Experiments 1, 2, 4, and 6, but with [$O_{3,i}$] = 100 ppb. The experiments with low [$O_{3,i}$] = 25 ppb represent concentrations found indoors due to outdoor-to-indoor transport (Weschler, 2000) or from indoor sources such as office equipment (Britigan et al., 2006) or portable ion generators (Waring and Siegel, 2009). The [$O_{3,i}$] = 100 ppb for the high ozone experiments are feasible in buildings with high air exchange rates in urban environments

(Weschler, 2000) or due to ozone generator use (e.g. Weschler and Shields, 1999; Hubbard et al., 2005). Combining the reactants in the manner herein simulates a transient release of terpenoids indoors without a substantial indoor ozone emission, since elevated ozone concentrations due to outdoor-to-indoor transport would not be immediately replenished after reactions commenced.

Phase II consisted of 11 experiments (Experiments Y1–Y11) and determined SOA yields, Y_g (-), for ozone reactions with single terpenoids. Known amounts of a terpene and ozone were combined in the Teflon chamber and allowed to react for one hour. After one hour, seven size-resolved particle samples were taken every two min, for a total of 14 min, and then one terpenoid sample was taken, on the order of 10 min after the last particle sample. Y_g were calculated as the ratio of the mass of SOA formed (assuming spherical particles with a density of 1 g/cm^3) and mass of terpenoid reacted.

Between all Phase I and Phase II experiments, reaction chambers were cleaned by first ozonating them at high concentrations (> 1 ppm) and then flushing at least six times. Analysis of both the treated, compressed air and the cleaned chamber by GC/MS revealed that any contaminants were below the part-per-trillion range. Results show that particle loss was negligible for both Phase I and II experiments.

RESULTS AND DISCUSSION

Phase I experiments

Table 1 lists the [terp$_i$], $k_{pseudo,i}$, the first peak of the total number concentrations, and the final total number and mass concentrations for Phase I experiments. Also, the lognormal parameters (number concentration, N; geometric mean diameter, GMD; and geometric standard deviation, GSD) for both the peak and final SOA number distributions are listed in Table 2. These were fit to minimize the sum of the squared difference between measured and modeled distributions, using either 2 or 3 modes. Comparing results from various experiments illustrates differences in the SOA formation trends: Experiments 1 vs. 2 vs. 3 demonstrates the differences in SOA formation among

ozone reactions with the single terpenoids, at low [$O_{3,i}$]; Experiments 1, 2, 3, and 7 vs. Experiments 4–6, 8, and 9 the differences for ozone reactions with single terpenoids vs. mixtures of terpenoids, respectively, at low [$O_{3,i}$]; and Experiments 1, 2, 4, and 6 vs. Experiments 10–13 the differences in low [$O_{3,i}$] vs. high [$O_{3,i}$], respectively.

Table 1. Phase I initial reactant concentrations, pseudo first-order reaction rates of terpenoids with ozone ($k_{pseudo,i}$), and the first peak number and final number and mass concentration results.

	Initial Reactant Concentrations					SOA Formation		
						Number		Mass
	$[O_{3,i}]$	$[d\text{-}lim_i]$	$[\alpha\text{-}terp_i]$	$[\alpha\text{-}pin_i]$	$k_{psuedo,i}$	Peak	Final	Final
Exp.	(ppb)	(ppb)	(ppb)	(ppb)	(h^{-1})	(#/cm^3)	(#/cm^3)	(μg/m^3)
1	25	50	0	0	0.9	13,628	7,430	4.2
2	25	0	33	0	0.9	547	486	0.33
3	25	0	67	0	1.8	7,257	5,626	7.2
4	25	50	33	0	1.8	8,567	5,991	4.6
5	25	50	67	0	2.7	11,284	9,064	8.9
6	25	50	33	118	2.7	12,854	7,578	7.7
7	25	0	0	118	0.9	4,044	1,985	2.1
8	25	0	33	118	1.8	9,232	4,406	6.6
9	25	0	67	118	2.7	12,693	7,982	11
10	100	50	0	0	0.9	16,326	17,699	3.7
11	100	0	33	0	0.9	20,857	21,014	34
12	100	50	33	0	1.8	39,022	30,383	31
13	100	50	33	118	2.7	50,152	40,787	84

Table 2. Lognormal distribution parameters (number concentration, N; geometric mean diameter, GMD; and geometric standard deviation, GSD) for both the first peak (P) and final (F) measured SOA distributions.

		Measured	Mode 1			Mode 2			Mode 3			Modeled
		number	N	GMD	GSD	N	GMD	GSD	N	GMD	GSD	number
Exp.		(#/cm^3)	(#/cm^3)	(nm)	(-)	(#/cm^3)	(nm)	(-)	(#/cm^3)	(nm)	(-)	(#/cm^3)
1	P	13,628	4,257	44	1.6	7,695	70	1.3	1,575	98	1.1	13,527
	F	7,430	5,221	85	1.3	2,088	113	1.2	-	-	-	7,309
2	P	547	25	16	1.0	511	48	1.6	15	78	1.0	551
	F	486	30	58	1.0	413	98	1.4	30	141	1.1	472
3	P	7,257	3,382	72	1.5	3,720	115	1.3	-	-	-	7,102
	F	5,626	88	53	1.0	1,249	157	1.2	4,179	112	1.3	5,516
4	P	8,567	4,422	66	1.5	3,894	102	1.2	-	-	-	8,317
	F	5,991	121	79	1.0	2,798	84	1.4	3,015	118	1.2	5,935
5	P	11,284	5,535	76	1.5	5,638	115	1.3	13	430	1.2	11,187
	F	9,064	6,254	98	1.3	2,726	137	1.2	-	-	-	8,980
6	P	12,854	6,001	68	1.5	6,735	105	1.3	15	356	1.2	12,751
	F	7,578	2,230	136	1.2	5,237	100	1.3	-	-	-	7,467
7	P	4,044	607	23	1.4	3,470	58	1.5	39	74	1.0	4,116
	F	1,985	552	84	1.3	562	100	1.1	843	140	1.2	1,956
8	P	9,232	4,022	84	1.5	5,114	128	1.3	-	-	-	9,137
	F	4,406	3,302	117	1.3	962	164	1.2	-	-	-	4,264
9	P	12,693	6,244	63	1.6	6,418	110	1.3	-	-	-	12,662
	F	7,982	6,524	115	1.3	1,184	160	1.1	72	58	1.0	7,781
10	P	18,827	9,412	38	1.4	9,335	59	1.2	-	-	-	18,746
	F	17,699	14,385	59	1.4	3,020	82	1.1	-	-	-	17,405
11	P	20,857	16,421	104	1.4	3,938	145	1.2	-	-	-	20,359
	F	21,014	14,597	118	1.3	5,985	163	1.2	-	-	-	20,582
12	P	39,022	19,853	56	1.4	13,498	80	1.3	5,443	104	1.1	38,795
	F	30,383	17,289	96	1.3	8,527	124	1.2	4,120	150	1.1	29,937
13	P	50,152	20,696	76	1.4	16,788	97	1.2	12,119	132	1.2	49,604
	F	40,787	27,770	128	1.3	4,789	153	1.1	7,446	187	1.1	40,005

To further reveal formation trends, Figure 1 displays the temporal development of the total number concentrations for Experiments 1, 2, 4, 6, and 10–13. Experiments 1, 2, 4, and 6 have the same [terp$_i$] at low [$O_{3,i}$] as for Experiments 10–13 at high [$O_{3,i}$]. Figure 2(a) and (b) display the first peak of the total number concentrations versus the

product of the $[O_{3,i}]$ and total $k_{pseudo,i}$ for each terpenoid. Figure 2(c) and (d) displays the final mass concentrations versus ($[O_{3,i}] \times k_{pseudo,i}$). Plotting the formation results versus ($[O_{3,i}] \times k_{pseudo,i}$) normalizes the SOA formation by the initial concentrations of ozone and either single terpenoids or mixtures. In Figure 2(b), (c), and (d), the different shades of the bars represent the contribution of each terpenoid to the total $k_{pseudo,i}$.

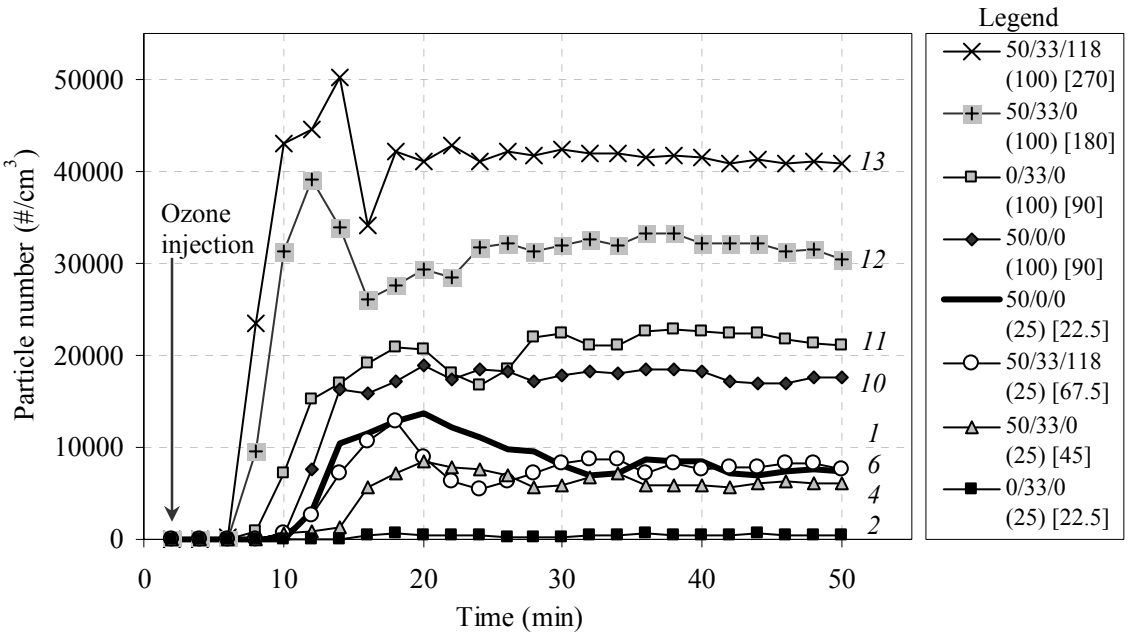

Figure 1. Temporal development of the SOA number concentration for 8 experiments in Phase I. Ozone was injected at 2 min. In the legend, the first set of numbers are [d-lim$_i$]/[α-terp$_i$]/[α-pin$_i$], the number in parentheses is $[O_{3,i}]$, and the number in brackets is ($[O_{3,i}] \times k_{pseudo,i}$). Italicized numbers correspond to the experiment number.

Figure 1 illustrates that for Experiments 11–13 with higher ($[O_{3,i}] \times k_{pseudo,i}$), initial SOA formation was detected 6 min after ozone was introduced into the chamber, but for Experiments 1, 2, 4, 6, and 10 with lower ($[O_{3,i}] \times k_{pseudo,i}$), initial SOA formation was detected 8–14 min after ozone injection. This detection time is a function of the time-scales of two processes, the SOA nucleation and the mixing of the air between the ozone injection port and the particle counting port (which were at opposite ends of the semi-rectangular chamber). These two processes occur in parallel, so the detection time

for Experiments 11–13 implies that the mixing time in the chamber is no more than 6 min. For Experiments 1, 2, 4, 6, and 10, the mixing time is less than the nucleation time.

The first peak of the number concentration occurred between 10–16 min after the ozone injection, after which particle number concentrations leveled off to a near-constant value. For Experiments 1–9 with low $[O_{3,i}]$, the first peak concentration was the highest observed concentration, and the final number concentration ranged between 48–89% of the peak. For Experiments 10–13 with high $[O_{3,i}]$, the first peak was not always the highest observed number concentration, and the final number concentration ranged between 78–110% of the first peak value.

SOA formation occurs by either nucleation or partitioning of products into a condensed phase onto preexisting particles (Pankow, 1994). There were no particles present in the chamber initially, so the initial particle formation was due entirely to nucleation. After the ozone injection into the chamber, reactions started and gaseous products accumulated. Once the lowest volatility products reached their supersaturation concentrations, nucleation commenced and SOA number concentrations increased rapidly. After peaking, the SOA concentrations decreased likely due to coagulation losses. With particles available, condensation of products onto these particles occurred in parallel to the continued nucleation. As the mass of organic aerosol increased, condensation occurred more rapidly (Pankow, 1994; Odum et al., 1996), slowing down the rate of and eventually precluding any new particle formation, thus stabilizing the SOA number concentration. Figure 1 shows that the particle number concentrations were near-constant through the end of the experiment, and deposition loss was neglected.

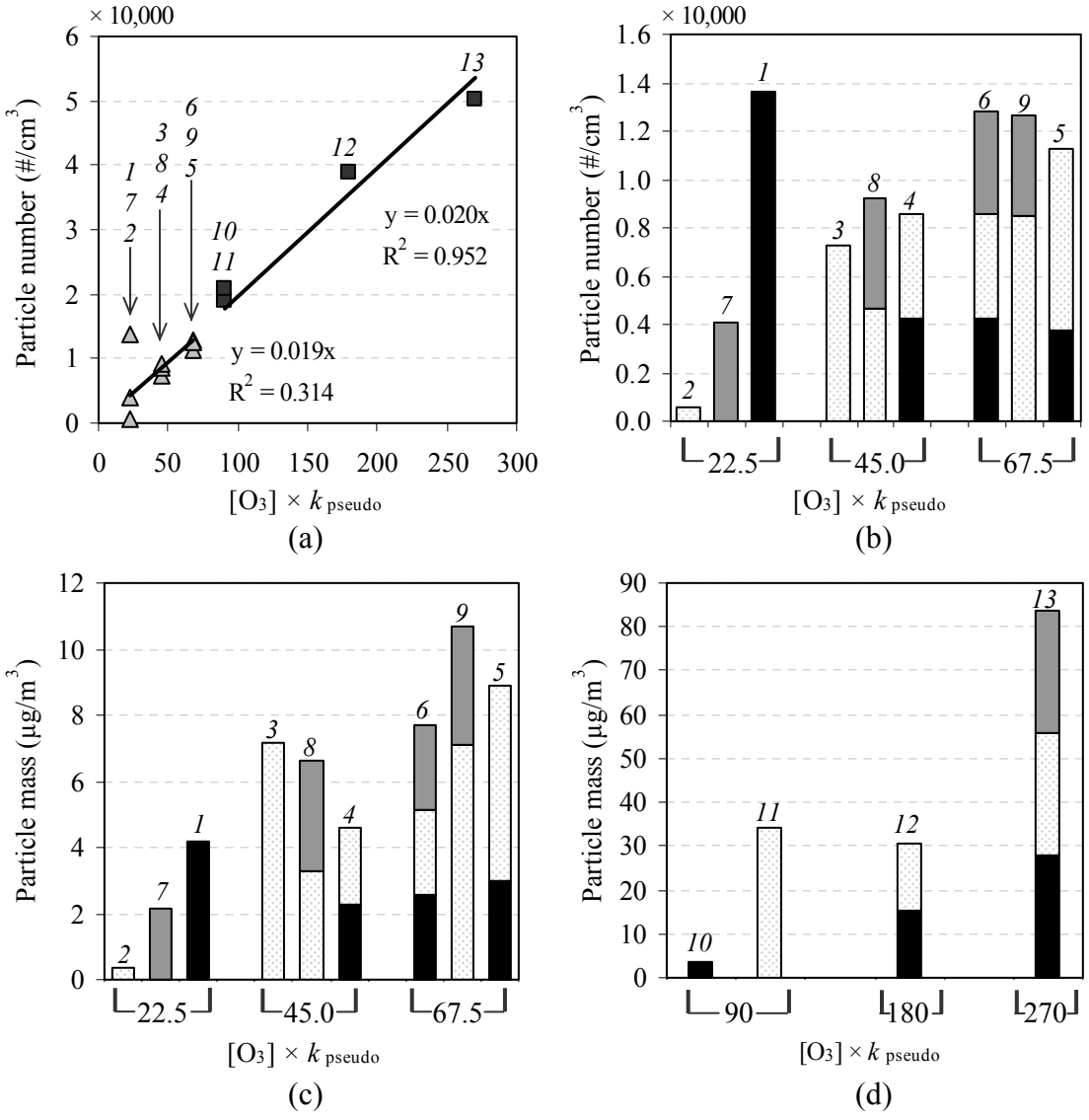

Figure 2. SOA concentration vs. ($[O_{3,i}] \times k_{pseudo,i}$). Plot (a) shows peak number concentrations for Experiments 1–13 on a linear x-axis. Plots (b)–(d) show as bar plots (b) peak number concentrations for Experiments 1–9, (c) final mass concentrations for Experiments 1–9, and (d) final mass concentrations for Experiments 10–13. For (b)–(d), the different shades represent the fraction of each terpenoid of the total $k_{pseudo,i}$. Black is for d-limonene, gray is for α-pinene, and dotted white is for α-terpineol. Italicized numbers correspond to experiment number.

For Experiments 1–9 with low $[O_{3,i}]$, Experiment 1 with $[\text{d-lim}_i]$ of 50 ppb yielded the largest peak total number concentration, higher than experiments with single

terpenoids or mixtures, even though some experiments had three times the total $k_{pseudo,i}$. Also, the final number concentrations for Experiment 1 were the third largest observed, at 93 and 98% of the those for Experiments 6 and 9, which had three times the total $k_{pseudo,i}$. Experiment 6 used a mixture with [d-lim$_i$] = 50 ppb, [α-terp$_i$] = 33 ppb, and [α-pin$_i$] = 118 ppb. Experiment 9 used a mixture of [α-terp$_i$] = 67 ppb and [α-pin$_i$] = 118 ppb.

These results reflect the large potential of ozone/d-limonene reaction products to nucleate at these low ozone conditions. For experiments with identical [d-lim$_i$], the addition of another reactive terpenoid appears to lessen its nucleation potential greatly, which is illustrated by the results of Experiments 4, 5, and 6 exhibiting lower peak number formation than Experiment 1. Also, Experiment 1 yielded more SOA number than the other experiments with single terpenoids. Experiment 2, with [α-terp$_i$] = 33 ppb, resulted in the lowest peak and final particle number concentrations, illustrating a possible low number formation potential of α-terpineol at these conditions. Experiment 7, which had [α-pin$_i$] = 118 ppb, resulted in modest number formation.

Though results of peak number formation for Experiments 1, 2, and 7 with single terpenoids at low [$O_{3,i}$] were very different from each other, for experiments with single terpenoids or mixtures of terpenoids that result in a system with higher total $k_{pseudo,i}$, the results are more predictable. Figure 2(a) and (b) show that for values of ([$O_{3,i}$] × $k_{pseudo,i}$) ≥ 45 ppb/h, the relationship between ([$O_{3,i}$] × $k_{pseudo,i}$) and peak number concentration is linear. The linear fit to experiments with low [$O_{3,i}$] was $y = 0.019x$ ($R^2 = 0.314$) and for high [$O_{3,i}$] was $y = 0.020x$ ($R^2 = 0.952$). The R^2 value for the low ozone experiments is small since the experiments with ([$O_{3,i}$] × $k_{pseudo,i}$) = 25 h^{-1} affected the goodness of the fit. However, the slopes of the fits from Experiments 1–9 and 10–13 are nearly identical. For the terpenoids studied, the prediction of peak number concentration is possible with knowledge of ([$O_{3,i}$] × $k_{pseudo,i}$), if ([$O_{3,i}$] × $k_{pseudo,i}$) ≥ 45 ppb/h.

The reason for the large nucleation potential of products of ozone/d-limonene reactions at low ozone conditions appears to be more complicated than simply that less ozone is available to react with d-limonene in a mixture, since the same trend was not observed with Experiment 10, which equivalent [d-lim$_i$] to Experiment 1 but at high

$[O_{3,i}]$. Reactions of ozone with d-limonene, which has two unsaturated carbon-carbon bonds, is a complex process that can lead to first or second generation products, depending on whether ozone is limited or in excess (Ng et al., 2006). For experiments with low $[O_{3,i}]$, ozone was the limiting reagent, so first generation products were likely responsible for most all nucleation that occurred. Nucleation for a single product occurs when the saturation ratio, S_{sat} (-), which is the ratio of the partial pressure of the compound to the saturation vapor pressure of the compound, is greater than unity. For nucleation due to multiple products, S_{sat} for each product need not exceed unity for nucleation to occur (Seinfeld and Pandis, 1998). Thus, it is speculated that the ozone-limited reaction with d-limonene yields a set of byproducts with higher nucleation potential than those that occur with ozone reactions with mixtures of terpenoids or ozone-excess reactions with d-limonene.

From a mass perspective, all experiments reached a steady concentration by the end of the sampling time, except for Experiment 13, which was still increasing. For Experiments 1–9 with low $[O_{3,i}]$, the linear fit of the final mass concentration versus ($[O_{3,i}] \times k_{pseudo,i}$) was $y = 0.133x$ ($R^2 = 0.799$). For Experiments 10–13 with high $[O_{3,i}]$, the linear fit of the final mass concentration versus ($[O_{3,i}] \times k_{pseudo,i}$) was $y = 0.259x$ ($R^2 = 0.717$). The slopes of the mass fits for experiments with low $[O_{3,i}]$ and high $[O_{3,i}]$ are not approximately equal, as they were with the peak number formation. However, for the low $[O_{3,i}]$, Figure 2(c) shows that the SOA formation follows a more predictable trend from a mass than a number perspective. The average mass concentrations for experiments with ($[O_{3,i}] \times k_{pseudo,i}$) of 22.5, 45.0, and 67.5 ppb/h were 2.2, 6.1, 9.1 $\mu g/m^3$, respectively, and the factor increase in SOA mass was approximately proportional to the increase in $k_{pseudo,i}$.

The mass results for Experiments 10–13 with high $[O_{3,i}]$ are less predictable. Figure 2(d) shows that Experiment 10, with $[\text{d-lim}_i] = 50$ ppb, led to a low amount of total mass formed. Experiment 11, with $[\alpha\text{-terp}_i] = 33$ ppb, led to an SOA mass concentration that was 9.2 times greater, even though its peak number concentration was only 1.2 times greater. This is a surprising result, given that for the low ozone

experiments, Experiment 1 with [d-lim$_i$] = 50 ppb yielded 15 times the final number and 13 times the final mass concentration of Experiment 2 with [α-terp$_i$] = 33 ppb. Also not expected was the fact that Experiment 12 yielded a similar mass concentration to Experiment 11, rather than yielding more SOA mass. At these high [$O_{3,i}$], the d-limonene appears to have a dampening effect on the mass formation that occurs from α-terpineol alone, since [d-lim$_i$] = 50 ppb and [α-terp$_i$] = 33 ppb led to less SOA mass than [α-terp$_i$] = 33 ppb alone. Experiment 13, which had 3 times the total $k_{pseudo,i}$ of Experiments 10 and 11 and 1.5 times the total $k_{pseudo,i}$ of Experiment 12, exhibited the largest formation of SOA mass.

Phase II experiments

A total of 11 experiments in Phase II (Experiments Y1–Y11) were performed. Phase II experiments determined the SOA yields, Y_g (-), for ozone reactions with single terpenoids. The different [terp$_i$], ΔC_{terp}, ΔC_{SOA}, and resulting Y_g are listed in Table 3.

Table 3. For Phase II experiments, [$O_{3,i}$], [terp$_i$], and the results, which determined SOA yields, Y_g, for ozone reactions with d-limonene, α-pinene, and α-terpineol.

		Initial Concentrations				
		[$O_{3,i}$]	[terp$_i$]	ΔC_{terp}	ΔC_{SOA}	Y_g
Exp.	Terpenoid	(ppb)	(ppb)	(μg/m^3)	(μg/m^3)	(-)
Y1	d-limonene	25	50	193	3.00	0.016
Y2	d-limonene	50	50	243	25.6	0.11
Y3	d-limonene	25	100	269	33.1	0.12
Y4	d-limonene	150	100	482	118	0.25
Y5	α-pinene	25	235	83.4	7.71	0.092
Y6	α-pinene	75	235	274	73.8	0.27
Y7	α-pinene	150	235	521	144	0.28
Y8	α-terpineol	25	50	137	2.83	0.021
Y9	α-terpineol	25	67	168	5.28	0.031
Y10	α-terpineol	75	67	330	50.7	0.15
Y11	α-terpineol	150	67	422	114	0.27

For each terpenoid, the different [terp$_i$] and [$O_{3,i}$] were chosen to yield a range of resulting ΔC_{SOA}, which is important because the Y_g is a function of the total organic aerosol mass concentration, M_o (μg/m^3). This dependency arises because SOA is formed through partitioning of semi-volatile reaction products into the condensed organic phase in particles, and more organic material present in the particle phase allows for greater partitioning capacity of semi-volatile products (Pankow, 1994). The expression for Y_g is as in Equation 1 (Odum et al., 1996):

$$Y_g = \sum_i Y_{g,i} = M_o \sum_i \left(\frac{\alpha_i K_{om,i}}{1 + K_{om,i} M_o} \right) \quad (1)$$

where $K_{om,i}$ (m^3/μg) is a partitioning coefficient for species i , in terms of the organic mass concentration, and α_i is a proportionality constant relating the concentration of reactant that reacts to the total concentration of product i that is formed. For Equation 1, two products are usually used to fit the behavior of the SOA formation. Since the reactant air was free of particles before the ozone/terpenoid reactions commenced, $M_o = \Delta C_{SOA}$. Figure 3 shows the measured Y_g from experiments Y1–Y11, as well as the curves fitted with Equation 1 and the fitting parameters.

Figure 3 shows that the largest Y_g are for α-pinene, then for d-limonene, and then for α-terpineol. This trend is somewhat atypical of other results found in the literature. The Y_g for d-limonene is usually reported as being higher than that of α-pinene for ozone chemistry (Weschler and Shields, 1999; Ng et al. 2006). Y_g for α-terpineol have not been previously reported. The difference in reported Y_g between the results herein and those in the literature may be partially due to the small volume reactor chamber used in these experiments. Most research has determined Y_g in larger reaction chambers, which are on the order of at least 30 m^3 (e.g. Ng et al., 2006). A scaling estimate of surface-to-volume ratios (A/V) reveals that the A/V for a 90 L chamber is approximately an order of magnitude greater than that for a 30 m^3 chamber. This larger A/V in the 90 L chamber increases the influences of surface phenomena.

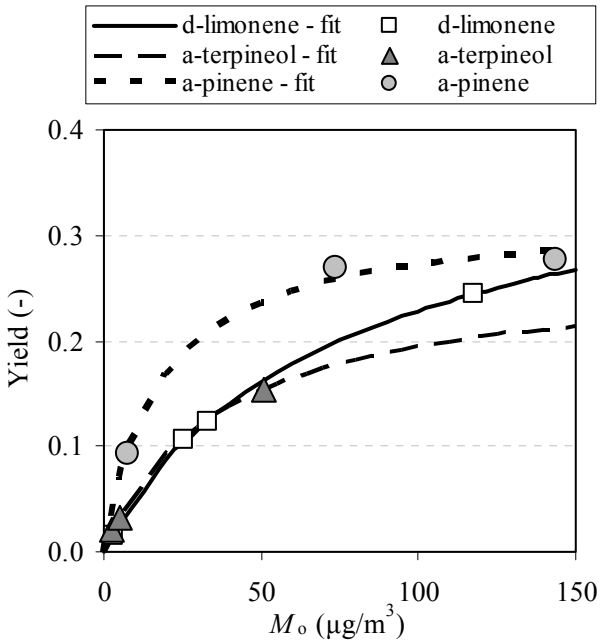

Figure 3. SOA yields, Y_g, for d-limonene, α-terpineol, and α-pinene as a function of M_o. Symbols are experimental values and lines are fits. Parameters used to generate fit lines are: d-limonene is $\alpha_1 = 0.351$, $K_{om,1} = 0.016$, $\alpha_2 = 0.539$, $K_{om,2} = 0.00028$; α-terpineol is $\alpha_1 = 0.268$, $K_{om,1} = 0.026$; and α-pinene is $\alpha_1 = 0.320$, $K_{om,1} = 0.056$.

The amount of that a compound adsorbs from the gas-phase onto a surface is dependent on the compound vapor pressure (Won et al., 2001; Weschler, 2003). α-Pinene has a boiling point of 156 °C and an approximate vapor pressure of 4 torr at 25 °C (Fichon et al., 1999); d-Limonene a boiling point of 176 °C and vapor pressure of 2 torr at 25 °C; and α-Terpineol a boiling point of 219 °C and vapor pressure of 0.04 torr at 25 °C. Thus, α-terpineol should adsorb to the chamber surfaces the most, followed by d-limonene, and α-pinene should adsorb the least. Since ΔC_{terp} was calculated as the difference of a measured amount and the known injected (but not measured) amount, adsorption to the chamber walls would bias the yields by inflating ΔC_{terp}. Since α-terpineol has the lowest vapor pressure, this bias should be the largest for it, then for d-limonene, then finally it should be the lowest for α-pinene. However, these Y_g were used to explore whether single terpenoid Y_g are additive for mixtures in the same experimental

apparatus, so the potential bias is less important from that perspective, assuming no influence of other surface phenomena.

Predicting SOA formation from yields from single terpenoids

The Y_g from single terpenoids determined with Phase II experiments can be used with Phase I results to estimate whether single terpenoid Y_g are additive in a mixed compound environment. Final terpenoid concentrations were not measured in Phase I experiments, so they were estimated for each concentration for 48 minutes after ozone injection by using a numerical approach. The concentration of reactant *i* at a particular time step, $C_i(t+1)$ (ppb), varied with each time step and is represented by Equation 2:

$$C_i(t+1) = C_i(t)\exp(L_i(t)\Delta t) \tag{2}$$

where $C_i(t)$ is the concentration of *i* from the previous time step (ppb), $L_i(t)$ is the pseudo first-order loss rate of *i* at that time step (h^{-1}), and Δt is the time step (h). L_i(t) was calculated with Equation 3:

$$L_i(t) = \sum_j k_j C_j(t) \tag{3}$$

where k_j (ppb^{-1} h^{-1}) and C_j (ppb) are the reaction rate constants and concentrations, respectively, from any compound *j* that reacts with *i* in the system. Ozone reacted with all terpenoids present, and each terpenoid present reacted only with ozone.

The Y_g for each terpenoid are listed in Table 4 and were calculated with Equation 1 and the fit parameters in the caption for Figure 3 for the final SOA mass measured at the end of Experiments 1–13. Using each terpenoid, *l*, in Experiments 1–13, the predicted change in SOA mass concentration, $\Delta C_{SOA,predicted}$ ($\mu g/m^3$) was calculated as the sum of the product of each yield, $Y_{g,l}$, and the corresponding estimated change in concentration, $\Delta C_{terp,l}$ ($\mu g/m^3$), as in Equation 4:

$$\Delta C_{SOA,predicted} = \sum_l Y_{g,l}\Delta C_{terp,l} \tag{4}$$

The final measured SOA concentrations and the predicted SOA concentrations for Experiments 1–13 are listed in Table 4, as well as the percent difference between the two values. A positive percent difference indicates that the measured value was larger than the predicted value of ΔC_{SOA}.

Table 4. Results exploring if SOA yields, Y_g, from Phase II experiments, which were for single terpenoids, are additive for mixtures in experimental Phase I. $[O_{3,i}]$, $[\text{d-lim}_i]$, $[\alpha\text{-terp}_i]$, and $[\alpha\text{-pin}_i]$ are the initial concentrations in Phase I for ozone, d-limonene, α-terpineol, and α-pinene, respectively. ΔC_{terp} was estimated with Equation 2 in the text. Y_g are from the curve fits in Figure 1, and they were used to calculate the predicted ΔC_{SOA} for Phase I experiments. The percent difference (% diff) is between the measured value at the end of Phase I and predicted value of C_{SOA}.

	Initial Concentrations (ppb)				ΔC_{terp} (μg/m^3)			Y_g (-)			ΔC_{SOA} (μg/m^3)		
Exp.	$[O_{3,i}]$	$[\text{d-lim}_i]$	$[\alpha\text{-terp}_i]$	$[\alpha\text{-pin}_i]$	d-lim	α-terp	α-pin	d-lim	α-terp	α-pin	Meas.	Pred.	% diff
1	25	50	0	0	71.1	0	0	0.022	0	0	4.2	1.6	62
2	25	0	33	0	0	70.7	0	0	0.0023	0	0.33	0.16	50
3	25	0	67	0	0	110	0	0	0.043	0	7.2	4.7	35
4	25	50	33	0	55.3	53.9	0	0.024	0.029	0	4.6	2.9	37
5	25	50	67	0	43.6	84.9	0	0.044	0.051	0	8.9	6.2	30
6	25	50	33	118	43.3	41.5	41.2	0.039	0.045	0.097	7.7	7.6	2.2
7	25	0	0	118	0	0	75.6	0	0	0.034	2.1	2.6	-21
8	25	0	33	118	0	53.3	54.4	0	0.040	0.087	6.6	6.8	-3.4
9	25	0	67	118	0	84.2	41.3	0	0.059	0.12	11	9.9	7.2
10	100	50	0	0	202	0	0	0.020	0	0	3.7	4.0	-7.8
11	100	0	33	0	0	176	0	0	0.13	0	34	22	35
12	100	50	33	0	178	156	0	0.12	0.12	0	31	40	-30
13	100	50	33	118	149	133	168	0.21	0.18	0.26	84	100	-20

The percent differences between the measured and an predicted values of ΔC_{SOA} range from −30 to 62%. The mean (s.d.) percent difference for all 13 experiments was 13 (29)%. The mean for experiments with only d-limonene was 27 (50)%, for only α-terpineol was 43 (11)%, and for only α-pinene was −21 (0)%. The mean for experiments with d-limonene and α-terpineol was 12 (37)%, for α-terpineol and α-pinene was 1.9 (7.5)%, and for all three terpenoids was −8.9 (16)%. Based on the mean results, this method appears to under-predict ΔC_{SOA} for α-terpineol the most. Moreover, this method also under-predicts ΔC_{SOA} for mixtures with α-terpineol, particularly for mixtures with α-

terpineol and d-limonene. This under-prediction is consistent with results shown in Figure 2(c) and (d). Overall, the results show that Y_g for single terpenoids can be used to predict SOA mass yields in mixed terpenoid environments reasonably well, which is a useful result since SOA yields for ozone reactions with single terpenoids are readily available in the literature.

Finally, ozone reactions with terpenoids yield hydroxyl radicals, which can react with terpenoids or other reaction products (Atkinson et al., 1992). Our experiments did not scavenge formed hydroxyl radicals, and our results are combined effects of terpenoid oxidation via both ozone and formed hydroxyl radicals. The chemistry due to the formed hydroxyl radicals are expected to increase the mass of SOA formed, but hydroxyl radicals are not expected to affect the initial nucleation of SOA (Colville and Griffin, 2004).

CONCLUSIONS

This paper investigated the number and mass concentrations of SOA that result from ozone reactions with single terpenoids and mixtures of terpenoids. Two phases of experiments were performed with d-limonene, α-pinene, and α-terpineol as the reactive terpenoids. Phase I explored the time- and size-resolved formation of SOA due to ozone reactions with single terpenoids and mixtures. Phase II calculated SOA yields, Y_g, for the single terpenoids. Then the Y_g from Phase II were used with the results from Phase I to assess whether single terpenoid Y_g are additive in a mixed compound environment. All experiments were carried out with transient conditions in a batch reactor experimental apparatus, and this work reached the following conclusions:

(1) At low initial ozone concentrations, $[O_{3,i}]$, ozone reactions with pure d-limonene produced larger peak total number concentrations than ozone reactions with any other single terpenoids or mixtures.

(2) For experiments where the product of $[O_{3,i}]$ and the pseudo first-order loss rate of ozone with terpenoid(s), $k_{pseudo,i}$, is greater than 45 ppb/h, the peak total number concentration is linearly related to $([O_{3,i}] \times k_{pseudo,i})$.

(3) Mass concentrations were more predictable with respect to ($[O_{3,i}] \times k_{pseudo,i}$) for experiments with low $[O_{3,i}]$ versus high $[O_{3,i}]$.

(4) Y_g from ozone reactions with single terpenoids can be used to approximate mass formation in a mixed terpenoid environment reasonably well.

These conclusions, particularly (1) and (2), have implications for indoor exposure to ultrafine and fine particles. Some research has suggested that particle number, rather than mass, may be more associated with adverse health effects (Harrison and Yin, 2000), and thus mixtures that have higher nucleation potential may be more harmful to human health than those with lower nucleation potential. This work highlights the need for further experiments that investigate SOA formation from ozone reactions with terpenoid mixtures.

ACKNOWLEDGMENTS

This work was funded by the National Institute of Occupational Safety and Health (NIOSH), a National Science Foundation IGERT Traineeship (Award DGE 0549428), and a Harrington Dissertation Fellowship from the University of Texas at Austin.

Appendix E

PAPER V

The Influence of Surface Reactions between Ozone and d-Limonene on Secondary Organic Aerosol Formation

(In Preparation for Submission to *Environmental Science and Technology*)

ABSTRACT

Reactions between ozone and terpenoids form products that partition to a condensed phase, yielding secondary organic aerosol (SOA). This work investigated the contribution to gas-phase SOA formation of ozone reactions with the surface-adsorbed terpenoid of d-limonene. A model framework was developed to describe SOA formation due to ozone/terpenoid surface reactions, and this framework was then used in conjunction with experiments in a 283 L chamber to determine $Y_{s,m}$ (the ratio of moles of SOA formed and moles of ozone consumed by ozone/terpenoid surface reactions) for ozone/d-limonene surface reactions. $Y_{s,m}$ ranged from 0.14–0.16 over a wide range of relative humidities. Also, the ratios of the SOA number concentration (#/cm^3) and the mass (μg/m^3) concentration formed for gas-phase (χ_g) and surface-phase (χ_s) reactions were determined. The χ_s ranged from 126–339 (#/cm^3)/(μg/m^3) and χ_g ranged from 51.1–60.2 (#/cm^3)/(μg/m^3), and lower relative humidity led to higher number formation from surface reactions, but not from gas-phase reactions. The model framework predicted that building materials on which ozone/d-limonene surface reactions lead to SOA formation are those with initially low surface reactivity, such as glass, sealed materials, or smooth metals. Using the experimentally determine $Y_{s,m}$ in the model framework, the SOA formation observed in a field study was reasonably predicted.

INTRODUCTION

This paper focuses on reactions between ozone and terpenoids that occur on indoor surfaces. Ozone (O_3) is often present indoors either due to outdoor-to-indoor transport of ozone-laden air (Sakersky et al., 1973; Weschler, 2000) or indoor emission

from devices such as portable ion generators (e.g. Niu et al., 2005a; Tung et al., 2005; Britigan et al., 2006) or office equipment (e.g. Lee et al., 2001; Destaillats et al., 2008). Terpenoids are emitted indoors from wood products and consumer products such as air fresheners, cleaning agents, and perfumes (e.g. Nazaroff and Weschler, 2004; Corsi et al., 2007). The most common indoor terpenoids are monoterpenes, which are composed of two isoprene units, have a molecular weight of 136.24 amu, and a molecular formula of $C_{10}H_{16}$. The most common monoterpenes indoors are d-limonene and α-pinene (Brown et al., 1994), which are often at concentrations that react with ozone in the gas-phase at fast enough rates to compete with loss due to air exchange (Weschler and Shields, 2000).

Ozone/terpenoid reactions can form secondary organic aerosol (SOA), free radicals, carbonyls, and carboxylic acids (Kamens et al., 1999; Leungsakul et al., 2005). The SOA formed is in the ultrafine (< 0.1 μm) and fine (0.1–2.5 μm) particle size ranges. Research on indoor SOA formation has focused almost solely on that which results from products of gas-phase reactions between ozone and either pure terpenoids or consumer products (Weschler and Shields, 1999, 2003; Long et al., 2000; Wainman et al., 2000; Rohr et al., 2003; Sarwar et al., 2003, 2004; Destaillats et al., 2006; Singer et al., 2006; Vartiainen et al., 2006; Alshawa et al., 2007; Sarwar and Corsi, 2007; Zuraimi et al., 2007; Coleman et al., 2008; Langer et al., 2008). However, this paper explores whether the chemistry that occurs due to heterogeneous reactions between ozone and terpenoids adsorbed to surfaces may also influence the formation of airborne SOA.

Terpenoids have vapor pressures that lead to modest adsorption to real building materials from the gas-phase (Won et al., 2001; Singer et al., 2004), and they are also applied directly to interior surfaces in the form of consumer products (Singer et al., 2006b). The primary loss mechanism of ozone indoors is deposition to and subsequent reaction on interior surfaces (Sabersky et al., 1973; Weschler, 2000). Thus it is very likely that ozone reacts with terpenoids adsorbed to surfaces in real buildings. Fick et al. (2005) studied ozonolysis of three monoterpenes in an experimental air handling system. When the system surface area was doubled, the reacted amount (independent of ozone and reaction time) of Δ^3-carene increased by a factor of 2.8 and d-limonene by 2.3.

Flemmer et al. (2007) continuously delivered 100 ppb of ozone-laden air for 72 hours to a vinyl tile surface onto which α-terpineol was applied before the experiment began. Derivatized products were measured in 12 hour intervals over 72 hours, and the yield to the gas-phase of one reaction product increased over the 72 hours and the yield to the gas-phase of another reaction product spiked after 36 hours and then decayed. Springs and Morrison (2008) measured reaction probabilities (ratio of reaction rate to collision rate) of ozone and monoterpenes on model beaded surfaces, and Δ^3-carene ranged from 2.9×10^{-6} to 3.0×10^{-5} and d-limonene from 2.8×10^{-5} to 3.0×10^{-4}. The authors noted that the results imply catalytic effects, as these surface reaction probabilities are 10 to 100 times more probable than gas-phase values for the same compounds.

The goal of this research was to investigate whether the products of ozone and terpenoids adsorbed to surfaces can contribute SOA formation in the gas-phase. The specific research objectives were (i) to articulate a model framework that describes SOA formation due to ozone/terpenoid surface reactions; (ii) to conduct experiments on ideal surfaces to quantify the yield to gas-phase SOA of surface reactions between ozone and adsorbed d-limonene, at different relative humidity (RH) values of 20, 50, and 70%; (iii) to discuss the potential effects for real indoor materials; and (iv) to model the potential SOA formation from surface reactions observed in a recent field study in a residential room. d-Limonene was used in the experiments because it adsorbs to surfaces (Singer et al., 2004), is the primary terpenoid in many consumer products (including the field study discussed herein) (Singer et al., 2006b), has been shown to react with ozone on surfaces (Fick et al., 2005; Springs and Morrison, 2008), and has high SOA mass yield potential (Ng et al., 2006).

MODEL FRAMEWORK

The model framework envisions a three-step mechanism by which ozone reactions with terpenoids adsorbed to surfaces increase gas-phase SOA concentrations. (1) Ozone either (a) adsorbs to the surface and then collides with an adsorbed terpenoid molecule or (b) collides directly from the gas-phase with the adsorbed terpenoid

molecule. (2) Some collisions cause the ozone and terpenoid molecules to react and form products. (3) The reaction products partition between the surface, the SOA and/or the gas-phase at fractions that depend on the product vapor pressures and polarity (Kamens et al., 1999; Leungsakul et al., 2005). Some reaction products on the surface or in the gas-phase can further react with ozone or the hydroxyl radical, which is a product of ozone/alkene chemistry (Atkinson et al., 1992), potentially leading to more products that partition between the SOA-, gas-, and surface-phases. This work does not separate any SOA formation by initial ozone versus secondary ozone or hydroxyl radical chemistry. Also, the effect of temperature is not considered, but temperature changes could affect the sorption rates of terpenoids to surfaces, the volatility of reaction products, and the rates of the chemical reactions.

Steps (1a) and (2), the rapid adsorption of ozone on a surface followed more slowly by a subsequent reaction, is the Langmuir-Hinshelwood mechanism. Dubowski et al. (2004) found evidence for this mechanism when ozone reacted with surface-adsorbed alkenes. However, precise knowledge of the actual mechanism is not necessary for this framework since steps (1) and (2) are incorporated into one mass transfer coefficient, the ozone deposition velocity, v_d (m/h). The definition of v_d is as in Equation 1:

$$v_d = \frac{J}{C_{O3}} \tag{1}$$

where J (μg/m^2·h) is the ozone mass flux to the surface, and C_{O3} (μg/m^3) is the mass concentration of ozone in indoor air. Assuming the bulk air is well-mixed and that the concentration at the edge of the boundary layer is equivalent to the bulk air concentration, the v_d is rate-controlled by the inverse sum of two resistances in series, the boundary layer resistance and the surface reaction resistance. The boundary layer resistance is determined by the rate of ozone transport through the concentration boundary layer, and the transport-limited deposition velocity, v_t (m/h), is the maximum mass transfer possible at given flow conditions. The surface reaction resistance of ozone with a particular surface is parameterized by the reaction probability, γ (-), which is the rate at which

ozone is irreversibly consumed at a surface divided by the rate at which ozone collides with that surface.

The original deposition velocity of ozone to a surface without any terpenoid adsorption, $v_{d,o}$ (m/h), is represented by Equation 2 (Cano-Ruiz et al., 1993):

$$v_{d,o} = \left(\frac{1}{v_t} + \frac{1}{\gamma_o < v > / 4} \right)^{-1} \quad (2)$$

where γ_o (-) is the original reaction probability of ozone for the surface without terpenoid adsorption, and ‹v› is the Boltzmann velocity (1.296×10^6 m/h for O_3 at 296 K). In Equation 2, as $\gamma_o \rightarrow 0$, the reactions are rate-limiting, and $v_{d,o}$ is approximated as $\gamma_o \cdot$‹v›/4. As $\gamma_o \rightarrow 1$, transport is rate-limiting, and $v_{d,o}$ approaches v_t.

Terpenoids adsorbed to a surface are expected to affect the γ of and potentially the v_d of ozone to that surface. The $\gamma_{(o + terp)}$ (-) and $v_{d,(o + terp)}$ (m/h) are the resulting reaction probability of and deposition velocity of ozone to a surface with terpenoid adsorption, respectively. The $\gamma_{(o + terp)}$ is defined as in Equation 3 (Springs and Morrison, 2008):

$$\gamma_{(o + terp)} = (1 - r_{terp})\gamma_o + r_{terp}\gamma_{terp} \quad (3)$$

where γ_{terp} (-) is the reaction probability of the adsorbed terpenoid, and r_{terp} (m^2 terpenoid/m^2 intrinsic surface area) is the fractional coverage of a surface with the adsorbed terpenoid, as in Equation 4:

$$r_{terp} = \frac{\left(M_{terp}\right)\left(A_{terp\text{-}molecule}\right)\left(N_A\right)}{\left(S\right)\left(MW_{terp}\right)} \quad (4)$$

where M_{terp} (µg/m^2 nominal surface area) is the mass concentration of the terpenoid on the surface; S (m^2 intrinsic/m^2 nominal surface area) is the ratio of the intrinsic (actual) to nominal (horizontally-projected) surface area of the material; N_A is Avogadro's number (6.022×10^{23} molecule/mol); $A_{terp\text{-}molecule}$ (m^2 terpenoid/molecule) is the cross-sectional area of the terpenoid molecule. Equation 2 can be modified to represent $v_{d,(o+terp)}$ as:

$$v_{d,(o+terp)} = \left(\frac{1}{v_t} + \frac{1}{\gamma_{(o+terp)} < v > / 4} \right)^{-1} \quad (5)$$

For ozone reactions with surfaces on which there are adsorbed terpenoids to contribute to gas-phase formation of SOA, the ozone must react with the adsorbed terpenoid and not another moiety of the building surface. The deposition velocity of ozone solely to an adsorbed terpenoid, $v_{d,terp}$ (m/h), is represented by Equation 6:

$$v_{d,terp} = f_{O3,terp} v_{d,(o+terp)} \quad (6)$$

where $f_{O3,terp}$ (-) is the fraction of ozone that reacts on the surface with the adsorbed terpenoid, as in Equation 7 (Coleman, 2009):

$$f_{O3,terp} = \frac{r_{terp} \gamma_{terp}}{\gamma_{(o+terp)}} \quad (7)$$

As in Equation 2, Equation 5 represents $v_{d,(o+terp)}$ as the inverse sum of the reaction-rate resistance and the mass-transport resistance. Thus, in Equation 5, as $\gamma_{(o+terp)} \rightarrow 0$, the reactions are rate-limiting and $v_{d,(o+terp)}$ is approximated as $\gamma_{(o+terp)} \cdot \langle v \rangle / 4$. As $\gamma_{(o+terp)} \rightarrow 1$, transport is rate-limiting and $v_{d,(o+terp)}$ approaches v_t.

If $v_{d,(o+terp)}$ is in the reaction rate-limited regime, then $v_{d,terp} = f_{O3,terp} v_{d,(o+terp)}$, the expression for $v_{d,terp}$, is the final term in Equation 8:

$$v_{d,terp} = \left(\frac{r_{terp} \gamma_{terp}}{\gamma_{(o+terp)}} \right) \left(\gamma_{(o+terp)} \frac{< v >}{4} \right) = r_{terp} \gamma_{terp} \frac{< v >}{4} \quad (8)$$

Thus, for surfaces for which ozone deposition is reaction rate-limited, $v_{d,terp}$ depends only on r_{terp}, assuming that γ_{terp} is the same for different surfaces.

Once ozone reacts with adsorbed terpenoids on surfaces, the products partition between the particle, gas, and surface phases. The fraction of products that partitions to the condensed particle phase yields SOA mass, which is step (3) of the mechanism outlined above. This fraction may be represented by the molar surface yield, $Y_{s,m}$ (-), defined as the ratio of moles of SOA formed and moles of ozone consumed by the

ozone/terpenoid reactions that occur on the surface. The molecular weight of SOA, MW_{SOA}, is assumed as 180 g/mol (Weschler and Shields, 1999) in all calculations. The contribution of ozone/terpenoid surface reactions to gas-phase SOA, E_s (μg/h), is related to the product of $v_{d,terp}$, the nominal surface-area, A (m^2), of the material, and C_{O3} by $Y_{s,m}$:

$$E_s = Y_{s,m} v_{d,terp} A C_{O3} \left(\frac{MW_{SOA}}{MW_{O3}} \right) \tag{9}$$

where MW_{O3} (g/mol) is the molecular weight of ozone. E_s can be used to predict SOA mass concentrations, C_{SOA} (μg/m^3). Assuming isothermal conditions, no particle resuspension or coagulation, and well-mixed air with only one reactive terpenoid that forms SOA, a mass balance on SOA results in Equation 10:

$$\frac{dC_{SOA}}{dt} = \lambda C_{SOA,out} + Y_{g,m} \Gamma \left(k C_{terp,m} C_{O3,m} \right) + Y_{s,m} \left(C_{O3} \sum_j v_{d,terp,j} \frac{A_j}{V} \right) \left(\frac{MW_{SOA}}{MW_{O3}} \right) - \lambda C_{SOA} - \beta_p C_{SOA} \tag{10}$$

where λ (h^{-1}) is the air exchange rate (which is the ratio of the flow through, Q (m^3/h), to the volume, V (m^3), of the air); $C_{SOA,out}$ (μg/m^3) is the mass concentration of SOA entering with the inlet air; $Y_{g,m}$ (-) is the molar yield of SOA for homogenous reactions between the terpenoid and ozone (defined as ratio of the moles of SOA formed and moles of terpenoid consumed by gas-phase reactions); Γ is a conversion factor to change the units of SOA formation from ppb/h to μg/m^3·h; k (ppb^{-1} h^{-1}) is the bimolecular gas-phase reaction rate constant between the terpenoid and ozone; $C_{terp,m}$ (ppb) and $C_{O3,m}$ (ppb) are the molar concentrations of the terpenoid and ozone, respectively; $v_{d,terp,j}$ is the same as $v_{d,terp}$ but for deposition to a particular surface, j; A_j (m^2) is the nominal surface area of surface, j; and β_p (h^{-1}) is the loss rate of SOA (and other particles) to all surfaces.

The term on the left-hand-side of Equation 10 is the rate of change of C_{SOA} in the air. The first three terms on the right-hand-side of Equation 10 are SOA gain mechanisms, which are introduction with air exchange, formation due to homogenous reactions, and formation due to heterogeneous reactions, respectively. The last two terms

are SOA loss mechanisms, which are removal with air exchange and deposition to indoor surfaces, respectively.

EXPERIMENTAL METHODOLOGY

The first section in this experimental methodology describes a procedure for calculating $Y_{s,m}$ (-), the yield of SOA due to ozone surface reactions with adsorbed d-limonene, that is based on the model framework outlined above. The second section describes the apparatus and instrumentation used in the experiments to determine $Y_{s,m}$.

Experimental procedure to determine $Y_{s,m}$

Experiments (L1–L12) were performed to determine the magnitude of $Y_{s,m}$ due to ozone reactions with adsorbed d-limonene, at RH values of 20, 50, and 70%. Since d-limonene was the reactive terpenoid used, in any equations used in reference to experiments or modeling, the subscript "terp" refers to d-limonene. In all experiments, inlet particle number concentrations were negligibly small (< 50 #/cm^3) and experiments were performed until steady-state. Thus, Equation 10 can be solved for C_{SOA} as in Equation 11. This equation shows that C_{SOA} is comprised of products of gas-phase reactions (first term in the numerator on the right-hand-side) and of products of surface reactions (second term in the numerator on the right-hand-side):

$$C_{SOA} = \frac{Y_{g,m} k C_{terp,m} C_{O3,m} \Gamma + Y_{s,m}\left(C_{O3} v_{d,terp} \frac{A}{V}\right)\left(\frac{MW_{SOA}}{MW_{O3}}\right)}{\left(\lambda + \beta_p\right)} \quad (11)$$

If the parameters in Equation 11 that control SOA formation due to gas-phase reactions are held constant or nearly constant while those that control formation due to surface reactions are varied, then the magnitude of the effect of surface reactions on C_{SOA} can be determined. SOA formation experiments were conducted with the air exchange rate, ozone, and d-limonene concentrations at approximately constant conditions, while A/V was varied for two different chamber conditions, Chambers 1 and 2. Thus,

differences in measured C_{SOA} in Chambers 1 and 2 were largely due to surface reactions. Subtracting $C_{SOA,1}$ ($\mu g/m^3$), the SOA mass concentration for Chamber 1, from $C_{SOA,2}$ ($\mu g/m^3$), the SOA mass concentration for Chamber 2, and solving for $Y_{s,m}$, generates Equation 12:

$$Y_{s,m} = \frac{L_1 L_2 \left(C_{SOA,2} - C_{SOA,1}\right) - L_1 Y_{g,m} k C_{terp,m,2} C_{O3,m,2} \Gamma + L_2 Y_{g,m} k C_{terp,m,1} C_{O3,m,1} \Gamma}{\left(L_1 v_{d,terp,2} \left(\frac{A}{V}\right)_2 C_{O3,2} - L_2 v_{d,terp,1} \left(\frac{A}{V}\right)_1 C_{O3,1}\right)\left(\frac{MW_{SOA}}{MW_{O3}}\right)} \quad (12)$$

where $L_1 = (\lambda + \beta_{SOA})_1$ (h^{-1}) and $L_2 = (\lambda + \beta_{SOA})_2$ (h^{-1}), and the previously defined concentrations and A/Vs with a number 1 or 2 in the subscript are the concentrations in Chambers 1 or 2. The different chamber A/V were Chamber 1 = the empty stainless-steel chamber, and Chamber 2 = the chamber plus 14 stainless-steel woven wire screens.

The addition of the stainless-steel screens increased the A by 460% and decreased V by 2%, respectively, which changed the total A/V by 469%. For the flow rate of 3.6 L/min, the chamber air exchange rates for Chamber 1 was $\lambda_1 = 0.76$ h^{-1} and for Chamber 2 was $\lambda_2 = 0.78$ h^{-1}. The SOA deposition was estimated from Lai and Nazaroff (2000) for Chamber 1 as $\beta_{SOA,1} = 0.03$ h^{-1}, which is a mean value for the particle size range that affects the SOA mass concentration the most. The SOA deposition for Chamber 2 was 4.6 times $\beta_{SOA,1}$ and was $\beta_{SOA,2} = 0.138$ h^{-1}. Thus, $L_1 = 0.79$ h^{-1} and $L_2 = 0.918$ h^{-1}. The geometric properties of the chamber for Chambers 1 and 2 are shown in Table 1.

Table 1. Geometry of the two experimental chamber conditions used in this study.

Experimental surface	A (m^2)	V (m^3)	A/V (m^{-1})	A/V variable name
(1) Experiments with empty chamber				
chamber walls	2.60	0.283	9.19	$(A/V)_1$
(2) Experiments with chamber + 14 screens				
chamber walls	2.60	0.277	9.37	$(A/V)_{2w}$
14 screens	9.36	0.277	33.74	$(A/V)_{2s}$
chamber walls + 14 screens	11.96	0.277	43.11	$(A/V)_2$

Equation 12 assumes that the surface properties of the stainless-steel screens are identical to the stainless-steel of the chamber walls. Equation 13 relaxes this assumption and calculates $Y_{s,m}$ and takes potential differences in surface properties into account:

$$Y_{s,m} = \frac{L_1 L_2 \left(C_{SOA,2} - C_{SOA,1}\right) - L_1 Y_{g,m} k C_{terp,m,2} C_{O3,m,2} \Gamma + L_2 Y_{g,m} k C_{terp,m,1} C_{O3,m,1} \Gamma}{\left(L_1 \left(\left(v_{d,terp,2w}\left(\frac{A}{V}\right)_{2w} + v_{d,terp,2s}\left(\frac{A}{V}\right)_{2s}\right) C_{O3,2}\right) - L_2 v_{d,terp,1}\left(\frac{A}{V}\right)_1 C_{O3,1}\right)\left(\frac{MW_{SOA}}{MW_{O3}}\right)} \quad (13)$$

where the subscript 2w indicates the variable is for the chamber walls in Chamber 2 and 2s for the screens in Chamber 2. The molar gas-phase yield, $Y_{g,m}$, is a function of the total SOA mass concentration (Pankow, 1994) and was determined as 0.22 with yield parameters for d-limonene in Appendix D for the SOA mass concentrations measured in the SOA formation experiments. The ozone/d-limonene reaction rate constant, k, has been previously determined 0.018 ppb^{-1} h^{-1} (Atkinson et al., 1992). In Equation 13, the concentrations were directly measured during the SOA formation experiments.

The determination of the $v_{d,terp,1}$, $v_{d,terp,2w}$, and $v_{d,terp,2s}$ used in Equation 13 for the SOA formation experiments was a multi-step process. First, before any SOA formation experiments and before any d-limonene was injected into the chamber, the deposition velocities of ozone to the surfaces in Chambers 1 and 2, which are $v_{d,o,1}$ (m/h) and $v_{d,o,2}$ (m/h), respectively, were determined. All experiments to determine $v_{d,o}$ were performed until steady-state was reached, allowing $v_{d,o}$ for Chambers 1 and 2 to be determined with Equation 14, which assumes that the chamber was well-mixed:

$$v_{d,o} = \frac{\lambda\left(C_{O3,\,inlet} - C_{O3}\right)}{(A/V)C_{O3}} \quad (14)$$

where $C_{O3,inlet}$ ($\mu g/m^3$) is the ozone mass concentration of the chamber inlet flow.

For Chamber 1, Equation 14 yields $v_{d,o,1}$, the deposition velocity of ozone to the only surface in the chamber, which are the stainless-steel chamber walls. However, for Chamber 2, Equation 14 yields $v_{d,o,2}$, the total deposition velocity to both the chamber walls and the 14 stainless-steel screens. By assuming that the deposition velocity

calculated for Chamber 1 is equivalent to the deposition velocity for Chamber 2 to the chamber walls (i.e., $v_{d,o,1} = v_{d,o,2w}$), the deposition velocity of ozone to the added stainless-steel screens in Chamber 2, $v_{d,o,2s}$, can be determined with Equation 15, which is a surface-to-volume ratio weighted average:

$$v_{d,o,2s} = \frac{(A/V)_2}{(A/V)_{2s}} v_{d,o,2} - \frac{(A/V)_{2w}}{(A/V)_{2s}} v_{d,o,2w} \tag{15}$$

A total of twelve experiments (O1–O12) were conducted to determine the $v_{d,o,1}$, $v_{d,o,2w}$, and $v_{d,o,2s}$ for the different chamber conditions, at the different RH of 20, 50, and 70%. Multiple $v_{d,o}$ experiments were performed with different steady-state values for C_{O3} for Chambers 1 and 2 at RH = 50% to ascertain how $v_{d,o}$ changes with C_{O3}.

Then, for the SOA formation experiments, all deposition velocities of ozone to surfaces with surface-adsorbed d-limonene in the chamber, $v_{d,(o+terp)}$, were calculated with Equation 16, which is similar to Equation 14 but with an additional loss term for ozone due to gas-phase reactions with d-limonene:

$$v_{d,(o+terp)} = \frac{\lambda C_{O3,\,inlet} - \left(\lambda + kC_{terp,m}\right) C_{O3}}{(A/V) C_{O3}} \tag{16}$$

Similarly to experiments for $v_{d,o}$, for Chamber 1 $v_{d,(o+terp),1}$ is the deposition to the chamber walls and for Chamber 2 $v_{d,(o+terp),2}$ is the total deposition velocity to the chamber walls and the 14 stainless-steel screens. Again, by assuming that the deposition velocity calculated for Chamber 1 is equivalent to the deposition velocity for Chamber 2 to the chamber walls (i.e., $v_{d,(o+terp),1} = v_{d,(o+terp),2w}$), the deposition velocity for the 14 stainless-steel screens in Chamber 2, $v_{d,(o+terp),2s}$, can be determined with Equation 17:

$$v_{d,(o+terp),2s} = \frac{(A/V)_2}{(A/V)_{2s}} v_{d,(o+terp),2} - \frac{(A/V)_{2w}}{(A/V)_{2s}} v_{d,(o+terp),2w} \tag{17}$$

The assumption that $v_{d,(o+terp),1} = v_{d,(o+terp),2w}$ is reasonable if there are similar d-limonene concentrations in experiments with Chambers 1 and 2.

Next, of the ozone that deposits to surfaces in the chamber, the fraction of ozone that reacts with adsorbed terpenes, $f_{O3,terp}$, can be calculated with Equation 17:

$$f_{O3,terp} = 1 - \frac{v_{d,o}}{v_{d,(o+terp)}} \quad (17)$$

for Chamber 1 for the chamber walls, $f_{O3,terp,1}$ (-), and for Chamber 2 for the chamber walls, $f_{O3,terp,2w}$ (-), and the screens, $f_{O3,terp,2w}$ (-). Finally, the $v_{d,terp,1}$, $v_{d,terp,2w}$, and $v_{d,terp,2s}$ for each surface can be calculated with Equation 5.

Experimental apparatus and instrumentation

Experiments were performed in a V = 283 L stainless-steel reaction chamber system, shown in Figure 1. The chamber was operated as a continuously mixed flow reactor (CMFR), which assumes that the volume of air in the chamber is well-mixed and that concentrations measured at the outlet are equivalent to the chamber concentrations. Tracer experiments were conducted to ensure that the chamber was well-mixed for both Chambers 1 and 2. The reaction chamber system was comprised of a dryer and humidifier, activated carbon filter, UV ozone generator, 283 L stainless-steel reaction chamber, ozone monitor, particle sizer and counter, d-limonene sampling train, and d-limonene introduction by a liquid diffuser. There were two inlet flows into the chamber (primary and d-limonene) and one outlet flow. The primary inlet flow introduced laboratory air, which was cleaned of organics, humidified and ozonated to a desired level, into the reaction chamber, at a volumetric flow rate of 3.6 L/min. The d-limonene flow introduced d-limonene into the reaction with nitrogen as a carrier gas, at a volumetric flow rate of 5 mL/min.

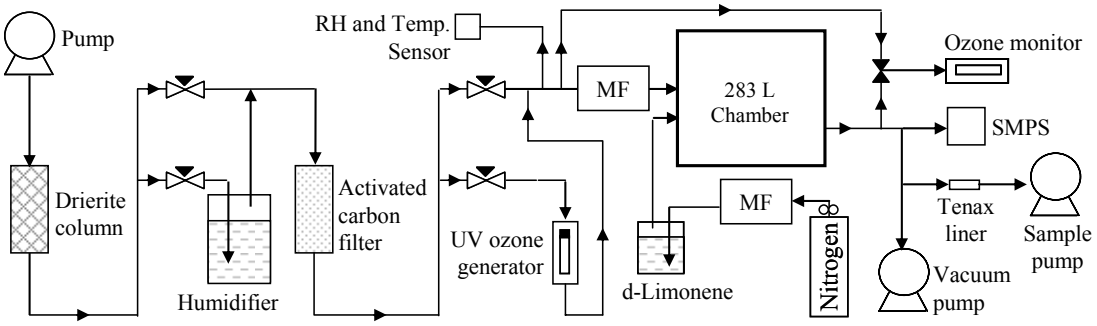

Figure 1. Experimental apparatus for measuring SOA formation due to chemical reactions with ozone and d-limonene. RH = relative humidity; Temp. = temperature; MF = mass flow controller; SMPS = scanning mobility particle sizer.

For the primary inlet flow, desired values of RH and ozone in the inlet air were achieved by manual adjustment of bypass valves, and the volumetric flow of air was controlled with a mass flow controller (Aarlborg GFC37) at a measured value of 3.6 L/min (Sensidyne Gilian Gilibrator-2). The RH and temperature (TSI Q-Trak 8551) and ozone concentration (2B Technologies 202, averaging time of 5 minutes) were measured at the chamber inlet. For the d-limonene inlet flow, the d-limonene was introduced by using a mass flow controller (Aarlborg GFC171S) to control the rate of nitrogen through a diffuser with liquid d-limonene (Sigma-Aldrich, 98% purity). For the outlet air, ozone could be sampled with the same ozone monitor as the primary inlet. Particle size distributions were sampled at the outlet with a scanning mobility particle sizer (SMPS) over 106 bins in the range of 15.1–661 nm (TSI 3936L85, every 5 minutes). The d-limonene was sampled at the outlet onto Tenax GR-packed focus liners (Atas A100094) for 4 minutes at a flow rate of 44 mL/min (Buck VSS-1), for a total sample volume of 0.176 L. Breakthrough was confirmed as less than 2% for the highest d-limonene concentration at this flow rate.

The d-limonene was analyzed by thermal desorption, gas chromatography, with flame-ionization detection, TD/GC-FID (Agilent G1530A equipped with Atas Optic 2 thermal desorber), for a run time of 22 min. The focus liners were thermally desorbed by ramping at 10 °C/s from an initial temperature of 60 °C up to a holding temperature of 280 °C. The split ratio for the thermal desorber was 10:1, and a sample transfer pressure

of 15 psi was held for 2 min before dropping to 14 psi and linearly increasing to 28.1 psi over the remainder of the run time. A Restek Rtx 5SilMS capillary column was used (30m length, 0.25mm internal diameter, 0.5 mm film thickness). The GC oven was held at the initial temperature of 40 °C for 2 min, after which it was ramped at 40 °C/min up to 95 °C and then 2 °C/min up to 125 °C then 60 °C/min from 125 to 270 °C, at which it was held for 1.2 min until the end of the run time. The FID was set at 250 °C with gas flows as follows: hydrogen, 35 mL/min; compressed air, 350 mL/min; and helium, 25 mL/min. Calibration standards for d-limonene were made from the same batch of d-limonene that was introduced into the chamber. Mass calibration was attained by injecting of methanol-diluted standards directly onto clean Texax-filled tubes, which were purged with nitrogen at 20 mL/min for 20 min, and analyzed using TC/GC-FID.

EXPERIMENTAL RESULTS

Experiments O1–O12 were conducted to determine the original deposition velocity of ozone without d-limonene adsorption, $v_{d,o}$, to the various surfaces of Chambers 1 and 2. The results from experiments O1–O12 are listed in Table 2, including the $C_{O3,m,inlet}$, the chamber $C_{O3,m}$, the resulting $v_{d,o,1}$ or $v_{d,o,2}$ (calculated with Equation 14) for Chambers 1 and 2. Seven experiments (O1–O7) were performed in Chamber 1 and five (O8–O12) were performed in Chamber 2. For experiments at RH = 50%, the $C_{O3,m,inlet}$ and thus the resulting $C_{O3,m}$ were varied to demonstrate the effect of $C_{O3,m}$ on $v_{d,o,1}$ or $v_{d,o,2}$. Figure 2 plots $v_{d,o,1}$ or $v_{d,o,2}$ versus $C_{O3,m}$.

Figure 2 shows that as $C_{O3,m}$ increased, the values for $v_{d,o,1}$ and $v_{d,o,2}$ decreased. The reason for this trend is not due to the deposition velocity transitioning between the reaction-rate limited and the mass-transport limited regimes. For all of the deposition velocities in Figure 2, the reaction probabilities ranged from $\gamma_o = 9.0\times10^{-7}$–$5.8\times10^{-7}$, when approximated with $v_{d,o} = \gamma_o \cdot \langle v \rangle / 4$. This range of γ_o lies in the reaction rate limited regime (Cano-Ruiz et al., 1993). However, the reaction probability has been shown to decease with prolonged ozone exposure, as some reaction sites are quenched (Morrison and Nazaroff, 2000). To determine the values for $v_{d,o}$ in the SOA formation experiments,

which is used to determine $v_{d,terp}$ in the calculation of $Y_{s,m}$ (Equation 13), power curves were fit to the values for Chambers 1 and 2 at RH = 50%. The experiments at lower RH resulted in slightly less ozone deposition and those at higher RH in slightly more ozone deposition, at comparable $C_{O3,m}$. This difference was neglected in the calculation of $Y_{s,m}$ since both it was small and there were not enough data to determine its effect in any robust manner. The total $v_{d,o,2}$ for Chamber 2 was lower than the $v_{d,o,1}$ for Chamber 1, implying that the screens were less reactive (i.e., lower γ_o) than the chamber walls.

Table 2. Results from experiments O1–O12. $v_{d,o,1}$ or $v_{d,o,2}$ were calculated with Equation 14 for Chambers 1 and 2.

Exp.	Chamber condition	RH (%)	$C_{O3,inlet}$ (ppb)	C_{O3} (ppb)	β_{O3} (h^{-1})	$v_{d,o,1}$ or $v_{d,o,2}$ (m/h)
O1	1	20	214 (1.1)	117 (0.86)	0.64	0.069 (0.001)
O2	1	50	27.1 (1.2)	8.26 (0.82)	1.7	0.19 (0.03)
O3	1	50	52.1 (0.66)	20.9 (0.77)	1.1	0.12 (0.008)
O4	1	50	104 (0.90)	50.1 (0.86)	0.82	0.089 (0.003)
O5	1	50	203 (0.67)	100 (1.5)	0.78	0.085 (0.003)
O6	1	50	400 (1.0)	242 (1.2)	0.49	0.054 (0.0007)
O7	1	70	203 (0.67)	88.6 (0.88)	0.98	0.11 (0.002)
O8	2	20	182 (1.6)	70.5 (1.9)	1.2	0.029 (0.001)
O9	2	50	104 (1.5)	18.7 (0.78)	3.6	0.085 (0.005)
O10	2	50	157 (1.9)	55.3 (1.0)	1.4	0.034 (0.001)
O11	2	50	394 (0.94)	141 (0.89)	1.4	0.033 (0.0004)
O12	2	70	197 (0.68)	32.9 (0.64)	3.9	0.09 (0.002)

Table 3 lists the results from experiments L1–L12, which were SOA formation experiments used calculate $Y_{s,m}$, grouped by RH. The $C_{O3,m,inlet}$ was necessarily higher for the experiments in Chamber 2 so that the $C_{O3,m}$ in Chamber 2 would approximately equal the $C_{O3,m}$ in Chamber 1, since much more of the ozone reacted with the additional surface area in Chamber 2. The $C_{O3,m}$, C_{SOA}, and $C_{SOA,N}$ (#/cm^3), which is the SOA number concentration, are mean (s.d.) values from the last hour of the experiments, once the formation had reached steady-state conditions. $C_{terp,m}$ was sampled at the end of the steady-state averaging hour, and $C_{terp,m}$ is lower for the experiments in Chamber 2 since

the emission into the chamber was not varied and more $C_{terp,m}$ adsorbed to the additional surface area and reacted with ozone. Even though the average $C_{terp,m}$ for Chamber 2 experiments was 66% of the average for Chamber 1 experiments, the overall trend is that the larger A/V in Chamber 2 led to higher concentrations of SOA.

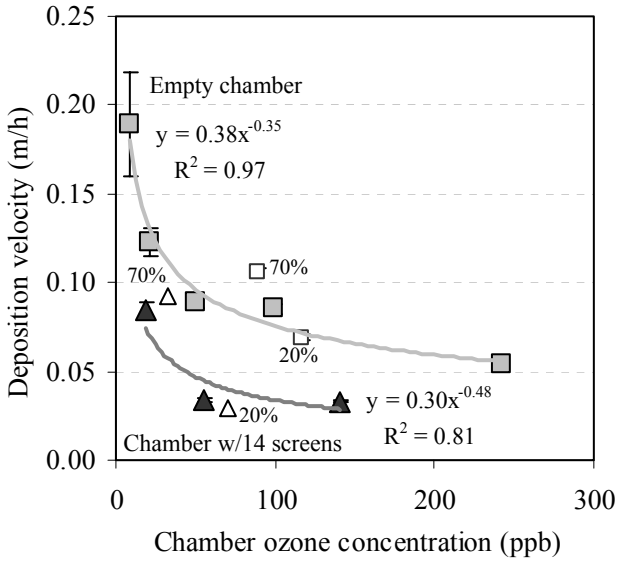

Figure 2. Plot of $v_{d,o,1}$ or $v_{d,o,2}$ versus $C_{O3,m}$, the chamber ozone concentration. Squares are for Chamber 1 and triangles for Chamber 2. Filled symbols are experiments at RH = 50%. Hollow symbols are at RH = 20 or 70% and are labeled on the plot.

The additional SOA formation in Chamber 2 versus Chamber 1 was much larger from a number than a mass perspective. For instance, for the experiments in Chamber 2 versus Chamber 1 at RH = 50%, the SOA mass concentration increase was 19% and the SOA number concentration increase was 56%. The SOA number distributions for the last hour of steady-state for the experiments in Chambers 1 and 2 with identical RH were averaged, and the mean (s.d.) are in Figure 3(a), (b), and (c). Additionally, Figure 3(d) shows the total mean distributions for Chambers 1 and 2 over the entire range of RH, as well as the difference between those means. In Figure 3, the number in parentheses represents either Chamber 1 or 2, which is followed by the experiment number (L1–L12) used to create the curve. The lognormal parameters for all SOA distributions displayed in Figure 3 are listed in Table 4.

Table 3. Results from experiments L1–L12.

Exp.	Chamber condition	RH (%)	$C_{O3,inlet}$ (ppb)	C_{O3} (ppb)	C_{terp} (ppb)	M_{SOA} ($\mu g/m^3$)	N_{SOA} ($\#/cm^3$)
L1	1	20	127	5.70 (0)	630	218 (2.7)	12,580 (280.4)
L2	2	20	221	5.25 (1.0)	483	266 (7.0)	24,690 (2086)
L3	2	20	217	6.92 (0.51)	-	250 (3.7)	25,616 (1451)
L4	2	20	215	7.08 (0.75)	417	248 (5.1)	24,489 (1244)
L5	1	50	120	5.35 (0.49)	632	193 (3.1)	11,912 (76.59)
L6	1	50	127	5.12 (0.72)	671	219 (2.6)	12,914 (149.7)
L7	2	50	227	4.39 (0.29)	469	227 (6.9)	17,690 (1145)
L8	2	50	226	6.45 (0.49)	388	262 (5.5)	20,938 (398.4)
L9	1	70	124	4.15 (0.45)	660	187 (5.7)	9,575.1 (164.7)
L10	2	70	251	4.83 (1.0)	400	250 (4.2)	17,447 (804.2)
L11	1	50	223	13.7 (0.43)	634	299 (7.8)	14,427 (489.3)
L12	1	50	409	28.7 (0.39)	413	359 (9.8)	15,656 (480.4)

The mean number distributions in Figure 3 display several interesting trends. First, more absolute SOA number formation occurred at lower RH, implying that reactions between ozone and d-limonene in the absence of water vapor forms products with higher nucleation potential. Second, the median diameter for the average distribution for Chamber 2 shifted slightly to the left with respect to the distribution in Chamber 1. The statistical differences between the distributions in Figures 3(a), (b), and (c) were evaluated with the Wilcoxon signed-ranks test. The p-values for the test that mean distributions for Chambers 1 and 2 were the same at RH = 20, 50, and 70% are 0 for all cases, indicating that the SOA distributions in Chambers 1 and 2 were not the same distribution.

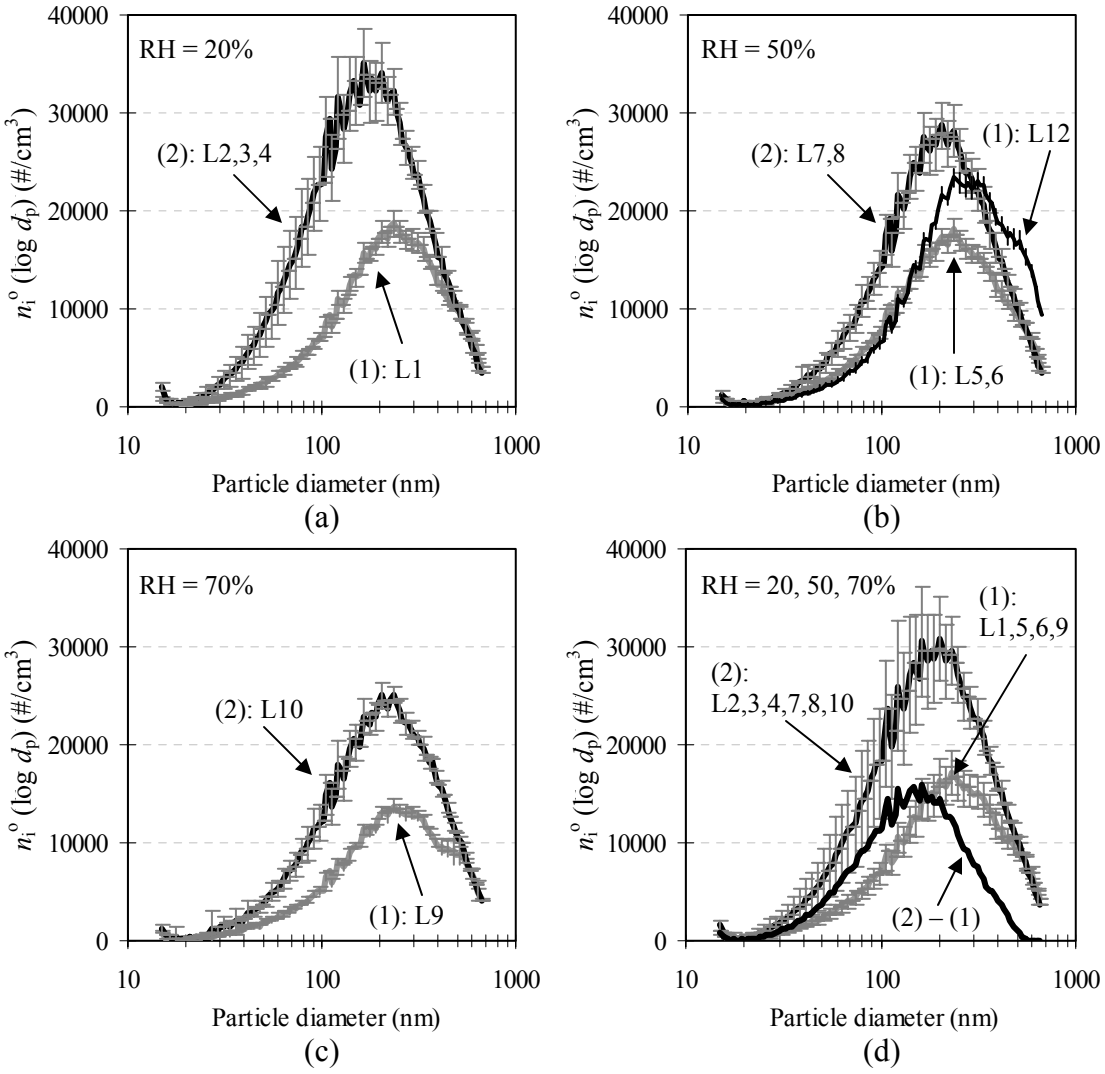

Figure 3. Average steady-state number concentrations for Chambers 1 and 2, for (a) RH = 20%, (b) RH = 50%, and (c) RH = 70%. The averages for Chambers 1 and 2 over all RH are shown in (d), as well as the difference between them.

To demonstrate that the SOA formation differences in Chambers 1 and 2 were due to surface effects as opposed to higher chamber concentrations, experiments L11 and L12 were performed with the A/V of Chamber 1 at RH = 50%, but with increased ozone concentrations. Results from experiments L11 and L12 are listed in Table 3, and L12 is also plotted on Figure 3(c). The SOA number formation trend for L12 is different than that observed for the average of experiments L7 and L8, which had the larger A/V

associated with Chamber 2. For experiment L12, the SOA formation diverged from the average for experiments L5 and L6 at approximately 105 nm particle diameter and never converged, as with experiments L7 and L8 in Chamber 2. The SOA mass concentration for experiment L12 was 359 μg/m^3 and for the average of experiments L5 and L6 was 206 μg/m^3, with the increased particle mass in the larger diameter range. Also, the median diameter for L12 shifted slightly to the right of the average of L6 and L6, rather than the left, as with the average of the L7 and L8 distributions from Chamber 2. Again using the Wilcoxon signed-ranks test, the p-values that the distributions for L11 and L12 are same as the average for L7 and L8 are 0 for both cases.

Table 4. Lognormal parameters (number concentration, N; geometric mean diameter, GMD; and geometric standard deviation, GSD) for SOA distributions in Figure 3.

	Measured	Mode 1			Mode 2			Mode 3			Modeled
	number	N	GMD	GSD	N	GMD	GSD	N	GMD	GSD	number
Chamber: Exp.	(#/cm^3)	(#/cm^3)	(nm)	(-)	(#/cm^3)	(nm)	(-)	(#/cm^3)	(nm)	(-)	(#/cm^3)
(1): L1	12,580	400	50	1.8	2,200	140	2.1	10,000	250	1.8	12,600
(2): L2,3,4	24,932	1,000	50	1.8	2,200	140	2.1	21,800	180	2.0	25,000
(1): L5,6	12,413	600	50	1.6	2,000	140	1.9	9,800	250	1.8	12,400
(1): L12	15,656	1,600	90	2.1	14,000	275	1.8	400	514	1.1	16,000
(2): L7,8	19,314	1,100	50	1.5	2,200	140	2.1	16,000	210	1.8	19,300
(1): L9	9,575	2,500	140	2.5	7,000	260	1.8	400	533	1.2	9,900
(2): L10	17,447	700	50	1.5	1,800	140	2.0	15,000	220	1.9	17,500
(1): L1,5,6,9	11,745	2,600	140	2.6	8,900	241	1.8	250	533	1.2	11,750
(2): L2,3,4,5,8,10	21,812	1,100	50	1.5	2,800	140	2.1	17,900	195	1.8	21,800
(2) - (1)	10,112	1,000	60	1.6	8,000	145	1.7	1,000	233	1.4	10,000

For each set of experiments grouped by RH, the average SOA, inlet ozone, chamber ozone, and d-limonene concentrations were used to calculate $Y_{s,m}$ with Equation 13. The $v_{d,terp,1}$, $v_{d,terp,2w}$, and $v_{d,terp,2s}$ in Equation 13 were calculated in the manner described in the experimental methodology, and the concentrations were measured. The calculated $Y_{s,m}$ values at RH = 20, 50, and 70% RH are in Figure 4(a). The $Y_{s,m}$ values ranged from 0.14 to 0.16, which is approximately two thirds of the gas-phase yield used in the calculations. Also shown in Figure 4(b) is the ratio of the SOA number

concentration formed (#/cm^3) and the mass concentration formed (μg/m^3) for the SOA formed from the gas-phase (χ_g) and surface-phase (χ_s) reactions, at the three different experimental RH values. The χ_s ranged from 126–339 #/cm^3 per μg/m^3 and χ_g ranged from 51.1–60.2 #/cm^3 per μg/m^3. The bars on Figure 4(a) and (b) represent the total experimental uncertainty in $Y_{s,m}$, χ_s, and χ_g.

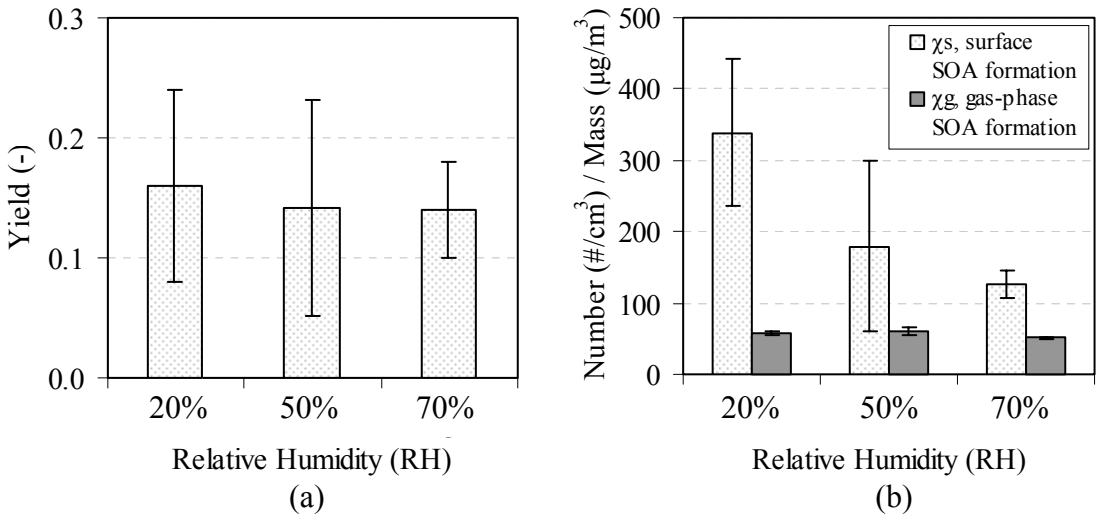

Figure 4. The (a) SOA yields ($Y_{s,m}$) due to surface reactions of ozone with surface-adsorbed d-limonene and (b) the ratio of the SOA number concentration formed (#/cm^3) and the mass concentration formed (μg/m^3) for gas-phase (χ_g) and surface-phase (χ_s) reactions, at RH = 20, 50, and 70%. Linear dependence to RH for χ_s is y = -4.34x + 417 (R^2 = 0.97) and for χ_g is y = -0.115x + 62.0 (R^2 = 0.37).

Both $Y_{s,m}$ and χ_s decreased as RH increased. The $Y_{s,m}$ was only slightly higher at the lower RH values, which is consistent with observations from other SOA formation experiments with gas-phase reactions of ozone and d-limonene (Leungsakul et al., 2005). However, χ_s was much higher at the lower RH values, which is consistent with the previous data shown in Table 3 and Figure 3 that more SOA particle formation occurred for ozone/d-limonene reactions at lower RH. More nucleation at lower RH is consistent with Bonn et al. (2002), and these authors hypothesize that nucleation is a function of the number of stabilized Criegee intermediates, which are scavenged by water vapor. In

Figure 4(b), the linear fit to χ_s is $y = -4.34x + 417$ ($R^2 = 0.97$) and the linear fit to χ_g is $y = -0.115x + 62.0$ ($R^2 = 0.37$), where the value for x is RH (%) and the value for y is χ_s or χ_g.

DISCUSSION

For a terpenoid with a constant γ_{terp} that is independent of the surface, the model framework predicts that $v_{d,terp}$ is a function of r_{terp} and γ_o, and it predicts that $v_{d,terp}$ is a function of only r_{terp} if $v_{d(o+terp)}$ is in the reaction rate limited regime. To further explore this distinction, Figure 5 plots $v_{d,terp}$ versus r_{terp} for a range of different γ_o that represent those common for building materials, using $\gamma_{terp} = 3\times10^{-4}$ for d-limonene of (Springs and Morrison, 2008) and a $v_t = 2.7$ m/h, which was estimated with $v_t = u^*/13.3$ (Morrison and Nazaroff, 2002) with $u^* = 1$ cm/s. The friction velocity, u^* (cm/s), is an empirical parameter that describes the level of turbulence intensity near a surface, and typical values indoors range from 0.3–3 cm/s (Lai and Nazaroff, 2000). For reference, the thick black line on the plot is the reaction rate limited $v_{d,terp}$, calculated with Equation 8.

In Figure 5, the $v_{d,terp}$ calculated for the reaction rate limited regime with Equation 8 is linear with r_{terp}, as shown in Equation 8. The $v_{d,terp}$ calculated for the surfaces with $\gamma_o \leq 10^{-6}$ are quite similar to each other. For values of $r_{terp} \leq 0.01$, the $v_{d,terp}$ for those surfaces are well-approximated with Equation 8, and for $r_{terp} > 0.01$, $v_{d,terp}$ for those surfaces deviate from the reaction rate limited approximation and approach $v_t = 2.7$ m/h. The surfaces with $\gamma_o \geq 10^{-5}$ are never in the reaction rate limited regime, and $v_{d,terp}$ for those surfaces is less that that calculated for surfaces with $\gamma_o \leq 10^{-6}$. For instance, when $v_{d,terp}$ for materials with $\gamma_o \leq 10^{-6}$ are fully in the reaction rate limited regime (i.e., $r_{terp} \leq 0.001$), the $v_{d,terp}$ for a surface with $\gamma_o = 10^{-5}$ is a factor of 2.2 less and for $\gamma_o = 10^{-4}$ is a factor of 13 less than those surfaces with $\gamma_o \leq 10^{-6}$. These results imply that contribution to SOA formation of ozone/d-limonene surface reactions is more important on surfaces with low initial reactivity than on surfaces with high initial reactivity.

This analysis can be extended to $v_{d,terp}$ for real building materials. For a real building material, the r_{terp} is dependent on two parameters as it is modeled (Equation 4), the M_{terp} (μg terpenoid/m^2 nominal surface area) and S (m^2 intrinsic/m^2 nominal surface

area). The M_{terp} is a function of the sorption characteristics of a material (Tichenor et al., 1991; Won et al., 2001), and S reflects the actual surface area of a material. Equilibrium values for M_{terp} can be calculated as $K_{eq}C_{terp}$, where K_{eq} (m) is the equilibrium sorption constant (Tichenor et al., 1991), and C_{terp} (μg/m^3) is the terpenoid mass concentration. Weschler (2003) noted that to a first approximation, the K_{eq} of a material linearly reflects the intrinsic surface area of a material. Thus, by this logic, K_{eq} increases linearly with S, and values for r_{terp} vary little from material to material, since r_{terp} is calculated with K_{eq}/S.

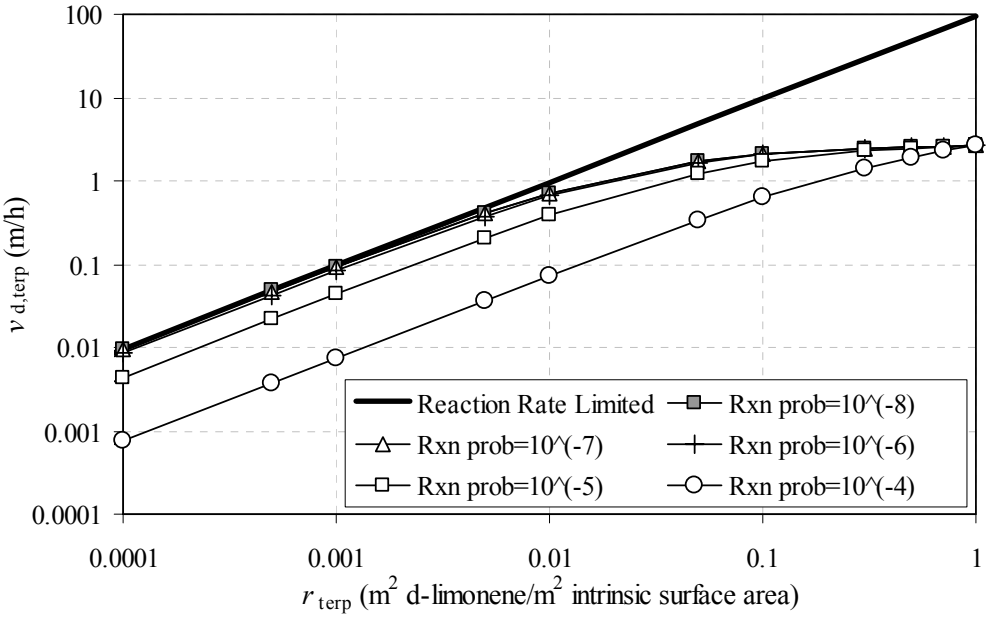

Figure 5. Plot of $v_{d,terp}$ versus r_{terp} for a range of different γ_o that represent those common for building materials, using $\gamma_{terp} = 3\times10^{-4}$ for d-limonene. The reaction probability (Rxn prob) in the legend are the γ_o without d-limonene adsorption.

Table 6 shows the predicted $v_{d,terp}$ for a variety of common indoor materials, for adsorption of d-limonene from the gas-phase at a concentration of 50 ppb. For many common building materials, values for K_{eq} versus saturation vapor pressure (p_L^o) of a compound are presented in Won et al. (2001). However, S for materials are not readily available, so these K_{eq} were used to estimate S for those materials, with an estimated reference point of S = 50 m^2 intrinsic/m^2 nominal surface area for the carpet (Morrison and Nazaroff, 2000). The p_L^o of d-limonene was 0.0054 atm in all calculations. For the

first four materials in Table 6, italicized values of S and K_{eq} were not available and are estimates. The γ_o in Table 6 were estimated from Cano-Ruiz et al. (1993) and Morrison and Nazaroff (2000). The $v_{d,o}$ was calculated with Equation 2, again assuming a v_t = 2.7 m/h. The $\gamma_{(o+terp)}$ was then calculated with Equation 3, again assuming a $\gamma_{terp} = 3\times10^{-4}$. Finally, $v_{d,(o+terp)}$ was calculated with Equation 5, $f_{O3,terp}$ was calculated with Equation 6, and $v_{d,terp}$ was calculated with Equation 7.

Table 6. Parameters that describe SOA formation due to ozone reactions with the d-limonene that results from a gas-phase concentration of 50 ppb, for different common building materials. The bold $v_{d,terp}$ can be estimated to within 85% of actual values with a reaction-rate-limited approach (described further in text). GB = gypsum board.

Material Surface	S[a] (m^2 int./ m^2 nom.)	K_{eq}[b] (m)	r_{terp} (m^2 terp./ m^2 int.)	γ_o[c] (-)	$v_{d,o}$ (m/h)	$\gamma_{(o+terp)}$ (-)	$v_{(d,o+terp)}$ (m/h)	$f_{O3,terp}$ (-)	$v_{d,terp}$ (m/h)
Glass	1*	0.2*	1.1E-03	1.0E-08	0.0032	3.3E-07	0.10	0.97	**0.10**
Sealant	1.2*	0.2*	8.9E-04	1.0E-07	0.032	3.7E-07	0.11	0.73	**0.083**
Stainless Steel	1.5*	0.2*	7.1E-04	1.0E-07	0.032	3.1E-07	0.098	0.68	**0.067**
Aluminum	3*	0.2*	3.6E-04	7.0E-07	0.21	8.1E-07	0.24	0.13	**0.032**
Apples	5	0.25	2.4E-04	1.0E-07	0.032	1.7E-07	0.055	0.42	**0.023**
Ceiling Tile	6	0.29	2.4E-04	5.0E-04	2.7	5.0E-04	2.7	0.00015	0.00039
Painted G.B.	11	0.52	2.4E-04	5.0E-05	2.3	5.0E-05	2.3	0.0015	0.0034
Vinyl Flooring	18	0.84	2.4E-04	1.0E-06	0.29	1.1E-06	0.31	0.068	**0.021**
Wallpaper G.B.	22	1.0	2.4E-04	5.0E-05	2.3	5.0E-05	2.3	0.0015	0.0034
Carpet	50	2.3	2.4E-04	1.0E-04†	2.5	1.0E-04	2.5	0.00073	0.0018
Carpet w/Pad	88	4.0	2.4E-04	1.0E-04†	2.5	1.0E-04	2.5	0.00073	0.0018

[a]From K_{eq} with reference point of S = 50 for carpet (Morrison and Nazaroff, 2000), except * which were estimated; [b]From Won et al. (2001), except * which were estimated; [c]Estimated from Cano-Ruiz et al. (1993), except † which were from Morrison and Nazaroff (2000).

The resulting r_{terp} values exhibited a small range from 2.4×10^{-4}–1.1×10^{-3} m^2 terpenoid/m^2 intrinsic surface area, a difference of less than an order of magnitude. Moreover, for the materials with S estimated by the K_{eq}, the $r_{terp} = 2.4\times10^{-4}$ for all materials. Even if this approach to estimating S from K_{eq} is only partially valid, this analysis implies that values for r_{terp} on real building materials may only span one or perhaps two orders of magnitude. If r_{terp} were the same for different materials, then r_{terp}

and thus $v_{d,terp}$ would only be a function of the gas-phase terpenoid concentration, for $v_{d,terp}$ in the reaction rate limited regime.

These calculated $v_{d,terp}$ range from 0.00039 m/h for the ceiling tile to 0.10 m/h for the glass surfaces. The largest of these $v_{d,terp}$ are approximately an order of magnitude below those measured for indoor surfaces (Wang and Morrison, 2006), and the smallest $v_{d,terp}$ are nearly inconsequential. The values of $v_{d,terp}$ listed in bold in Table 6 fall within 85% of the value estimated by the reaction rate limited approach. At this value for d-limonene of 50 ppb, the $v_{d,terp}$ in bold are one to four orders of magnitude higher than those that are not, which indicates that materials with $v_{d,terp}$ that will influence SOA concentrations the most can have their $v_{d,terp}$ estimated with Equation 8. The potential SOA contribution of the $v_{d,terp}$ for six of the common building materials listed in Table 6 are further explored in Figure 6.

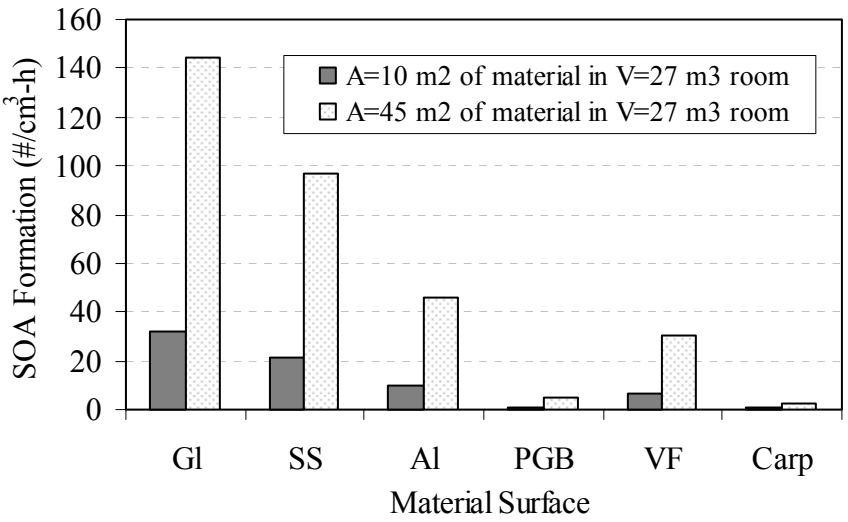

Figure 6. The (a) predicted steady-state SOA number formation from ozone deposition to d-limonene adsorbed to (Gl) glass, (SS) stainless steel, (Al) aluminum, (PGB) painted gypsum board, (VF) vinyl flooring, and (Carp) carpet, for two surface areas of 10 m^2 or 45 m^2, in a 27 m^3 indoor space with $C_{terp,m}$ = 50 ppb and $C_{O3,m}$ = 10 ppb.

Figure 6 displays the predicted steady-state SOA number formation rates (#/cm^3·h) from ozone deposition to d-limonene adsorbed to glass (Gl), stainless-steel (SS), aluminum (Al), painted gypsum board (PGB), vinyl flooring (VF), and carpet

(Carp). Contributions for these surfaces are determined for two surface areas, 10 m^2 or 45 m^2, in a 27 m^3 indoor space with concentrations of 10 ppb and 50 ppb for ozone and d-limonene, respectively. The SOA number formation rates (#/cm^3·h) were calculated as the product of term on the right-hand-side of the numerator in Equation 11 and χ_s for 50 RH. For reference, the SOA number formation rate from gas-phase reactions was calculated as the product of the term on the left-hand-side of the numerator in Equation 11 and χ_g for 50 RH. These calculations include $Y_{g,m}$ and $Y_{s,m}$, and $Y_{g,m}$ was set to 0.1 (a yield typical of these concentrations) and $Y_{s,m} = 0.65(0.1) = 0.065$, per the relationship determined in the experiments above. The SOA formation rate from the gas-phase reactions was 401 #/cm^3·h. For the low surface area (10 m^2) in the room, the surface contributions are a small fraction of the total SOA number formation, and the largest contributor, glass, was responsible for 7%. For the high surface area (45 m^2), the surface contributions are a larger fraction, and glass was responsible for 27% of the total number formation. For the 10 m^2 and 45 m^2 of glass, surface reactions were only responsible for 0.7 and 3% of the SOA mass formed.

As a screening test, the model framework was also applied to results with transient SOA formation for the field study described in Appendix B. The field study determined the SOA formation that occurred in a residential room with an ozone-emitting ion generator (3.3 mg/h) and a terpene-emitting liquid plug-in air freshener (total emission = 1.5 g/day). Tests at similar air exchange rates and ozone and d-limonene concentrations were conducted with different flooring surfaces in the room. Four tests used the original flooring of sealed/stained concrete, and two tests used carpet with padding that was installed over the original flooring. Figure 7(a) shows the change in average concentrations for each floor surface for ten hours of testing.

At time zero in Figure 7(a), the air exchange rate in the room decreased from approximately 1.3 h^{-1} to 0.4 h^{-1}, corresponding to the shutting off of the HVAC system supplying the room. After the air exchange rate decreased, the residence time of reactant concentrations increased and the loss rate of SOA due to ventilation decreased, resulting in increased formation of SOA particles. For the tests with carpet, the SOA concentration

reached steady-state after approximately three hours. However, for the tests with the sealed/stained concrete floor, steady-state was not reached after 10 hours and final SOA number concentrations were larger than the room with carpet.

The ozone and d-limonene concentrations in all tests were on the order of 10 ppb and 45 ppb, respectively (both were approximately constant due to their emissions in the room). The main variable that changed was flooring surface. The effect of this one variable change on SOA formation was explored with a numerically-solved transient version of the model framework. The model calculated $C_{SOA}(t)$ with Equation 9, with a constant ozone concentration of 10 ppb (as was measured in the room).

The time-varying d-limonene concentration, $C_{terp}(t)$ (μg/m^3), was calculated similarly to Tichenor et al. (1991), and its concentration was controlled by gains due to constant emission (the liquid plug-in air freshener) and desorption from surfaces, as well as losses due to air exchange, gas-phase reaction with ozone, and adsorption to surfaces, as in Equation 18:

$$\frac{\mathrm{d}C_{terp}(t)}{\mathrm{d}t} = \frac{E_{terp}}{V} - \lambda C_{terp}(t) - kC_{terp}(t)C_{O3} - k_a C_{terp}(t)\frac{A}{V} + k_d M_{terp}(t)\frac{A}{V} \tag{18}$$

where $M_{terp}(t)$ (μg/m^2 nominal surface area) is the time-varying mass concentration of the adsorbed terpene on the surface, k_a (m/h) is the adsorption rate coefficient, and k_d (h^{-1}) is the desorption rate coefficient. For time-varying adsorption to a surface, Tichenor et al. (1991) modeled $M_{terp}(t)$ as in Equation 19:

$$\frac{\mathrm{d}M_{terp}(t)}{\mathrm{d}t} = k_a C_{terp}(t) - k_d M_{terp}(t) \tag{19}$$

However, Equation 19 does not account for the loss of $M_{terp}(t)$ due to reactions that occur on the surface. This work modifies Equation 19 for $M_{terp}(t)$ to account for this loss:

$$\frac{\mathrm{d}M_{terp}(t)}{\mathrm{d}t} = k_a C_{terp}(t) - k_d M_{terp}(t) - v_{d,terp}(t)C_{O3}\left(\frac{MW_{terp}}{MW_{O3}}\right) \tag{20}$$

where $v_{d,terp}(t)$ (m/h) is time-varying deposition velocity of ozone to the adsorbed terpene, and MW_{terp} (μg/mol) is the molecular weight of the terpenoid, respectively. Since $v_{d,terp}(t)$ is a function of $M_{terp}(t)$ (see Equations 3–7), the last term in Equation 20 was recast to reflect this dependence, as follows.

Assuming that the ozone loss to the surface is dominated by surface reaction resistance, which is a valid assumption for reactions on surfaces that influence gas-phase SOA formation (see analysis above), $v_{d,terp}(t)$ can be expressed as in Equation 21:

$$v_{d,terp}(t) = r_{terp}(t)\gamma_{terp}\frac{<v>}{4} = \left(M_{terp}(t)\frac{\left(A_{terp\text{-}molecule}\right)\left(N_A\right)}{\left(S\right)\left(MW_{terp}\right)}\right)\left(\gamma_{terp}\frac{<v>}{4}\right) \quad (21)$$

After substituting Equation 21 into Equation 20, the new expression for $M_{terp}(t)$ is:

$$\frac{dM_{terp}(t)}{dt} = k_a C_{terp}(t) - M_{terp}(t)\left(k_d + k_{rxn}C_{O3}\right) \quad (22)$$

where k_{rxn} is constant for a given material surface, as in Equation 23:

$$k_{rxn} = \left(\frac{\left(A_{terp\text{-}molecule}\right)\left(N_A\right)}{\left(S\right)\left(MW_{O3}\right)}\right)\left(\gamma_{terp}\frac{<v>}{4}\right) \quad (23)$$

$A_{terp\text{-}molecule}$ was estimated as 5×10^{-19} m^2 with the bond lengths, bond angles, and Van der Waal's radii for d-limonene.

Numerical solutions for Equations 18, 21, and 22 were used to predict $C_{terp}(t)$, $v_{d,terp}(t)$, and $M_{terp}(t)$, as well as for Equation 9 for $C_{SOA}(t)$, the time-varying SOA mass concentration, with an additional term for particle loss due to the ion generator of 1.5 h^{-1}, calculated as CADR/V, assuming the CADR = 41 m^3/h, as in Appendix A. For the stained/sealed concrete floor, values for S and γ_o from the sealant material in Table 6 were used to model SOA from the sealed/stained concrete, and k_a was estimated as 0.1 m/h and k_d as 0.5 h^{-1}. The $Y_{g,m} = 0.075$ was fit to achieve the observed concentration in the room with the carpet flooring, and $Y_{s,m} = (0.65)Y_{g,m} = 0.049$. The χ_g and χ_s were used to calculate the SOA number concentrations, for the average RH for the tests of 45%.

The modeled results of the field study tests are shown in Figure 15(b). The time-resolved model predicted the SOA number concentrations reasonably well, with the modeled final number concentration falling near the observed final concentration. However, it is worth noting that this modeling work is only of a screening nature, and further attention should be focused on designing experiments that allow observation of this effect indoors, as well as validating the model framework as ideal with a more controlled data set than was available with the field study results.

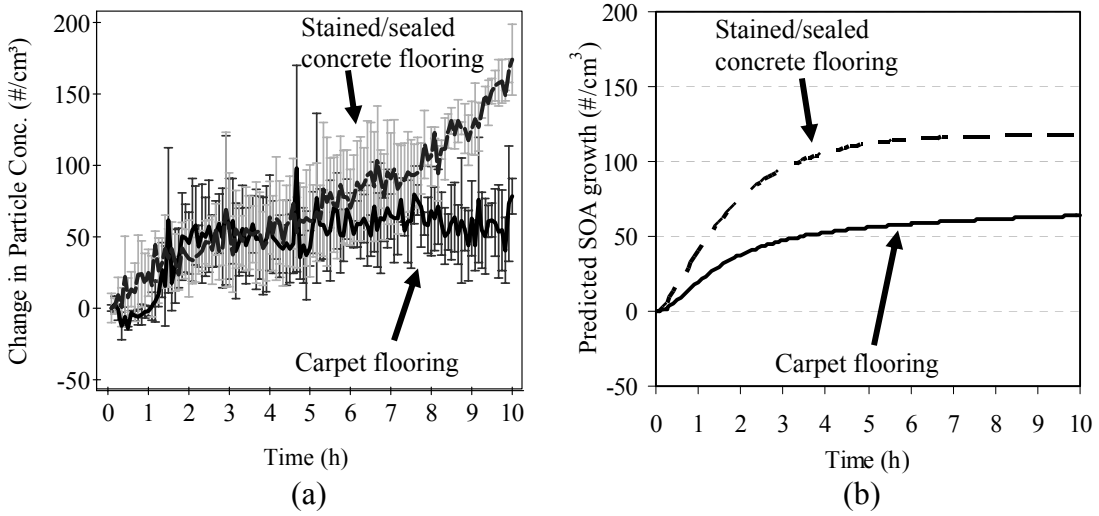

Figure 15. (a) Change in mean particle concentrations (0.015–0.53 μm) vs. time for four nights of testing with stained/sealed concrete flooring and for two nights with carpet flooring, in the same 27 m^3 room. Error bars represent one standard deviation from the mean value. An operating ion generator and energized air freshener were present during all tests. (b) Modeled results. (See text for more information.)

CONCLUSIONS

This work investigated the contribution to gas-phase SOA formation of ozone reactions with the surface-adsorbed terpenoids. The monoterpene d-limonene was used in the experiments because it adsorbs to surfaces (Singer et al., 2004), is the primary terpenoid constituent in many consumer products (Singer et al., 2006b), has been shown to react with ozone on surfaces (Fick et al., 2005; Springs and Morrison, 2008), and has

high SOA mass yield potentials (Ng et al., 2006). A model framework was developed to describe SOA formation due to ozone/terpenoid surface reactions, and it predicted that building materials on which surface reactions lead to SOA formation are those with initially low surface reactivity, such as glass, sealed materials, or smooth metals. For these materials, a reaction rate limited approximation is sufficient to adequately describe $v_{d,terp}$, the deposition velocity of ozone to the adsorbed terpenoid molecules.

Experiments were conducted in a 283 L stainless-steel chamber to determine the yield, $Y_{s,m}$, for ozone/d-limonene surface reactions. For the experiments herein, this yield ranged from 0.14–0.16, for relative humidity values of 20, 50, and 70%. Also determined was the ratio of the SOA number concentration (#/cm^3) and the mass concentration (μg/m^3) formed for gas-phase (χ_g) and surface-phase (χ_s) reactions, at RH = 20, 50, and 70%. The χ_s ranged from 126–339 (#/cm^3)/(μg/m^3) and χ_g ranged from 51.1–60.2 (#/cm^3)/(μg/m^3), and lower RH led to higher number formation from the surface reactions, but not from the gas-phase reactions. Using the experimentally determined values for $Y_{s,m}$ and χ_s within the model framework, the differences in SOA number formation observed in a residential room with different flooring surfaces was successfully modeled. Surface reactions were responsible for approximately 50% of SOA number formation in the room when the flooring was sealed/stained concrete.

ACKNOWLEDGMENTS

This work was funded by a National Science Foundation IGERT Traineeship (Award DGE 0549428), and a Harrington Dissertation Fellowship from the University of Texas at Austin.

REFERENCES

Alshawa, A., Russell, A.R., Nizkorodov, S.A. (2007). Kinetic analysis of competition between aerosol particle removal and generation by ionization air purifiers. *Environmental Science and Technology* 46: 2498-2504.

ASHRAE (2004). *Ventilation and Acceptable Indoor Air Quality in Low-Rise Residential Buildings*. Atlanta, GA: American Society of Heating, Refrigerating, and Air-Conditioning Engineers. ASHRAE Standard 62.2-2004.

ASHRAE (2005). *Handbook of Fundamentals*. Atlanta GA, American Society of Heating, Refrigerating, and Air-Conditioning Engineers.

ASHRAE (2007). *Method of Testing General Ventilation Air-Cleaning Devices for Removal Efficiency by Particle Size*. Atlanta, GA: American Society of Heating, Refrigerating, and Air-Conditioning Engineers. ASHRAE Standard 52.2-2007.

Atkinson, R., Aschmann, S.M., Arey, J., et al. (1992). Formation of OH radicals in the gas-phase; Reactions of O3 with a series of terpenes. *Journal of Geophysical Research-Atmospheres* 97: 6065-6073.

Atkinson, R., Arey, J. (2003) Gas-phase tropospheric chemistry of biogenic volatile organic compounds: A review. *Atmospheric Environment* S197-S219.

Baumann, M.G.D., Batterman, S.A., Zhang, G.Z. (1999a). Terpene emissions from particleboard and medium density fiberboard products. *Forest Products Journal* 49: 49-56.

Baumann, M.G.D., Lorenz, L.F., Batterman, S.A., Zhang, G.Z. (1999b). Aldehyde emissions from particleboard and medium density fiberboard products. *Forest Products Journal* 50: 75-82.

Bekö, G., Halás, O., Clausen, G., Weschler, C.J. (2006). Initial studies of oxidation processes on filter surfaces and their impact on perceived air quality. *Indoor Air* 16: 56-64.

Bekö, G., Clausen, G., Weschler, C.J. (2007). Further studies of oxidation processes on filter surfaces: Evidence for oxidation products and the influence of time in service. *Atmospheric Environment* 41: 5202–5212.

Bell, M.L., McDermott, A., Zeger, S.L., Samet, J.M., Dominici, F. (2004). Ozone and short-term mortality in 95 US urban communities, 1987-2000. *Jama-Journal of the American Medical Association* 292: 2372-2378.

Bonn, B., Schuster, G., Moortgat, G.K. (2002). Influence of water vapor on the process of new particle formation during monoterpene ozonolysis. *Journal of Physical Chemistry A* 106: 2869-2881.

Britigan, N., Alshawa, A., Nizkorodov, S.A. (2006). Quantification of ozone levels in indoor environments generated by ionization and ozonolysis air purifiers. *Journal of the Air & Waste Management Association* 56: 601-610.

Brown, S.K., Sim, M.R., Abramson, M.J., Gray, C.N. (1994). Concentrations of volatile organic compounds in indoor air – A review. *Indoor Air* 4: 123-134.

California Air Resources Board (2007). *Survey of the Use of Ozone Generating Air Cleaners by the California Public*. Principal Investigator: Thomas Piazza. University of California, Berkeley, 05-301.

Cano-Ruiz, J.A., Kong, D., Balas, R.B. and Nazaroff W.W. (1993). Removal of reactive gases at indoor surfaces: Combining mass transport and surface kinetics, *Atmospheric Environment* 27: 2039-2050.

Cogliano, J.V., Grosse, Y., Baan, R.A., Straif, K., Secretan, M.B., El Ghissassi, F., and the Working Group for Volume 88 (2005). Meeting report: Summary of IARC monographs on formaldehyde, 2-butoxyethanol, and 1-tert-butoxy-2-propanol. *Environmental Health Perspectives* 113: 1205-1208.

Coleman, B., Lunden, M.M., Destaillats, H., and Nazaroff, W.W. (2008). Secondary organic aerosol from ozone-initiated reactions with terpene-rich household products. *Atmospheric Environment* 42: 8234-8245.

Coleman, B. (2009). *Exposure-Relevant Ozone Chemistry in Occupied Spaces*. Dissertation, University of California, Berkeley.

Colville, C.J., Griffin, R.J. (2004). The roles of individual oxidants in secondary organic aerosol formation from Δ^3-carene: 2. soa formation and oxidant contribution. *Atmospheric Environment* 38: 4013-4023.

Corsi, R.L., Siegel, J., Karamalegos, A., Simon, H., Morrison, G.C. (2007). Personal reactive clouds: Introducing the concept of near-head chemistry. *Atmospheric Environment* 41: 3161-3165.

Dennekamp, M., Howarth, S., Dick, C.A., Cherrie, J.H.W., Donaldson, K., Seaton, A. (2001). Ultrafine particles and nitrogen dioxides generated by gas and electric cooking. *Occupational Environmental Medicine* 58: 511-516.

Destaillats, H., Lunden, M.M., Singer, B.C., Coleman, B.K., Hodgson, A.T., Weschler, C.J., Nazaroff, W.W. (2006). Indoor secondary pollutants from household product emissions in the presence of ozone: A bench-scale chamber study. *Environmental Science and Technology* 40: 4421-4428.

Destaillats, H., Maddalena, R.L., Singer, B.C., Hodgson, A.T., McKone, T.E. (2008). Indoor pollutants emitted by office equipment: A review of reported data and information needs. *Atmospheric Environment* 42: 1371-1388.

Devos, M., Patte, F., Rouault, J., Laffort, P., Van Gemert, L.J. (1990). *Standardized Human Olfactory Thresholds*. New York: Oxford University Press.

Dubowski, Y., Vieceli, J., Tobias, D.J., Gomez, A., Lin, A., Nizkorodov, S.A., McIntire, T.M., Finlayson-Pitts, B.J. (2004). Interaction of gas-phase ozone at 296 K with unsaturated self-assembled monolayers: A new look at an old system. *Journal of Physical Chemistry* 108: 10473-10485.

Fan, Z., Lioy, P., Weschler, C., Fielder, N., Kipen, H., Zhang, J. (2003). Ozone-initiated reactions with mixtures of volatile organic compounds under simulated indoor conditions. *Environmental Science and Technology* 37: 1811-1821.

Ferro, A.R., Kopperud R.J., Hildemann L.M. (2004). Elevated personal exposure to particulate matter from human activities in a residence. *Journal of Exposure Analysis and Environmental Epidemiology* 14: S34-S40.

Flemmer, M.M., Ham, J.E., Wells, J.R. (2007). Field and laboratory emission cell automation and control system for investigating surface chemistry reactions. *Review of Scientific Instruments* 78, 014101.

Fick, J., Pommer, L., Åstrand, A., Östin, R., Nilsson, C., Andersson, B. (2005). Ozonolysis of monoterpenes in mechanical ventilation systems. *Atmospheric Environment* 39: 6315-6325.

Grosjean, E., Grosjean, D. (1998). Rate constants for the gas-phase reaction of ozone with unsaturated oxygenates. *International Journal of Chemical Kinetics* 30: 21-29.

Guenther A., Hewitt, C.N., Erickson, D., et al. (1995). A global model of natural volatile organic compound emissions. *Journal of Geophysical Research-Atmospheres* 100: 8873-8892.

Hanley, J.T., Esnor, D.S., Smith, D.D., Sparks, L.E. (1994). Fractional aerosol filtration efficiency of in-duct ventilation air cleaners. *Indoor Air* 4: 169-178.

Harrison, R.M., Yin, J. (2000). Particulate matter in the atmosphere: Which particle properties are important for its effects on health? *The Science of the Total Environment* 249: 85-101.

Hinds, W.C. (1999). *Aerosol technology : Properties, behavior, and measurement of airborne particles*. New York: Wiley.

Hines, W.W., Montgomery, D.C. (1990). *Probability and Statistics in Engineering and Management Science*. 3rd ed. New York: Wiley, p. 310.

Hodgson, A.T., Rudd, A.F., Beal, D., Chandra, S. (2000). Volatile organic compound concentrations and emission rates in new manufactured and site-built houses. *Indoor Air* 10:178-192.

Hubbard H.F., Coleman B.K., Sarwar G., Corsi R.L. (2005). The effects of an ozone generating air purifier on indoor secondary particles in three residential dwellings. *Indoor Air* 15: 432-444.

Hyttinen, M., Pasanen, P., Salo, J., Björkroth, M., Vartianen, M. and Kalliokoski, P., (2003). Reactions of ozone on ventilation filters. *Indoor and Built Environment* 12: 151-158.

Hubbard H.F., Coleman B.K., Sarwar G., Corsi R.L. (2005). The effects of an ozone generating air purifier on indoor secondary particles in three residential dwellings. *Indoor Air* 15: 432-444.

Ito, K., De Leon, S.F., Lippmann, M. (2005). Associations between ozone and daily mortality: analysis and meta-analysis. *Epidemiology* 16: 446-457.

Jaenicke, R. (1993). Tropospheric aerosols. In: Hobbs, P.V. (ed.) *Aerosol–Cloud–Climate Interactions*, San Diego, Academic Press, 1-31.

Jonsson, A. M., Hallquist, M., Ljungstrom, E. (2006). Impact of humidity on the ozone initiated oxidation of limonene, Δ^3-carene, and α-pinene. *Environmental Science and Technology* 40: 188-194.

Kamens, R., Jang, M., Chien, C.J., Leach, K. (1999) Aerosol formation from the reaction of a-pinene and ozone using a gas-phase kinetics-aerosol partitioning model. *Environmental Science and Technology* 33: 1430–1438.

Klenø J.G., Clausen, P.A., Weschler, C.J., Wolkoff, P. (2001) Determination of ozone removal rates by selected building products using the FLEC emission cell. *Environmental Science and Technology* 35: 2548-2553.

Klepeis, N.E., Nelson, W.C., Ott, W.R., Robinson, J.P., Tsang, AM., Switzer, P., Behar, J.V., Hern, S.C., Engelmann, W.H. (2001). The National Human Activity Pattern Survey (NHAPS): a resource for assessing exposure to environmental pollutants. *Journal of Exposure Analysis and Environmental Epidemiology* 11: 231-252.

Klepeis, N.E., Apte, M.G., Gundel, L.A., Sextro, R.G., Nazaroff, W.W. (2003). Determining size-specific emission factors for environmental tobacco smoke particles. *Aerosol Science and Technology* 37: 780–790.

Lai, A.C.K., Nazaroff, W.W. (2000). Modeling indoor particle deposition from turbulent flow onto smooth surfaces. *Journal of Aerosol Science* 31: 463-476.

Langer, S., Moldanova, J., Arrhenius, K., Ljungstrom, E., Ekberg, L. (2008). Ultrafine particles produced by ozone/limonene reactions in indoor air under low/closed ventilation conditions. *Atmospheric Environment* 42: 4149-4159.

Lee, K., Vallarino, J., Dumyahn, T., Ozkaynak, H., Spengler, J.D. (1999) Ozone decay rates in residences. *Journal of Air and Waste Management Association* 49: 1238-1244.

Lee, S.C., Lam, S., Fai, H.K. (2001). Characterization of VOCs, ozone, and PM10 emissions from office equipment in an environmental chamber. *Building and Environment* 36: 837–842.

Lee, B.U., Yermakov, M., Grinshpun, S.A. (2004). Removal of fine and ultrafine particles from indoor air environments by the unipolar ion emission. *Atmospheric Environment* 38: 4815-4823.

Leungsakul, S., Jaoui, M., Kamens, R.M. (2005). Kinetic mechanism for predicting secondary organic aerosol formation from the reaction of d-limonene with ozone. *Environmental Science and Technology* 39: 9583-9594.

Levy, J.I., Chemerynski, S.M., Sarnat, J.A. (2005). Ozone exposure and mortality: an empiric bayes metaregression analysis. *Epidemiology* 16: 458-468.

Liu, D.L., Nazaroff, W.W. (2001). Modeling pollutant penetration across building envelopes. *Atmospheric Environment* 35: 4451-4462.

Long C.M., Suh H.H., Koutrakis P. (2000). Characterization of indoor particle sources using continuous mass and size monitors. *Journal of Air and Waste Management Association* 50: 1236-1250.

Long, C.M., Suh, H.H., Catalano, P.J., Koutrakis, P. (2001) Using time- and size-resolved particulate data to quantify indoor penetration and deposition behavior, *Environmental Science and Technology* 35: 2089–2099.

Leungsakul, S., Jaoui, M., and Kamens, R.M. (2005). Kinetic mechanism for predicting secondary organic aerosol formation from the reaction of d-limonene with ozone. *Environmental Science and Technology* 39: 9583-9594.

Li, Q., Hu, D., Leungsakul, S., Kamens, R. (2007). Large outdoor chamber experiments and computer simulations: (I) Secondary organic aerosol formation from the oxidation of a mixture of d-limonene and a-pinene. *Atmospheric Environment* 41: 9341–9352.

McDonnell, W.F., Abbey, D.E., Nishino, N., Lebowitz, M.D. (1999). Longterm ambient ozone concentration and the incidence of asthma in nonsmoking adults: the AHSMOG Study. *Environmental Research* 80:110–121.

Miller-Leiden, S., Lobascio, C., Nazaroff, W.W., Macher, J.M. (1996). Effectiveness of in-room air filtration and dilution ventilation for tuberculosis infection control. *Journal of Air and Waste Management Association* 46: 869-882.

Mølhave, L., Kjaergaard, S., Hempel-Jorgensen, A., et al. (2000). The Eye irritation and odor potencies of four terpenes which are major constituents of the emissions of VOCs from nordic softwoods. *Indoor Air* 10: 315-318.

Morrison, G.C., Nazaroff, W.W., Cano-Ruiz, J.A., Hodgson, A.T., Modera, M.P. (1998). *Journal of Air and Waste Management Association* 48: 941-952.

Morrison, G.C., Nazaroff, W.W. (2000). Rate of ozone uptake on carpets: experimental studies. *Environmental Science and Technology* 34: 4963-4968.

Morrison, G.C., Nazaroff, W.W. (2002). Ozone interactions with carpet: Secondary emissions of aldehydes. *Environmental Science and Technology* 36: 2185-2192.

Mullen, N., Yu, X., Zhao, P., Corsi, R.L., Siegel, J.A. (2005). Experimental characterization of portable ion generators. *Indoor Air 2005: Proceedings of the 10th International Conference on IAQ and Climate*, 2957-2961.

Murray, D.M., Burmaster, D.E. (1995). Residential air exchange-rates in the United-States—Empirical and estimated parametric distributions by season and climatic region. *Risk Analysis* 15: 459-465.

Nazaroff, W.W., Klepeis, N.E. (2004) Environmental tobacco smoke particles. In: *Indoor Environment: Airborne Particles and Settled Dust*, Morawska, L. and Salthammer, T. (eds), Weinheim, Wiley VCH, pp. 245-274.

Nazaroff, W.W., Weschler, C.J. (2004). Cleaning products and air fresheners: Exposure to primary and secondary air pollutants. *Atmospheric Environment* 38: 2841-2865.

Ng, N.L., Kroll, J.H., Keywood, M.D., Bahreini, R., Varutbangkul, V., Flagan, R.C., Seinfeld, J.H. (2006). Contribution of first- versus second-generation products to secondary organic aerosols formed in the oxidation of biogenic hydrocarbons. *Environmental Science and Technology* 40: 2283-2297.

Niu, J., Thomas, C.W., Tung, J.B. (2001a). Ozone emission rate testing and ranking method using environmental chamber. *Atmospheric Environment* 35: 2143-2151.

Niu, J.L., Tung, T.C.W., Burnett, J. (2001b). Quantification of dust removal and ozone emission of ionizer air-cleaners by chamber testing. *Journal of Electrostatics* 51: 20-24.

Nøjgaard, J.K., Bilde, M., Stenby, C., Nielsen, O.J., Wolkoff, P. (2006). The effect of nitrogen dioxide on particle formation during ozonolysis of two abundant monoterpenes indoors. *Atmospheric Environment* 40, 1030-1042.

Odum, J.R., Hoffmann, T., Bowman, F., Collins, D., Flagan, R.C., Seinfeld, J.H. (1996). Gas/particle partitioning and secondary organic aerosol. *Environmental Science and Technology* 30: 2580-2585.

Offermann, F.J., Sextro, R.G., Fisk, W.J., Grimsrud, D.T., Nazaroff, W.W., Nero, A.V., Revzan, K.L., Yater, J. (1985). Control of respirable particles in indoor air with portable air cleaners. *Atmospheric Environment* 19: 1761-1771.

Pankow, J.F. (1994). An absorption model of the gas/aerosol partitioning involved in the formation of secondary organic aerosol. *Atmospheric Environment* 28: 189-193.

Pekkanen, A. Peters, G. Hoek, P. Tittanen, B. Brunekreef, J. De Hartog, J.U. Heinrich, A. Ibald-Mulli, W.G. Kreyling, T. Lanki, K.L. Timonen and E. Vanninen. (2002). Particulate air pollution and risk of ST-segment depression during repeated submaximal exercise tests among subjects with coronary heart disease. *Circulation* 106: 933-944.

Persily, A. (1989). Ventilation rates in office buildings. In*: IAQ '89, The Human Equation: Health and Comfort, Atlanta, GA*, American Society of Heating, Refrigerating, and Air Conditioning Engineers, pp. 128–136.

Piazza, T, Lee, R.H., Hayes, J. (2007). *Survey of the Use of Ozone Generating Air Cleaners by the California Public*. California Air Resources Board.

Pope, C.A., Dockery, D.W. (2006). Health effects of fine particulate air pollution: Lines that connect. *Journal of Air and Waste Management Association* 56: 709-742.

Reiss, R., Ryan, P.B., Koutrakis, P. (1994). Modeling ozone deposition onto residential surfaces. *Environmental Science and Technology* 28: 504-513.

Reiss, R., Ryan, P.B., Koutrakis, P., Tibbetts, S.J. (1995). Ozone reactive chemistry on interior latex paint. *Environmental Science and Technology* 29: 1906-1912.

Riley, W.J., McKone, T.E., Lai, A.C.K., Nazaroff, W.W. (2002). Indoor particulate matter of outdoor origin: Importance of size-dependent removal mechanisms. *Environmental Science and Technology* 36: 200-207.

Robinson, J., Nelson, W.C. (1995). *National Human Activity Pattern Survey Data Base*. United States Environmental Protection Agency, Research Triangle Park, N.C.

Rohr, A.C., Wilkins, C.K., Clausen, P.A., Hammer, M., Nielsen, G.D., Wolkoff, P., Spengler, J.D. (2002). Upper airwary and pulmonary effects of oxidation products of (+)α-pinene, d-limonene, and isoprene in balb/c Mice. *Inhalation Toxicology* 14: 663-684.

Rohr, A.C., Shore, S.A., Spengler, J. D. (2003). Repeated exposure to isoprene oxidation products causes enhanced respiratory tract effects in multiple murine strains. *Inhalation Toxicology* 15: 1191-1207.

Saarela, K. (1999). Emissions from floor coverings. In: Salthammer, T., (ed). *Organic Indoor Air Pollutants: Occurrence, Measurement, Evaluation*. Wiley-VCH.

Sabersky, R.H., Sinema, D.A., Shair, F.H. (1973). Concentrations, decay rates, and removal of ozone and their relation to establishing clean indoor air. *Environmental Science and Technology* 7: 347-353.

Salthammer, T., Boehme, C., Meyer, B., Siwinski, N. (2003). Release of primary compounds and reaction products from oriented strand board (OSB). In: *Proceedings of Healthy Buildings 2003, Singapore*, vol. 1, pp. 160–165.

Sarwar, G., Corsi, R., Allen, D., Weschler, C.J. (2003). The significance of secondary organic aerosol formation and growth in buildings: Experimental and computational evidence. *Atmospheric Environment* 37: 1365-1381.

Sarwar, G., Olson, D.A., Corsi, R.L., Weschler, C.J. (2004). Indoor fine particles: The role of terpene emissions from consumer products. *Journal of Air and Waste Management Association* 54: 367-377.

Sarwar, G., Corsi, R.L. (2007). The effects of ozone/limonene reactions on indoor secondary organic aerosols. *Atmospheric Environment* 41: 959-973.

Seinfeld, J.H., Pandis, S.N. (1998). *Atmospheric Chemistry and Physics*. New York: Wiley.

Shaughnessy, R.J., Levetin, E., Blocker, J., Sublette, K. L. (1994). Effectiveness of portable indoor air cleaners: Sensory testing results. *Indoor Air* 4: 179-188.

Shaughnessy, R.J., Sextro, R.G. (2006). What is an effective portable air cleaning device? A review. *Journal of Occupational and Environmental Hygiene* 3: 169–181.

Singer B.C., Revzan K.L., Hotchi T., Hodgson A.T., Brown N.J. (2004). Sorption of organic gases in a furnished room. *Atmospheric Environment* 38: 2483-2494.

Singer, B.C., Coleman, B.K., Destaillats, H., Hodgson, A.T., Lunden, M.M., Weschler, C.J., Nazaroff, W.W., (2006a). Indoor secondary pollutants from cleaning product and air freshener use in the presence of ozone. *Atmospheric Environment* 40: 6696-6710.

Singer, B., Destaillats, H., Hodgson, A.T., and Nazaroff, W.W. (2006b). Cleaning products and air fresheners: Emissions and resulting concentrations of glycol ethers and terpenoids. *Indoor Air* 16: 179-191.

Springs, M., Morrison, G.C., 2008. Reaction probability between terpenes and ozone on model indoor surfaces. *Indoor Air 2008: Proceedings of the 11th International Conference on IAQ and Climate*.

Tichenor, B.A., Guo, A., Dunn, J.E., Sparks, L.E., Mason, M.A. (1991). The interaction of vapour phase organic compounds with indoor sinks. *Indoor Air* 1: 23-35.

Thatcher, T.L., Layton, D.W. (1995). Deposition, resuspension, and penetration of particles within a residence. *Atmospheric Environment* 29: 1487-1497.

Tung, T.C.W., Niu, J., Burnett, J., Hung, K. (2005). Determination of ozone emission from a domestic air cleaner and decay parameters using environmental chamber tests. *Indoor Built Environment* 14: 29-37.

US Bureau of the Census (2005). *American Housing Survey*. Washington, DC

U.S. Environmental Protection Agency (1999). *Compendium of Methods for the Determination of Toxic Organic Compounds in Ambient Air*. EPA/625/R-96/010b. Office of Research and Development, Center for Environmental Research Information: Washington, DC.

Vartiainen, E., Kulmala, M., Ruuskanen, T.M., Taipale, R., Rinne, J., Vehkamaki, H. (2006). Formation and growth of indoor air aerosol as a result of d-limonene oxidation. *Atmospheric Environment* 40: 7882-7892.

Viner, A., Lawless, P.A., Ensor, D.S., Sparks, L.E. (1992). Ozone generation in dc-energized electrostatic precipitators. *IEEE Transactions on Industry Applications* 28: 504-512.

Wainman, T., Zhang, J.F., Weschler, C.J., Lioy P.J. (2000). Ozone and limonene in indoor air: A source of submicron particle exposure. *Environmental Health Perspectives* 108: 1139-1145.

Wallace, L., Nelson, C.W., Pellizzari, E. (1991). Identification of polar volatile organic compounds in consumer products and common microenvironments. In: *Proceedings of the Air and Waste Management Association's 1991 Annual Meeting*.

Wallace, L.A. (2000). Real-time monitoring of particles, PAH, and CO in an occupied townhouse. *Applied Occupational Environmental Hygiene* 15, 39-47.

Wallace, L., Emmerich, S.J., Howard-Reed, C. (2004). Effect of central fans and in-duct filters on deposition rates of ultrafine and fine particles in an occupied townhouse. *Atmospheric Environment* 38: 405-413.

Wallace, L.A. (2005). Ultrafine particles from a vented gas clothes dryer. *Atmospheric Environment* 39: 5777-5786.

Wallace, L. (2006). Indoor sources of ultrafine and accumulation mode particles: Size distributions, size-resolved concentrations, and source strengths. *Aerosol Science and Technology* 40: 48-360.

Wang, H., Morrison, G.C. (2006) Ozone-initiated secondary emission rates of aldehydes from indoor surfaces in four homes. *Environmental Science and Technology* 40: 5263-5268.

Ward, M., Siegel, J.A. (2005). Modeling filter bypass: Impact on filter efficiency. *ASHRAE Transactions* 111: 1091-1100.

Waring, M.S., Siegel, J.A. (2007). An evaluation of the indoor air quality in bars before and after a smoking ban in Austin, Texas. *Journal of Exposure Science and Environmental Epidemiology* 17: 260-268

Waring, M., Siegel, J. (2008). Particle loading rates for HVAC filters, heat exchangers, and ducts. *Indoor Air* 18: 209-224.

Waring, M.S., Siegel, J.A., Corsi, R.L. (2008). Ultrafine particle removal and generation by portable air cleaners. *Atmospheric Environment* 42: 5003-5014.

Wells, J.R. (2005). Gas-phase chemistry of α-terpineol with ozone and OH radical: Rate constants and products. *Environmental Science and Technology* 39: 6937-6943.

Weschler, C.J., Hodgson, A.T., Wooley, J.D. (1992). Indoor chemistry: Ozone, volatile organic compounds, and carpets. *Environmental Science and Technology* 26: 2371-2377.

Weschler, C.J., Shields, H.C. (1996). Production of hydroxyl radical in indoor air. *Environmental Science and Technology* 30: 3250-3258.

Weschler, C.J., Shields, H.C. (1997). Measurement of the hydroxyl radical in a manipulated but realistic indoor environment. *Environmental Science and Technology* 31: 3719-3722.

Weschler, C.J., Shields, H.C. (1999). Indoor ozone/terpene reactions as a source of indoor particles. *Atmospheric Environment* 33: 2301-2312.

Weschler, C.J. (2000). Ozone in indoor environments: Concentration and chemistry. *Indoor Air* 10: 269-288.

Weschler, C.J., Shields, H.C. (2000). The influence of ventilation on reactions among indoor pollutants: Modeling and experimental observations. *Indoor Air* 10: 92-100.

Weschler, C.J. (2003). Indoor/outdoor connections exemplified by processes that depend on an organic compound's saturation vapor pressure. *Atmospheric Environment* 37: 5455-5465.

Weschler, C.J., Shields, H.C. (2003). Experiments probing the influence of air exchange rates on secondary organic aerosols derived from indoor air chemistry. *Atmospheric Environment* 37: 5621–5631.

Weschler, C.J. (2004). New Directions: Ozone-initiated reaction products indoors may be more harmful than ozone itself. *Atmospheric Environment* 38: 5715–5716.

Weschler, C.J. (2006). Ozone's impact on public health: Contributions from indoor exposures to ozone and products of ozone-initiated chemistry. *Environmental Health Perspectives* 114: 1489-1496.

Wolkoff, P., Schneider, T., Kildesø, J., Degerth, R., Jaroszewski, M., Schunk, H. (1998). Risk in cleaning: Chemical and physical exposure. *The Science of the Total Environment* 215: 135-156.

Won, D., Corsi, R.L., Rynes, M. (2001). Sorptive interactions between VOCs and indoor materials. *Indoor Air* 11: 246-256.

Zhao, P., Siegel, J.A., Corsi, R.L. (2007). Ozone removal by HVAC filters. *Atmospheric Environment* 41: 3151-3160.

Zuraimi, M.S., Weschler, C.J., Tham, K.W., Fadeyi, M.O. (2007). The impact of building recirculation rates on secondary organic aerosols generated by indoor chemistry. *Atmospheric Environment* 41: 5213-5223.

Vita

Michael Shannon Waring attended Cypress Creek High School, in Houston, Texas. In 1996, he entered the University of Texas at Austin as an undergraduate. He received the degree of Bachelor of Arts from UT-Austin in May, 2000, and he received the degree of Bachelor of Science in Engineering in May, 2005. In August, 2005, he entered the Graduate School at the University of Texas at Austin.

Permanent Address: 202 E. 45th St. #301, Austin, Texas, 78751

This manuscript was typed by the author.